

**A PATH INTEGRAL MONTE CARLO STUDY
OF QUANTUM SOLUTES IN LIQUID AMMONIA
AND AMMONIA CLUSTERS**

by

© Massimo Marchi

A Thesis

Submitted to the School of Graduate Studies
in Partial Fulfilment of the Requirements

for the Degree
Doctor of Philosophy

McMaster University
(July 1988)

QUANTUM SOLUTES IN LIQUID AMMONIA

DOCTOR OF PHILOSOPHY (1988)

McMASTER UNIVERSITY

Hamilton, Ontario

TITLE: A Path Integral Monte Carlo Study of Quantum Solutes in
Liquid Ammonia

AUTHOR: Massimo Marchi, Laurea in Chimica (Università di Firenze)

SUPERVISOR: Professor Michael L. Klein

NUMBER OF PAGES: xiii, 158

Abstract

The path integral Monte Carlo method is applied to some solvation problems involving quantum solutes. Thermodynamics quantities like partial molar volume and entropy change associated with the electron solvation process are calculated. The ionization of alkali atoms in liquid ammonia and the electron attachment to ammonia clusters are investigated.

Path integral MC simulations at constant pressure lead to an expansion of the simulation box in satisfactory agreement with the experimental molar volume. The structure of the solvated electron at constant pressure was found to be very similar to the one at constant volume. The electron wavefunction was only slightly expanded.

The Debye charging trick is used to calculate the free energy of the solvated electron at constant volume. The experimental solvation entropy at constant pressure is reproduced only when a correction due to the volume expansion is introduced. The contribution to the entropy due to the ordering of the ammonia molecules induced by the electron is negative. The expansion work, performed by the liquid when the electron is introduced, is responsible for the positive experimental entropy.

Spontaneous ionization is observed only for Na and Cs when a hard core (HC) pseudopotential is employed. A soft core (SC) pseudopotential leads to the formation of dipolar atoms when tested with Li and Cs. A dipolar Li atom is observed even for the HC model. These calculations

predict that the minimum energy state for at least Na and Cs is indeed the separately solvated ions. This is agreement with the experimental evidence.

The nature of electron attachment to ammonia clusters composed of 16, 36 and 54 molecules is studied. At 100K, a negatively charged cluster of 16 molecules appears to be unstable in the sense that the electron binding energy is less than $k_B T$. For both the 36 and 54 molecule clusters the electron binds to the cluster surface. The 54 molecule cluster also supports a (meta) stable interior solvated state. These findings are discussed in the light of experimental data on the same system.

Acknowledgements

In first place, I would like to acknowledge my supervisor Mike L. Klein for his guidance through the marshy grounds of statistical mechanics. Most of my knowledge on simulation techniques was acquired through the nurturing discussions I had with him, mainly by telephone. In that respect, I would like express my gratitude to Bell Canada for the superb service they have provided us.

I greatly benefitted from Roger W. Impey's knowledge of supercomputers. His help in the computational problems faced in these years is deeply appreciated. I would like to acknowledge John S. Tse for his continuous encouragement and scientific assistance. I thank both for their friendship.

The NSERC financial support for the years 1984-86 is appreciated. The Government of Ontario is gratefully acknowledged for an Ontario Differential Fee Waiver in 1987-88. In addition, I would like to thank the John Von Neumann Center for Scientific Computing for the abundant CYBER 205 computer time provided.

I would like to express my appreciation to Jim Bareman and Michael Moller who contributed to improve my spoken and written English enduring endless discussions on that subject.

Last, but not the least, I would like to thank Michiel Sprik for

showing me that only hard and punctilious work is rewarded in science. Throughout the years I spent working on my thesis project his assistance and scientific knowledge as well as his kindness and friendship have been invaluable. Again, I would like to stress my profound appreciation for him.

LE

in memoria di mio padre

Contents

1	Introduction	1
2	Intermolecular Interactions and Pseudopotentials	5
2.1	Intermolecular Potentials	5
2.1.1	Ab Initio Calculations	6
2.1.2	Atom-atom Potential Method	8
2.2	Electron Pseudopotentials	11
3	Path Integral Monte Carlo Method	16
3.1	Path Integral Representation of the Partition Function	18
3.1.1	High Temperature Approximation	19
3.1.2	Classical Isomorphism	20
3.2	The Monte Carlo Method	22
3.3	Classical Monte Carlo Simulations	25
3.4	Path Integral Monte Carlo	27
3.5	The Staging Algorithm	29
3.5.1	The Choice of P	30

3.5.2	Staging	31
3.6	Equilibrium Correlation Functions	34
4	The Solvated Electron in Liquid Ammonia at Constant Pressure	39
4.1	Potentials	40
4.2	Path Integral Monte Carlo at Constant Pressure	42
4.3	Simulation Details and Results	46
4.3.1	Simulations in the (NvT) Ensemble	47
4.3.2	Simulations in the (NpT) Ensemble	51
4.3.3	Partial Volume of Electron Solvation	53
5	Free Energy of Electron Solvation in Liquid Ammonia	61
5.1	Free Energy from MC Simulations	61
5.2	Application to the Electron in Liquid Ammonia	66
5.3	Simulation Details	68
5.4	Results	69
5.4.1	The Discharge Process	69
5.4.2	Free Energy of Solvation	71
5.5	Discussion	74
6	Ionization of Alkali Atoms in Ammonia : Li, Na, Cs	84
6.1	Li ⁺ , Na ⁺ and Cs ⁺ in Liquid Ammonia	87
6.1.1	Ion-ammonia Potentials	87
6.1.2	Classical MC Calculations	88

6.2	Alkali Atoms in Ammonia	91
6.2.1	The Pseudopotential Problem	91
6.2.2	The Li Atom in Liquid Ammonia	93
6.2.3	Cs and Na in Liquid Ammonia	99
7	Electron Attachment to Ammonia Clusters	127
7.1	Preparation of the clusters	128
7.1.1	Neutral Clusters	128
7.1.2	Charged Clusters	130
7.2	Structural Properties	132
7.2.1	Neutral Clusters	132
7.2.2	Charged Clusters	133
7.3	Energetics of Electron Attachment	136
8	Conclusions	146

List of Tables

6.1	Ion-Ammonia Lennard-Jones Parameters	103
6.2	Structural Data	103
6.3	Energetics of Ionic Solvation	103
6.4	Parameters of the soft and hard core pseudopotentials . . .	104
7.1	Energetics of the Neutral and Charged Clusters.	138

List of Figures

4.1	Pair distribution functions $g_{N-N}(r)$	55
4.2	(cm-NH ₃) pair correlation functions at constant volume . .	56
4.3	Dipole correlation function	57
4.4	Convergence of the simulation box	58
4.5	Complex time correlation functions	59
4.6	(cm-NH ₃) pair correlation functions at constant pressure . .	60
5.1	Complex time correlation functions	76
5.2	Asymptotic values of the complex time correlation function	77
5.3	(cm-N) distribution functions	78
5.4	Configuration of electron and solvent at $c = 0.9e^-$	79
5.5	Configuration of electron and solvent at $c = 0.5e^-$	80
5.6	Configuration of electron and solvent at $c = 0.25e^-$	81
5.7	The electron-solvent potential V_{ep}	82
5.8	Entropy cycle	83
6.1	Molar conductivity of sodium-ammonia solutions	105

6.2	(X-N) pair correlation functions	106
6.3	(X-H) pair correlation functions	107
6.4	Ions dipole correlation functions	108
6.5	Complex time correlation functions : SC and HC Li	109
6.6	Electron-Li ⁺ charge site correlation functions : SC and HC Li	110
6.7	(Li-N) distribution functions : SC and HC Li	111
6.8	(Li-H) distribution functions : SC and HC Li	112
6.9	(cm-N) distribution functions: SC and HC Li	113
6.10	(cm-H) distribution functions: SC and HC Li	114
6.11	Electron-ammonia dipole correlation functions	115
6.12	Li ⁺ -ammonia dipole correlation functions	116
6.13	Instantaneous configuration from the SC Li calculation . . .	117
6.14	Instantaneous configuration from the HC Li calculation . . .	118
6.15	Instantaneous configuration from the SC Cs calculation . . .	119
6.16	Complex time correlation function from the SC Cs calculation	120
6.17	Cs-electron chain radial correlation from the SC Cs simulation	121
6.18	(Cs-NH ₃) pair correlation from the Cs SC simulation	122
6.19	(Cs-NH ₃) dipole correlations from the SC Cs simulation . . .	123
6.20	(cm-NH ₃) pair correlations from the Cs SC simulation	124
6.21	Configuration after 2000 passes of the Na HC simulation . .	125
6.22	e ⁻ -Cs ⁺ charge site distribution from the Cs HC simulation .	126
7.1	Neutral cluster: distribution functions for the nitrogen atoms	139
7.2	Configuration of an electron in an interior solvated state . .	140

7.3	(cm-NH ₃) distribution functions	141
7.4	Instantaneous configurations of the N = 16, 36 and 54 clusters	142
7.5	Clusters complex time correlation functions	143
7.6	Dipole correlation functions	144
7.7	(cm-N) correlation functions for the surface states.	145

Chapter 1

Introduction

The increasing power and speed of the modern computers in the past two decades have produced a flourish of studies on classical molecular systems by means of molecular dynamics (MD)[1] and Monte Carlo (MC)[2] calculations. Recently, simulation techniques, somewhat related to MD and MC, have been used to investigate quantum systems.[3-8] The most popular of these techniques is derived from the Feynman path integral formulation of quantum equilibrium statistical mechanics.[9,10] Here a quantum particle acting in a potential field is represented by an isomorphic closed chain polymer (necklace) composed of P classical particles. Each particle interacts with its adjacent neighbours in the polymer and with the external field. The interaction between adjacent polymer units is directly related to the path integral free particle density matrix.

If exchange is neglected, this approach projects a system of N inter-

acting quantum particles into an isomorphic classical system of N flexible ring molecules formed by P atoms.[11] The advantages of the path integral method are now clear. Since the quantum many-body problem can be reduced to a classical many-body problem, the canonical averages of such a system can be calculated by using MC or MD simulation techniques.

Path integral MC[12,5,6] or MD[3,13] simulations have been performed on a variety of systems. Although in the past quantum many-body problems have been treated with this technique,[12,14] most of the investigations have been focused on quantum solvation problems involving a quantum particle (electron or muonium) interacting with the solvent molecules, which in turn were dealt with as classical objects.

The theoretical interest in this latter kind of problems lies in the relation between electron solvation and fundamental physical chemistry processes such as electron transfer in solution, at an electrode and in biological molecules, ionization and electron-ion recombinations in solution. Several solvents have now been studied. The first pioneering work was carried out by Parrinello et al.[3] on an electron in molten KCl using path integral MD. More recently the attention has been focused on the electron in rare gases,[15] water[13,6] and liquid ammonia.[5,16] Both MD and MC methods have been used for these systems.

The first path integral simulation of an electron in a molecular liquid[5] was carried out in ammonia and was mainly centered on the structural aspects of the solvent molecules, in the vicinity of the solvated elec-

tron, and the electron state. That work has been taken as a starting point for this thesis. This thesis is concerned with some aspects of the solvation of quantum solutes in liquid ammonia and in ammonia clusters. The quantum solute studied has been the electron and alkali atoms : Li, Na and Cs. What follows is an outline of the problems this thesis deals with.

The discovery of solvated electrons in liquid ammonia goes back to 1863.[17] Since then a wide variety of experimental techniques have been used to study this phenomenon.[18] The easiest way of preparing a solvated electron is by dissolution of alkali metals in ammonia at low concentration.[17] Another technique involves the pulse radiolysis of the pure liquid.[19] The thermodynamics of the electron-ammonia system (free energy and entropy) can be probed either by photoemission experiments[20,21] or indirectly by standard electrochemical techniques applied to low concentration alkali metal solutions.[22] Some noticeable properties of the electron-ammonia solutions include intense blue colour, high electronic mobility, large positive molar volume and positive entropy.

The study of the absorption spectrum and the mobility of the solvated electron would involve access to real time electron correlation functions. Because of the limitation set by the complex time formalism, the path integral simulation methods cannot provide such information. Nevertheless, this technique can now be used to investigate the volume and the entropy change on solvation. Part of this thesis deals in fact with these two problems after a few theoretical issues are answered.

To provide some insight to the experimentally observed phenomenon of spontaneous ionization of alkali metals in liquid ammonia,[23,22] the next problem tackled in this thesis is the solvation of alkali atoms in liquid ammonia. Issues like structure of solvent near the atoms, ions and electron, which are not experimentally accessible, are at the center of the discussion.

In very recent times, experimental studies on negatively charged ammonia clusters have appeared in literature.[24,25] In these clusters the excess electron is bound to a neutral body of molecules. The experiment has provided only information about the critical size of the ammonia cluster, no information about the structure of the electron state can be gathered from experiment. This thesis will provide a few answers to the latter issue in light of the results obtained from path integral simulations.

The various chapters of this thesis are arranged as follows : Chapter 2 presents a discussion of the intermolecular potentials and electronic pseudopotentials. In Chapter 3 the path integral Monte Carlo method is described in some detail. After these two introductory chapters, Chapter 4 and 5 deals respectively with the volume and entropy change on electron solvation. Chapter 6 is devoted to the study of some alkali atoms in liquid ammonia. The study on electron attachment in ammonia clusters is presented in Chapter 7.

Chapter 2

Intermolecular Interactions and Pseudopotentials

2.1 Intermolecular Potentials

Intermolecular forces play a central role in the structure and thermodynamics of liquids and solids.[26] The problem of calculating the potential surface in phase space on which the molecular system is evolving can in theory be solved directly from first principles. In effect only in a few cases [27,7] has such an approach revealed to be feasible with the currently available computational resources. In more common circumstances one is obliged to adopt very crude potential models to represent the interactions amongst molecules.

The potential energy $V(\mathbf{r}_1, \mathbf{r}_2, \dots, \mathbf{r}_N)$ of a system composed by N

molecules can be expanded in contributions each deriving from different orders of additive interactions :

$$V(\mathbf{r}_1, \mathbf{r}_2, \dots, \mathbf{r}_N) = \frac{1}{2} \sum_{i,j} u_2(\mathbf{r}_i, \mathbf{r}_j) + \frac{1}{2 \cdot 3} \sum_{i,j,k} u_3(\mathbf{r}_i, \mathbf{r}_j, \mathbf{r}_k) + \dots \quad (2.1)$$

Studies[28,29,30] have shown that many-body effects are not generally negligible in most of the liquid and solid state applications. For practical reasons, however, only the first term in Eq. 2.1 is usually retained.

2.1.1 Ab Initio Calculations

One way of calculating the intermolecular potential acting between molecules is to use the perturbation theory. When the intermolecular distances are in the same order in magnitude of the dimensions of the molecules or larger, the interaction energy through second order in the interaction Hamiltonian can be derived from so-called *exchange perturbation theories*. [31,32] Schematically the intermolecular potential is given by

$$\epsilon = \epsilon_{exch} + \epsilon_{elat} + \epsilon_{ind} + \epsilon_{diap} \quad (2.2)$$

The first term in the above equation represents the repulsive exchange interactions acting between the molecules when the wavefunctions overlap is not negligible. In the perturbative calculation at short range, ϵ_{exch} derives directly from the antisymmetry requirements on the molecular wavefunctions. It contains first and, in smaller extent, second order contributions and vanishes as the intermolecular separation goes to infinity.

ϵ_{elst} is the quantum mechanical counterpart of the classical electrostatic interaction energy between two charge distributions and coincides with it at large intermolecular distances. It is a first order contribution. At shorter distances, this term differs from the classical energy of two interacting arrays of multipoles by a contribution sometimes called "penetration energy"

$$\epsilon_{pen} = \epsilon_{elst} - \epsilon_{mult}, \quad (2.3)$$

where ϵ_{mult} is the energy calculated from the electrostatic multipole expansion.

The last two terms in Eq. 2.2 are purely second order contributions. The induction (ϵ_{ind}) and dispersion (ϵ_{disp}) energies are originated respectively by (permanent-induced) and (induced-induced) multipole interactions between the two molecules.

The explicit expressions for the four terms in Eq. 2.2 involve a complex dependence from the center of mass separation between the molecules and the relative molecular orientations. Additionally, it requires the evaluation of matrix elements of the interaction Hamiltonian between antisymmetric products of the two sets of molecular eigenfunctions. Due to such complexity only in the past few years the calculation of ab initio intermolecular potentials has become computationally feasible. So far mainly small molecules have been the subject of investigations (see for instance [33,34,35,36]).

2.1.2 Atom-atom Potential Method

When repeated evaluations of the interaction potentials for many configurations are required like in applications to statistical mechanics and solid state physics, the use of the *ab initio* approach is out of the question because of the enormous computer resources needed. An easy and quick calculation of the intermolecular energy and its derivatives is achieved by using analytical functions to approximate the effective potential acting between molecules. Multicenter analytical functions, instead of an explicit angular dependence, are generally used to mimic the anisotropy of the molecule-molecule interaction. Many-body simulation studies such as molecular dynamics (MD) and Monte Carlo (MC) are then possible within reasonable computer resources.

In the past there has been a great deal of discussion about the partitioning of molecules in fragments whose properties are transferable amongst different molecular species.[37,32] According to one possible approach, the molecular Hartree-Fock orbitals are projected by an unitary transformation onto orbitals localized on interatomic bonds, inner shell of the nuclei and lone pairs.[37] It has been shown that molecular quantities can be expressed as a sum of contributions from bonds and lone pairs. In addition to being additive, the properties of the fragment are, in a certain extent, transferable amongst different, but chemically related, molecular species.

Bader et al.[38,39,40,41,42] have followed a different route. In their view, the most transferable fragments in a molecule are delimited by a so-called "zero flux" surface for which the gradient of the electron density,

$\bar{\nabla}\rho(\mathbf{r})$, is equal to zero. Such fragments possess physical properties and satisfy theorems that are those of the isolated atom.

In principle, both approaches could be used to partition the molecules in pieces whose interaction potentials are the same independently from which molecule the fragments happen to be.

As mentioned in the previous section, *ab initio* intermolecular potentials are difficult to calculate and the estimated error large. At present, there is not a reliable way to calculate the contributions from bonds and lone pairs to the molecular interaction, the results depending mostly on the wavefunction used in such calculations. Moreover, Bader's approach has not been widely applied to intermolecular interactions.

Because of these aspects, the atom-atom method is generally adopted. This consists in considering the center of each atom in the molecule as the molecular fragment. The interaction between two molecules is then calculated by adding up together the contributions from each pair of atoms on different molecules.

The atom-atom potentials have a variety of analytical forms involving many parameters. These parameters are generally fitted either to physical properties of gaseous and condensed phases or to *ab initio* calculations of the dimer. They are respectively classified as semi-empirical and *ab initio* atom-atom potentials.

The functions used in representing the atom-atom interaction are composed of different contributions which, in part, derive their analytical

expressions from a series expansion of the terms in Eq. 2.2.

Commonly, the electrostatic atom-atom potential consists of a charge-charge term. In some case atomic dipole-dipole, dipole-quadrupole and quadrupole-quadrupole contributions have been added.[43,44] The charges or higher order multipoles are distributed on the molecule in order to reproduce the molecular multipole moments known from experiment or *ab initio* calculations.

The series expansion of the dispersion energy for two interacting atoms leads to a sequence of contributions from instantaneous multipole interactions. The leading terms go with $1/R^6$ (instantaneous dipole-dipole interactions), $1/R^8$ (instantaneous dipole-quadrupole interactions),... etc.

The intermolecular exchange interaction, which gives a repulsive contribution to the total energy, cannot be represented analytically according to an expansion like the one for the dispersion energy. Therefore, the potential function in an atom-atom potential is totally empirical and goes commonly with $1/R^{12}$ or has an exponential dependence.

The induction effects are commonly negligible in solids and liquids. In the few cases in which induction has been explicitly included in condensed matter calculations, the potential is expanded in terms containing the static molecular multipoles and polarizabilities leading terms. Induction has never been incorporated explicitly in atom-atom potentials. Often, its effects are included in the attractive and repulsive terms of the interatomic potential.

The most common analytical forms used are the Lennard-Jones and exp-6 functions :

$$V_{LJ}(r) = 4\epsilon \left[\left(\frac{\sigma}{r} \right)^{12} - \left(\frac{\sigma}{r} \right)^6 \right] \quad (2.4)$$

$$V_{exp-6}(r) = A \exp(-Br) - \frac{C}{r^6} \quad (2.5)$$

The relatively few parameters contained in the above expressions and their simplicity make them suitable for use in MD and MC simulations. Only in few cases *ab initio* atom-atom potentials include contributions from multi-body interactions, deriving from higher order terms in Eq. 2.1 (see for instance [29]). This, in part, explains why most of the available *ab initio* potentials do not satisfactorily reproduce the behaviour of liquids and solids where those interactions are important.

At present, semiempirical atom-atom potentials are the most popular in statistical mechanics calculations. In fact, although designed to reproduce only a few physical properties of the molecules in a particular region of the phase diagram, they can be successfully used to study other regions of importance for the same system. In addition, they can have in some case a certain degree of transferability amongst chemically related molecular species (see for instance [45,46]).

2.2 Electron Pseudopotentials

Pseudopotentials have been used in the past to calculate the electronic properties of a variety of systems such as metals, semiconductors, atoms

and molecules. The pseudopotential method is based on the assumption that the interaction amongst core and valence electrons can be handled by an effective potential acting on the valence electrons. Such a potential averages out the contributions from all the core electron states.

In the past the first pseudopotentials were used in single electron band structure calculations. Their parameters were empirically chosen to fit first ionization energies of the isolated atoms and some experimentally available features of the energy bands, such as form factors.

The earliest formulation of the pseudopotential method is due to Philips and Kleinman.[47] They considered a single electron wavefunction Ψ solution of the Schrodinger equation for a valence electron¹

$$\{T + V(r)\}\Psi(r) = \epsilon\Psi(r), \quad (2.6)$$

where T and $V(r)$ constitute the appropriate single electron Hamiltonian (namely Hartree-Fock or density functional Hamiltonian). $\Psi(r)$ is divided in a *smooth* part, Φ , and a linear combination of the core wavefunctions ϕ_α

$$\Psi(r) = \Phi(r) - \sum_{\alpha} b_{\alpha}\phi_{\alpha}(r). \quad (2.7)$$

Inside the core, where the potential energy is strongly negative and, consequently, the kinetic energy of the valence electron is matchingly high, Ψ is rapidly oscillating. The oscillatory contribution to Ψ is totally due to the second term in Eq. 2.7. The cancellation of the negative potential energy

¹Unless otherwise stated, atomic units are adopted throughout this thesis

with the positive kinetic energy inside the core[48] suggests the use of an effective Hamiltonian whose eigenfunction is Φ . Φ coincides with the *exact* wavefunction outside a certain core radius, is nodeless and goes smoothly to zero when r goes to zero.

Since Ψ is orthogonal to the core levels, the coefficient of the linear combination of core orbitals is given by

$$b_\alpha = \langle \phi_\alpha | \Phi \rangle. \quad (2.8)$$

Inserting 2.8 into 2.6 and using $H\phi_\alpha = \epsilon_\alpha\phi_\alpha$, one obtains

$$\{T + V(r) + V_R(r)\}\Phi(r) = \epsilon\Phi(r), \quad (2.9)$$

where

$$V_R(r) = -\frac{\sum_\alpha (\epsilon_\alpha - \epsilon)\phi_\alpha(r)\langle \phi_\alpha | \Phi \rangle}{\Phi(r)}. \quad (2.10)$$

The term in brackets in Eq. 2.9 acts as an effective Hamiltonian. The altered potential contained in this Hamiltonian is the pseudopotential, namely

$$V_{ps}(r) = V(r) + V_R(r). \quad (2.11)$$

The above pseudopotential is not only a function of the electron position, but also of core state projection operators (see, Eq. 2.10). This is then called a *non local* pseudopotential.[49]

To discuss the various contributions to the pseudopotential an explicit expression for the single electron Hamiltonian has to be used. The most natural choice is to employ the standard Hartree-Fock formalism. One

obtains the following eigenvalue equation for the valence electron[50,51]

$$[T + V_C(\mathbf{r}) - \epsilon] \Psi(\mathbf{r}) = \sum_{\alpha} \phi_{\alpha}(\mathbf{r}) \int \frac{\phi_{\alpha}^*(\mathbf{r}') \Psi(\mathbf{r}')}{|\mathbf{r} - \mathbf{r}'|} d\mathbf{r}', \quad (2.12)$$

where $V_C(\mathbf{r})$ is the Coulombic potential felt by the electron given by

$$V_C(\mathbf{r}) = -\frac{Z}{r} + 2 \sum_{\alpha} \int \frac{\phi_{\alpha}^*(\mathbf{r}') \phi_{\alpha}(\mathbf{r}')}{|\mathbf{r} - \mathbf{r}'|} d\mathbf{r}'. \quad (2.13)$$

The sum of exchange terms on the right hand side of Eq. 2.12 is *non local*. This part of the Hamiltonian can be replaced by some attractive potential $V_E(\mathbf{r})$ if a local exchange approximation is used. The Hartree-Fock approach does not include any effect from electron polarization (i.e. correlation). It is common to introduce an additional term in the potential $V_P(\mathbf{r})$ which accounts for this effect.

The one electron potential which now acts on the electron in the outer shell is

$$V(\mathbf{r}) = V_C(\mathbf{r}) + V_E(\mathbf{r}) + V_P(\mathbf{r}). \quad (2.14)$$

Thus, combining Eq. 2.14 with Eq. 2.11 one obtains the following expression for the pseudopotential

$$V_{ps}(\mathbf{r}) = V_C(\mathbf{r}) + V_E(\mathbf{r}) + V_P(\mathbf{r}) + V_R(\mathbf{r}). \quad (2.15)$$

Although Eq. 2.15 has been derived for valence electron of atoms, the electron-molecule scattering theory can show that an identical equation holds for the interaction between an electron and a closed shell molecule.[51] In this case one has to substitute in the Eqs. 2.6 and 2.15 the core wavefunctions with the ground state wavefunctions of the molecule. Additionally,

the coulombic interaction has to be modified to include the electrostatic potential deriving from all the nuclei. It is clear, however, that the nature of the interaction in the two cases is different; the electron-molecule potential is much less attractive than the interaction between valence and core electrons.

Chapter 3

Path Integral Monte Carlo Method

The thermodynamic properties of a quantum many-body system are directly obtainable from its partition function which, in turn, can be expressed as the trace of the so-called density matrix ρ , namely

$$Q = \text{Tr}(\rho). \quad (3.1)$$

ρ is the statistical mechanics equivalent of the wave function in quantum mechanics. The Feynman path integral representation of the partition function can be exploited to study quantum systems by computer simulation.

The density matrix of a quantum many-body system in thermal equilibrium with the surroundings and composed of N particles is obtainable

by solving the Bloch equation

$$\frac{\partial \rho(\beta)}{\partial \beta} = -H \rho(\beta), \quad (3.2)$$

with boundary condition

$$\lim_{\beta \rightarrow 0} \rho(\beta) = 1, \quad (3.3)$$

where $\rho(\beta)$ is the density matrix relative to the reciprocal temperature $\beta = 1/k_B T$ and H is the system Hamiltonian. Equation 3.2 has formal solution

$$\rho(\beta) = e^{-\beta H}. \quad (3.4)$$

Adopting the Dirac notation, the density matrix in the coordinate representation has the form

$$\rho(\mathbf{R}, \mathbf{R}', \beta) = \langle \mathbf{R} | e^{-\beta H} | \mathbf{R}' \rangle, \quad (3.5)$$

where \mathbf{R} and \mathbf{R}' refer to all the phase space coordinates of the N particles. It is clear that $\rho(\mathbf{R}, \mathbf{R}', \beta)$ has the physical meaning of the probability amplitude distribution, at reciprocal temperature β , relative to the transition between the phase space configurations \mathbf{R} and \mathbf{R}' .

The other possible interpretation is related to the dimensionality of the reciprocal temperature β . By comparison of $\rho(\beta)$ in Eq. 3.4 with the quantum propagator e^{-iHt} , it is evident that β has the dimension of an imaginary time.[10] Consequently, the density matrix can be thought of as an imaginary time propagator giving the probability that the system at imaginary time τ in \mathbf{R} moves to \mathbf{R}' at time $\tau + \beta$.

3.1 Path Integral Representation of the Partition Function

To derive the path integral representation of the partition function, one can transform Eq. 3.5 using the identity

$$e^{-\beta H} = (e^{-\frac{\beta H}{P}})^P, \quad (3.6)$$

and inserting $P-1$ intermediate states; namely

$$\begin{aligned} \langle R | e^{-\beta H} | R' \rangle &= \int dR_1 \int dR_2 \cdots \int dR_{P-1} \langle R | e^{-\frac{\beta H}{P}} | R_1 \rangle \\ &\times \langle R_1 | e^{-\frac{\beta H}{P}} | R_2 \rangle \cdots \langle R_{P-1} | e^{-\frac{\beta H}{P}} | R' \rangle. \end{aligned} \quad (3.7)$$

In imaginary time the integrand in Eq. 3.7 gives the probability that a system at time $\tau = 0$ in R moves to R' at time $\tau = \beta$ through a path of intermediate points in phase space. The system is found in R_1 at time $\tau = \frac{\beta}{P}$, in R_2 at time $\tau = \frac{2\beta}{P} \cdots$ and in R_{P-1} at time $\tau = \frac{(P-1)\beta}{P}$. The total amplitude to go from R to R' is given by a sum over all possible paths.

As mentioned previously, the trace of the density matrix, namely the integral over the diagonal matrix elements, gives the partition function of the system. Thus, from Eqs. 3.7 and 3.5

$$\begin{aligned} Q(N, \beta) &= \int dR \rho(R, R, \beta) \\ &= \int dR \int dR_1 \int dR_2 \cdots \int dR_{P-1} \langle R | e^{-\frac{\beta H}{P}} | R_1 \rangle \\ &\times \langle R_1 | e^{-\frac{\beta H}{P}} | R_2 \rangle \cdots \langle R_{P-1} | e^{-\frac{\beta H}{P}} | R \rangle. \end{aligned} \quad (3.8)$$

3.1.1 High Temperature Approximation

The appearance on the right hand side in Eq. 3.8 of the density matrices relative to a temperature higher than the one on the left side enables one to use the high temperature approximation of the density matrix to evaluate the integrand.

At first, one has to assume a pair product form for the density matrix, namely

$$\rho\left(\mathbf{R}_s, \mathbf{R}_{s'}, \frac{\beta}{P}\right) = \prod_{i=1}^N K_0\left(\mathbf{r}_s^i, \mathbf{r}_{s'}^i, \frac{\beta}{P}\right) \prod_{i < j}^N \rho_2\left(\mathbf{r}_s^{ij}, \mathbf{r}_{s'}^{ij}, \frac{\beta}{P}\right), \quad (3.9)$$

where \mathbf{r}_s^i is the position of the particle i at "time" s , $K_0\left(\mathbf{r}_s^i, \mathbf{r}_{s'}^i, \frac{\beta}{P}\right)$ is the free particle density matrix[10]

$$K_0\left(\mathbf{r}_s^i, \mathbf{r}_{s'}^i, \frac{\beta}{P}\right) = \left(\frac{PM}{2\pi\beta}\right)^{3/2} \exp\left(-\frac{P}{2\beta}(\mathbf{r}_s^i - \mathbf{r}_{s'}^i)^2\right), \quad (3.10)$$

with M the particle mass; ρ_2 is the two-body density matrix divided by the free particle contribution; and

$$r_s^{ij} = |\mathbf{r}_s^i - \mathbf{r}_s^j|. \quad (3.11)$$

By using the perturbation theory at the first order in $\frac{\beta}{P}$, one can show that[10]

$$\rho_2\left(\mathbf{r}_s^{ij}, \mathbf{r}_{s'}^{ij}, \frac{\beta}{P}\right) \simeq \exp\left[-\frac{\beta}{2P}\left(V(r_s^{ij}) + V(r_{s'}^{ij})\right)\right], \quad (3.12)$$

where $V(r_s^{ij})$ is the interaction potential between the particles i and j at "time" s . The so-called asymptotic formula for the density matrix at high

temperature in Eq. 3.12 can approximate ρ_2 when P is large enough. In addition to the condition on the temperature, Eq. 3.12 is a good approximation if the potential acting on the particles does not vary significantly in the space $\Delta r = \lambda_T(1/P)^{1/2}$ spanned by the particles during the "time" $\Delta \tau = \beta/P$ which separates s from s' . Here λ_T is the particle thermal wavelength

$$\lambda_T = (\beta/m)^{1/2}. \quad (3.13)$$

The use of Eqs. 3.9 through 3.12 into Eq. 3.8 brings to the partition function

$$Q(N, P, \beta) = \left(\frac{MP}{2\pi\beta} \right)^{3N/2} \int \exp(-\beta S_{eff}) \prod_{s=1}^P \prod_{i=1}^N d\mathbf{r}_s^i, \quad (3.14)$$

with the Euclidian action

$$S_{eff} = \sum_{s=1}^P \sum_{i=1}^N \left[\frac{MP}{2\beta^2} (\mathbf{r}_s^i - \mathbf{r}_{s+1}^i)^2 + \frac{1}{P} \sum_{i < j}^N V(\mathbf{r}_s^{ij}) \right], \quad (3.15)$$

and

$$\mathbf{r} = \mathbf{r}_1 = \mathbf{r}_{P+1}. \quad (3.16)$$

It is clear that when $P \rightarrow \infty$ Eqs. 3.14 and 3.8 coincide.

3.1.2 Classical Isomorphism

The present discussion is concerned with the special case in which all the particles of the system except one have a very short thermal wavelength compared with the interparticle distances and can be considered classical

while an electron does not. The electron is, undoubtedly, a quantum particle.

The partition function of the mixed quantum-classical system composed of N molecules and one electron is obtainable from Eq. 3.14 when the path integral discretization of the N classical particles is removed. This means inserting $P = 1$ for those particles in Eq. 3.14. One obtains

$$Q(N, P, \beta) = \left(\frac{mP}{2\pi\beta}\right)^{3/2} \left(\frac{MP}{2\pi\beta}\right)^{3N/2} \int \prod_{i=1}^N d\mathbf{R}_i \prod_{s=1}^P e^{-\beta(V_{e--N} + V_{N-N})} \quad (3.17)$$

where m is the quantum particle mass,

$$V_{e--N} = \sum_{s=1}^P \left[\frac{mP}{2\beta^2} (\mathbf{r}_s - \mathbf{r}_{s+1})^2 + \frac{1}{P} \sum_{i=1}^N V(|\mathbf{r}_s - \mathbf{R}_i|) \right] \quad (3.18)$$

and

$$V_{N-N} = \sum_{i < j}^N U(\mathbf{R}_i, \mathbf{R}_j). \quad (3.19)$$

The set $\{\mathbf{r}^P\}$ denotes the electron coordinates at different imaginary time-points, $\{\mathbf{R}^N\}$ represents the molecular coordinates; P is now the discretization of the electron, M and m are respectively the molecular and electronic mass.

The next problem to be tackled is the evaluation of $Q(N, P, \beta)$ for the mixed quantum-classical system. It has been noticed in the past that the partition function in Eq. 3.17 is equivalent to the one of a purely classical system formed by a closed chain flexible polymer (or necklace) and N molecules. The potential field acting on this *isomorphic* classical system is given by Eqs. 3.18 and 3.19. This connection between the electron and the

necklace polymer is called "Classical Isomorphism".[11] The isomorphism becomes eventually exact when $P = \infty$.

Each bead of the isomorphic necklace, onto which the electron at a certain imaginary time has been mapped out, interacts with two adjacent beads through a harmonic potential of spring constant $Pm/2\beta^2$ and with the molecules. The latter interaction occurs through the electron-molecule pseudopotential scaled by P (second term in Eq. 3.18).

The "Classical Isomorphism" enables one to take full advantage of the classical theories of polyatomic fluids and the related simulation techniques to compute the physical properties of a quantum particle in a liquid. Both molecular dynamics and Monte Carlo simulations have shown to be able to sample the particle quantum paths.[13,5,52] This thesis will discuss only the latter approach to the problem.

3.2 The Monte Carlo Method

In the past, large use has been made of the Monte Carlo (MC)[2] method to simulate classical solids and liquids. A standard MC simulation samples the configurational space of a given many-body system in the canonical ensemble.

One can begin a more detailed discussion by looking at the canonical average on the (NvT) ensemble of an arbitrary quantity of interest A

$$\langle A \rangle = \frac{\int A \exp(-\beta U_N) d\mathbf{p}^N d\mathbf{r}^N}{\int \exp(-\beta U_N) d\mathbf{p}^N d\mathbf{r}^N}, \quad (3.20)$$

where U_N is the configurational energy, $\{p^N\}$ and $\{r^N\}$ are respectively the particles momentum and position coordinates. Since U_N is momentum independent, the integrals over dp^N in the numerator and denominator cancel out. Thus, one obtains

$$\langle A \rangle = \frac{\int A \exp(-\beta U_N) dr^N}{\int \exp(-\beta U_N) dr^N}. \quad (3.21)$$

The traditional MC method for many dimensional integrals, which samples the integral on a random grid of configuration space points, is not practical in this case. In fact, only certain physically accessible regions of the phase space contribute substantially to the integral in Eq. 3.21. This makes a random sampling of the phase space extremely inefficient.

The importance sampling MC method due to Metropolis et al.[53,54] uses another approach. It samples preferentially from the regions of the phase space which give the greatest contribution to the configurational integral in Eq. 3.21. This biased sampling is carried out picking up configurations according to a probability distribution Π corresponding to the canonical distribution. Here Π can be regarded as a vector of finite dimensionality in which the element Π_m gives the probability of occurrence of the m -th system with energy $U_N(m)$. The importance sampling algorithm uses the Boltzmann factor $\exp(-\beta U_N(m))$ as probability of the state m , namely

$$\Pi_m = \exp(-\beta U_N(m)). \quad (3.22)$$

The Metropolis algorithm is a procedure (series of stochastic processes) that, in the end, generates a sequence of systems distributed in

phase space according to the unique steady-state distribution Π . It can be shown that if each system of a stochastic sequence has probability of occurrence that depends only on the previously generated system, then after a sufficiently long chain the distribution of systems reaches a steady-state probability distribution. A stochastic process that satisfies those conditions is called a Markov chain.[55]

However, the process being a Markov chain *per se* does not assure its ergodicity. Different steady-state probability distributions can be reached from distinct initial conditions. The process of generating a sequence of systems becomes ergodic if the transition probability, $P_{n \rightarrow m}$, between two states in the chain, n and m , obeys the so-called "microscopic reversibility" (or "detailed balance") property

$$\Pi_m P_{n \rightarrow m} = \Pi_n P_{m \rightarrow n}. \quad (3.23)$$

In such a case, an unique steady-state distribution is approached irrespective of the form of Π .

The transition probability matrix for the systems generated in the chain is

$$P_{s \rightarrow s'} = P_{s \rightarrow s'}^* \min \left[1, \frac{\Pi_{s'} P_{s \rightarrow s'}^*}{\Pi_s P_{s' \rightarrow s}^*} \right], \quad (3.24)$$

where $P_{s \rightarrow s'}^*$ is an *a priori* transition probability matrix and the second factor is an acceptance probability.

The Markov chain generated according to the transition probability matrix in Eq. 3.24 converges to a steady-state distribution which coincides with the canonical distribution.

The biased sampling of the configurational space according to the distribution Π affects the way one does the average on the ensemble. Each equilibrium property of the system in the state m has to be weighted by the probability Π from which one samples. The integrals in Eq. 3.21 has to be substituted by a discrete sum over the N states generated by the MC sampling. Thus

$$\langle A \rangle \simeq \frac{\sum_m A(m) \exp(-\beta U_N(m)) / \Pi_m}{\sum_m \exp(-\beta U_N(m)) / \Pi_m} \quad (3.25)$$

If the expression of Π_m in Eq. 3.22 is substituted in Eq. 3.25, one obtains

$$\langle A \rangle \simeq \frac{1}{N} \sum_{m=1}^N A(m). \quad (3.26)$$

3.3 Classical Monte Carlo Simulations

Generally, classical MC simulations of liquids are carried out on systems composed of few hundreds atoms (or molecules) contained in a cubic box. To avoid surface effects, the so-called periodic boundary conditions are imposed in which the simulation box is periodically repeated in space along the three cartesian axes. For each particle which exits the box its reflected image enters from the opposite direction.

For a system composed of atoms, the *a priori* transition probability $P_{i \rightarrow j}^*$ corresponds to the displacement of a particle chosen at random from an initial position (X_0, Y_0, Z_0) to a final position X_t, Y_t, Z_t

$$X_t = X_0 + \xi_x X_{max}$$

$$\begin{aligned} Y_t &= Y_0 + \xi_y Y_{\max} \\ Z_t &= X_0 + \xi_z Z_{\max} \end{aligned} \quad (3.27)$$

where ξ_x, ξ_y, ξ_z are random numbers from $0 \rightarrow 1$, $X_{\max}, Y_{\max}, Z_{\max}$ are the maximum displacements of the particle allowed for each move.

It is obvious that in this case $P_{s \rightarrow s'}^* = P_{s' \rightarrow s}^*$, therefore the transition probability in Eq. 3.24 takes the simpler form

$$P_{s \rightarrow s'} = P_{s' \rightarrow s}^* \min[1, \exp(-\beta(U_N(s') - U_N(s)))] \quad (3.28)$$

where the expression of Π_s in Eq. 3.22 has been used.

Each move is accepted or rejected according to $\min[1, \frac{\Pi_{s'}}{\Pi_s}]$ which is sometime called the Metropolis function. In practise this means that when $U_N(s') < U_N(s)$ the move is accepted and when, instead, the reverse occurs the move is accepted with probability $\exp(-\beta(U_N(s') - U_N(s)))$. In the latter case a random number ξ between 0 to 1 is generated; if $\xi < \exp(-\beta(U_N(s') - U_N(s)))$ the move is accepted. If the move is finally rejected the configuration s is counted again in every average.

In case of molecular liquids, rotational degrees of freedom also have to be sampled by a MC simulation. Quaternions[56] are generally preferred to Euler angles to define the orientation of a molecule in space because they give rise to a rotation matrix of the molecule which is non-singular. The quaternions coordinates along with the molecular center of mass are moved according to rules similar to those specified previously for monoatomic systems.[57]

It is obvious that a particular choice of maximum coordinate displacement does not affect the final distribution. It alters, instead, the rate at which the moves are accepted and the velocity with which the steady-state probability distribution is reached.

A high acceptance rate can be achieved with small maximum displacements. Unfortunately, this brings to a slow convergence of the simulation since the phase space is sampled slowly. On the other hand, a large maximum displacement also leads to a slow sampling of the phase space, because of the low acceptance rate. It follows that an intermediate value of the acceptance rate is usually preferred. A typical value that maximizes the convergence of the simulation is $\sim 30 - 40\%$.

3.4 Path Integral Monte Carlo

So far only the application of the MC importance sampling method to classical systems has been discussed. Nevertheless, by exploiting the "Classical Isomorphism" examined in section 3.1.2, the MC technique can be employed to simulate quantum-classical systems. In accordance with Eq. 3.17, in these circumstances the probability distribution from which one has to sample is

$$\Pi = \exp \left(-\beta(V_{e-N} + V_{N-N}) \right). \quad (3.29)$$

Here V_{e-N} and V_{N-N} are respectively the contributions from the electron-molecule and molecule-molecule interactions to the average potential energy

of the system. Before discussing the problems that this type of simulations generates and how the difficulties can be overcome, it is opportune to examine the non obvious relation between the energies of the quantum particle and the isomorphic system.

While in quantum mechanics the energy of a particle is interpreted as the expectation value of the Hamiltonian operator evaluated in the occupied state, in statistical mechanics the energy has to be related to the partition function of the system. In particular, in the canonical ensemble the energy is given by

$$E = -\frac{\partial \ln Q}{\partial \beta} \quad (3.30)$$

If the path integral approximation of the partition function of a mixed quantum-classical system ($Q(N, P, \beta)$ in Eq. 3.17) is substituted in the above equation, one obtains the following energy estimator

$$E = \frac{3P}{2\beta} - \frac{Pm}{2\beta^2} \left\langle \sum_{s=1}^P (\mathbf{r}_s - \mathbf{r}_{s+1})^2 \right\rangle + \langle V_{e-N} \rangle + \langle V_{N-N} \rangle. \quad (3.31)$$

Consequently, the quantum particle kinetic energy is given by

$$K = \frac{3P}{2\beta} - \frac{Pm}{2\beta^2} \left\langle \sum_{s=1}^P (\mathbf{r}_s - \mathbf{r}_{s+1})^2 \right\rangle. \quad (3.32)$$

The above estimator is, however, not suitable to be used in a MC simulation. In fact, with large P values the kinetic energy is given by a sum of two large numbers of opposite sign. This brings a high numerical uncertainty on the average. Herman et al.[58] circumvented this problem showing that in the (NvT) ensemble

$$K = \frac{3}{2\beta} + \frac{1}{2P} \left\langle \sum_{s=1}^P \mathbf{r}_{s,P} \cdot \sum_{i=1}^N \frac{\partial V(\mathbf{r}_s - \mathbf{R}_i)}{\partial \mathbf{r}_s} \right\rangle, \quad (3.33)$$

where $r_{,P}$ stands for $r_s - r_P$. This expression for the kinetic energy is legitimate only if the external pressure acting on the quantum particle is zero.[10] The same authors showed that if $P \rightarrow \infty$ the mean square fluctuation in the kinetic energy given by Eq. 3.32 grows as $O(P)$, while the energy estimator in Eq. 3.33 is insensitive to P .

3.5 The Staging Algorithm

Due to the increase in strength of the harmonic spring that connects two adjacent beads, the Monte Carlo importance sampling of the isomorphic polymer chain becomes more inefficient when the number of beads in the chain increases. When P is big, moving a vertex of the polymer has very few chances to be accepted unless the associated maximum allowed displacement is very small. As mentioned previously, both a low acceptance rate and a slow sampling of the phase space produce an inadequate convergence of the simulation. Since P in the order of 10^3 is the usual number for an electron in polar liquids (see later in this section for details on how P is chosen), an alternative to the importance sampling must be found.

In the past, two approaches have been devised which partially solve the problem. In one case the standard Metropolis algorithm is substituted by a biased importance sampling.[12] An approximate transition probability is used to chose a new point in the path from the actual position and the position after the next imaginary time interval. Because of this, only moves

with a high probability of being accepted are actually attempted, while, at the same time, the phase space is sampled efficiently. This method has been used to study solid and liquid helium[12,14] and an excess electron in water[52] and rare gas liquids.[15] The other sampling method which has been used in the past is the so-called staging[59,60,5] and will be the one used throughout this thesis.

Before discussing this technique in detail, it is useful to specify what size of discretization is needed in order to adopt the high temperature approximation of the density matrix in a MC simulation of a solvated electron in ammonia.

3.5.1 The Choice of P

The average distance covered by a bead in the imaginary time $\tau = \frac{\beta}{P}$ in one direction is equal to

$$\begin{aligned}\Delta r &= v\tau \\ &= \lambda_T(1/P)^{\frac{1}{2}}\end{aligned}\tag{3.34}$$

where λ_T is the de Broglie wavelength. This average distance corresponds also to the average link length.

The high temperature approximation of the two body density matrix is valid if in Δr the potential acting on the bead does not change appreciably. For the type of electron-ammonia pseudopotential used in this thesis (see next chapter for details) the former condition is likely to be

satisfied when Δr is in the order of a_0 , the Bohr radius. Accordingly, the average MC move of each bead is of the same size as a_0 .

Since the average distance between two ammonia molecules in the liquid, $l = (V/N)^{1/3}$, is almost one order of magnitude larger than a_0 , it is evident that the significant phase space of the electron will be sampled very slowly. This argument is exactly equivalent to the one addressed at the beginning of this section.

It follows that what one really needs is an average MC move in the order of l and, at the same time, an average link length in the order of a_0 . These two, apparently, irreconcilable requirements can be composed by the staging algorithm.

3.5.2 Staging

The staging technique divides the polymer chain in two subsections. A primary chain composed of P_a beads and a series of P_a secondary chains of P_b beads inserted between each two adjacent primary chain beads. The primary chain is sampled using the Metropolis importance sampling algorithm while a direct sampling technique is used to handle the secondary chain.

Analytically, this means that V_{e-N} in Eq. 3.18 will be changed to

$$V_{e-N} = \sum_{s_a=1}^{P_a} \left\{ \sum_{s_b=0}^{P_b-1} \frac{m P_a P_b}{2\beta^2} (r_{s_a, s_b} - r_{s_a, s_b+1})^2 + \frac{1}{P_a P_b} \sum_{s_b=0}^{P_b-1} \sum_{i=1}^N V(|r_{s_a, s_b} - R_i|) \right\}, \quad (3.35)$$

where r_{s_a, s_b} is the position of the s_b -th bead of the secondary chain inserted

between s_a and $s_a + 1$, $r_{s_a} = r_{s_a,0}$ and $r_{s_a+1,0} = r_{s_a,P_b}$. It is convenient to write r_{s_a,s_b} as the sum of classical path between r_{s_a} and r_{s_b} and the deviation from it

$$r_{s_a,s_b} = r_{s_a,s_b}^d + \Delta r_{s_a,s_b}. \quad (3.36)$$

where

$$r_{s_a,s_b}^d = r_{s_a} + s_b(r_{s_a+1} - r_{s_a})/P_b \quad (3.37)$$

$$\Delta r_{s_a,0} = \Delta r_{s_a,P_b} = 0 \quad (3.38)$$

The first term in Eq. 3.35, say $V_{e--N}^{(1)}$, can be manipulated by the introduction of Eqs. 3.36 through 3.38. Finally, one obtains

$$V_{e--N}^{(1)} = \frac{mP_a}{2\beta^2} \sum_{s_a=1}^{P_a} (r_{s_a} - r_{s_a+1})^2 + \frac{mP_a P_b}{2\beta^2} \sum_{s_a=1}^{P_a} \sum_{s_b=1}^{P_b} (\Delta r_{s_a,s_b} - \Delta r_{s_a,s_b+1})^2. \quad (3.39)$$

The second term in Eq. 3.35, say $V_{e--N}^{(2)}$, can, instead, be approximated by the sum of two contributions, one deriving from the interactions amongst the secondary beads and the nearby molecules, the other from the interaction of the primary beads and the rest of the molecules, namely

$$V_{e--N}^{(2)} \simeq \frac{1}{P_a} \sum_{s_a=1}^{P_a} \sum_{\alpha} V(|r_{s_a} - R_{\alpha}|) + \frac{1}{P_a P_b} \sum_{s_a=1}^{P_a} \sum_{s_b=1}^{P_b} \sum_{\gamma} V(|r_{s_a,s_b} - R_{\gamma}|). \quad (3.40)$$

The sum over γ includes only the molecules which are close to the link associated with the vertices s_a and $s_a + 1$, while the index α runs over all the other molecules. Technically, for each link all the molecules inside an ellipsoid of volume Ω_b and centered on the two vertices of the link are

included in the secondary chain contribution to $V_{e--N}^{(2)}$. In other word, this signifies that the molecules farther away from the links see a necklace with less beads, while the ones closer feel the interaction with the full chain.

The real trick that makes the staging algorithm worth using is that now the Metropolis algorithm can be used for the primary chain beads while a direct sampling of the secondary chains is performed. It is therefore convenient to rearrange V_{e--N} in two contributions from the primary and secondary chains, namely

$$V_{e--N} \simeq V_{e--N}^a + V_{e--N}^b \quad (3.41)$$

$$V_{e--N}^a = \frac{mP_a}{2\beta^2} \sum_{s_a=1}^{P_a} (r_{s_a} - r_{s_a+1})^2 + \frac{1}{P_a} \sum_{s_a=1}^{P_a} \sum_{\alpha} V(|r_{s_a} - R_{\alpha}|) \quad (3.42)$$

$$V_{e--N}^b = \frac{mP_a P_b}{2\beta^2} \sum_{s_a=1}^{P_a} \sum_{s_b=1}^{P_b} (\Delta r_{s_a, s_b} - \Delta r_{s_a, s_b+1})^2 + \frac{1}{P_a P_b} \sum_{s_a=1}^{P_a} \sum_{s_b=1}^{P_b} \sum_{\gamma} V(|r_{s_a, s_b} - R_{\gamma}|). \quad (3.43)$$

For each link the direct sampling involves the evaluation of $\exp(-\beta V_{e--N}^b)$ for a fixed number of gaussianly distributed[61] secondary chain paths. The weight to the importance sampling function from the set of paths is

$$\Pi^D = \exp(-\beta \sum V_{e--N}^b), \quad (3.44)$$

where the sum in the exponential is over the paths. The total probability distribution from which one samples is therefore

$$\Pi^T = \Pi^M \Pi^D = \exp(-\beta V_{e--N}^a) \exp(-\beta \sum V_{e--N}^b). \quad (3.45)$$

Basically, the actual computational procedure associated with the staging algorithm consists of three steps. Firstly, a randomly chosen bead in the primary chain is moved according to Eq. 3.27. Secondly, the direct sampling weight from the two links affected by the move is recalculated. Finally, the move is accepted or rejected in conformity with Π^T in Eq. 3.45.

The staging algorithm not only affects the way one samples from the phase space associated with the quantum-solute, but also the computation of the average kinetic and potential energies. It is clear that contributions from the primary as well as secondary chains have to be included.

To conclude this section, it must be pointed out that the staging technique is a very good candidate for vectorization on modern supercomputers. In fact, the evaluation of each path of a secondary chain does not depend on the others in the set. For each primary chain link the direct sampling of the corresponding secondary chains can be done in a single shot on a vector machine.

3.6 Equilibrium Correlation Functions

What follows is a discussion of the various time independent correlation functions used throughout this thesis to probe the equilibrium structure of the systems studied.

Classical Liquids The most common way to discuss the structure of a liquid is to utilize the site-site correlation functions. One defines $g_{\alpha\beta}(r)$

as the density of sites of type α occurring at distance r from the site of type β normalized to the liquid average density ρ . In the computation of the distribution function only sites belonging to different molecules are included. The formal definition of $g_{\alpha\beta}(r)$ is given by

$$g_{\alpha\beta}(r) = \frac{1}{\rho^2} \left\langle \sum_{i=1}^N \sum_{j>i} \delta(\mathbf{r}_{i\alpha}) \delta(\mathbf{r}_{j\beta} - \mathbf{r}) \right\rangle. \quad (3.46)$$

Information on the atomic-pair correlation functions of liquids and solids can be gathered from neutron diffraction and X-rays experiments.

Electron To characterize the form of the quantum particle wavefunction and the structure of the nearby liquid molecules different correlation functions are commonly used. The functions utilized in this thesis are determined by including in the computation only statistics associated with the primary chain beads.

The electron center of mass site correlation function probes the radial distribution of the molecules in the surroundings of the electron and give some crude information on their orientation. It is defined as

$$g_{cm-\alpha}(r) = \frac{1}{\rho} \left\langle \sum_{n \in \alpha} \delta(\mathbf{r}_{cm}) \delta(\mathbf{r} - \mathbf{r}_n) \right\rangle, \quad (3.47)$$

where the sum runs over the sites α on the molecules and \mathbf{r}_{cm} is the center of mass of the P_A primary chain beads. The orientation of the molecules in the vicinity of the electron cloud is better described by calculating the electron c.m.-molecule dipole correlation function

$$P_{cm}(\theta) \propto \left\langle \sum_i \delta(\cos(\theta_{cm-i}) - \cos(\theta)) \right\rangle, \quad (3.48)$$

where

$$\cos(\theta_{cm-i}) = \frac{(\mathbf{R}_i - \mathbf{r}_{cm}) \cdot \mathbf{d}_i}{|\mathbf{R}_i - \mathbf{r}_{cm}| d_i}, \quad (3.49)$$

with \mathbf{R}_i and \mathbf{d}_i , respectively, the position vector of the center of mass of the solvent molecule with the index i and its dipole moment vector. The sum over the index i includes only those molecules in the vicinity of the electron c.m. belonging to a given solvation shell.

Some insights on the spatial extension and the nature of the electron state are provided by the complex time correlation function defined as [62,63,64]

$$\mathcal{R}^2(\tau) = \frac{1}{P_A} \left\langle \sum_i |\mathbf{r}(\tau_i + \tau) - \mathbf{r}(\tau_i)| \right\rangle, \quad (3.50)$$

where the sum is extended to all the contributions from the electron at imaginary times differing from each other by τ , multiple of β/P_A .

Electron excitation energies large compared to β^{-1} are a sign of dominance of the ground state in the electron wavefunction. It can be shown [11,13] that for small τ 's with the exception of $\tau = 0$, the deviation of $\mathcal{R}^2(\tau)$ from its maximum value at $\tau = \beta/2$ is proportional to

$$\begin{aligned} \Delta \mathcal{R}^2(\tau) &= \mathcal{R}^2(\tau) - \mathcal{R}^2(\beta/2) \\ &\propto \left\langle \mathcal{R}_{01}^2 \exp \left[-\frac{\beta(E_0 + E_1)}{2} \right] \right. \\ &\quad \times \left. \exp [(E_0 - E_1)\tau - \beta/2] - 1 \right\rangle, \end{aligned} \quad (3.51)$$

where E_0 and E_1 are respectively the electron ground state and first excited state energy. \mathcal{R}_{01}^2 is the matrix element

$$\mathcal{R}_{01}^2 = \int d\mathbf{r} \int d\mathbf{r}' \Psi_0(\mathbf{r}) \Psi_1^*(\mathbf{r}) |\mathbf{r} - \mathbf{r}'|^2 \Psi_0^*(\mathbf{r}') \Psi_1(\mathbf{r}'), \quad (3.52)$$

where $\Psi_0(\mathbf{r})$ and $\Psi_1(\mathbf{r})$ are the respective electron wavefunctions. It must be pointed out that \mathcal{R}_{01} is proportional to the electron dipole moment for the transition $0 \rightarrow 1$. Additionally, at larger τ values $\mathcal{R}^2(\tau)$ reaches a plateau value given by

$$\mathcal{R}^2(\tau) \propto \langle \mathcal{R}_{00}^2 \exp(-\beta E) \rangle. \quad (3.53)$$

The complex time correlation function for a free electron shows a strikingly different behaviour. In fact, \mathcal{R}_{free} has a parabolic dependence on τ according to

$$\mathcal{R}_{free}(\tau) = \frac{\lambda_T}{\beta} [3\tau(\beta - \tau)]^{1/2}. \quad (3.54)$$

Moreover, at $\tau = \beta/2$ Eq. 3.54 provides an useful relation between λ_T and the electron correlation length $\mathcal{R}(\beta/2)$. One obtains

$$\mathcal{R}(\beta/2) = \frac{\sqrt{3}}{2} \lambda_T. \quad (3.55)$$

To conclude, two aspects of $\mathcal{R}(\tau)$ reveal the nature of the electron state. An initial rapid rise with τ followed by a nearly constant region signals that the electron is in a compact state and the ground state is dominant. On the contrary, a parabolic dependence implies an extended electron state.

Atoms In the discussion regarding the solvation of atoms in ammonia two additional distribution functions will be used to analyze the results.

The first is the electron-ion correlation function

$$g_a(r) = \frac{1}{\rho} \left\langle \sum_{n \in \alpha} \sum_{s=1}^{P_A} \delta(\mathbf{r}_s) \delta(\mathbf{r} - \mathbf{r}_n) \right\rangle, \quad (3.56)$$

where \mathbf{r}_s is the position of the s -th primary chain bead. The second correlation function is the ion-molecule dipole correlation function which characterizes the orientation of the molecules around the positive ion. It is defined in a similar way as $P_{cm}(\theta)$, namely

$$P_X(\theta) \propto \left\langle \sum_i \delta(\cos(\theta_{X-i}) - \cos(\theta)) \right\rangle, \quad (3.57)$$

where

$$\cos(\theta_{X-i}) = \frac{(\mathbf{R}_i - \mathbf{r}_X) \cdot \mathbf{d}_i}{|\mathbf{R}_i - \mathbf{r}_X| d_i}, \quad (3.58)$$

with \mathbf{r}_X the position of the ion X .

Chapter 4

The Solvated Electron in Liquid Ammonia at Constant Pressure

In the past, path integral Monte Carlo (PIMC) simulations which used the staging algorithm have been performed on an excess electron in liquid ammonia.[5,65] The electron was found to produce a hole in the solvent and become self-trapped in it in a rather compact (localized) state. Since the simulation was carried out in the (NvT) ensemble, no theoretical estimate of the experimental partial molar volume was given. This chapter describes a PIMC simulation carried out in the (NpT) ensemble which enabled the calculation of the liquid ammonia volume expansion produced by the localized electron.

4.1 Potentials

The intermolecular potential used for ammonia in Ref. [5,65] is composed of an electrostatic simple point charge type potential and a N-N Lennard-Jones interaction. The ammonia molecule is assumed to have a C_{3v} symmetry with hydrogens placed at 1.0126 Å from the nitrogen. The angle between two N-H bonds is 106.72 degrees. The electrostatic potential consists of charges distributed in four sites on the molecule: $Q^+ = 0.485$ on the hydrogens and $Q^- = -1.455$ on a site 0.156 Å from the nitrogen along the C_{3v} axis. This charge distribution reproduces the experimental dipole moment of $\mu = 1.47D$. The additional atom-atom interaction center is placed on the nitrogen with $\epsilon = 1.16 \text{ KJ mol}^{-1}$ and $\sigma = 3.40 \text{ Å}$.

This potential was obtained from a fit of the set of parameters to the physical properties of liquid ammonia. It must be pointed out that this potential model does not include explicitly polarizability interactions many-body effects. They are taken into account only in an "effective" way.

It has been shown in Chapter 2 that the electron-molecule pseudopotential can be written as

$$V_{ps}(\mathbf{r}) = V_C(\mathbf{r}) + V_E(\mathbf{r}) + V_P(\mathbf{r}) + V_R(\mathbf{r}). \quad (4.1)$$

There seems to be agreement that for the similar case of an electron-water pseudopotential the dominant contribution is provided by the electrostatic term V_C . It was shown in Ref. [66] that $\langle V_E(\mathbf{r}) \rangle$ is negative, while $\langle V_P(\mathbf{r}) \rangle$ and $\langle V_R(\mathbf{r}) \rangle$ are positive. Moreover, the sum of the positive contributions

to $V_{ps}(r)$ tends to cancel out $V_E(r)$. A more serious error may arise in the estimate of the electron kinetic energy where the first derivative of the pseudopotential is employed (see Eq. 3.33).

Since at the present time there is no reliable model potential that includes all the terms in Eq. 4.1, the pseudopotential used in this thesis includes only the electrostatic contribution and neglects all the others.

A purely electrostatic pseudopotential possesses a singularity at the origin. In the presence of singularities the direct sampling of the secondary chain experiences crucial attrition problems. Moreover, a large discretization of the electron polymer may be needed for the high temperature approximation of the imaginary time propagator to hold.

To eliminate these problems, the Coulombic potential can be replaced by a quantum effective pair potential which in the past, has been used in Plasma Physics.[67] Here the interaction between the site α on a given ammonia molecule and the electron is given by

$$V_{e-\alpha}(|r - R_\alpha|) = -\frac{Q_\alpha e^2}{|r - R_\alpha|} \left\{ 1 - \exp \left[-\frac{(2\pi P)^{\frac{1}{2}}}{\lambda_T} |r - R_\alpha| \right] \right\}, \quad (4.2)$$

where Q_α is the fractional charge placed on the α -th site of the molecule positioned at R_α and e is the electronic charge. The quantum effective potential in Eq. 4.2 arises as a direct consequence of the diffraction effects due to the uncertainty principle.

Although, the regularized Coulombic potential is adequate for the repulsive interaction between electron and nitrogen, it does not work as well for the attractive interactions. Since the electron and the molecular

eigenfunctions have to be orthogonal to each other, the probability of finding the excess electron located on the hydrogen of the ammonia molecule must be very low. Because of the deep minima on the hydrogens, such a requirement cannot be fulfilled when the quantum effective potential in Eq. 4.2 is utilized.

A way to get around the problem is to use a model potential like those widely used in the past in band structure calculations of metals. Shaw[68] proposed the following pseudopotential

$$\begin{aligned} V_{e-H} &= -Q_H e^2 / |r - R_H| & |r - R_H| \geq R_c \\ V_{e-H} &= -Q_H e^2 / R_c & |r - R_H| < R_c. \end{aligned} \quad (4.3)$$

A similar model pseudopotential was used by Parrinello and Rahman[3] in a path integral simulation of an F center in molten KCl to handle the interactions between the polymer chain and the potassium ion. The choice of R_c for the electron-hydrogen interaction is somewhat arbitrary. $R_c = 1$ Å was used throughout this thesis.

4.2 Path Integral Monte Carlo at Constant Pressure

Following McDonald,[69] the average of a classical dynamical variable in the canonical ensemble at constant pressure can be derived from Eq. 3.21 by adding a pressure dependent energy term to the total energy of the system

and averaging over all possible molar volumes. Thus one obtains

$$\langle A \rangle = \frac{\int_0^\infty dv \exp(-\beta pv) \int_v A(\mathbf{R}^N, v) \exp[-\beta U_N(\mathbf{R}^N, v)] d\mathbf{R}^N}{\int_0^\infty dv \exp(-\beta pv) \int_v \exp[-\beta U_N(\mathbf{R}^N, v)] d\mathbf{R}^N}. \quad (4.4)$$

The integral over the variable v has to be evaluated for a constant shape of the volume enclosing the particles. In a MC simulation the volume must be sampled as well as the particle coordinates. To do so a new set of particle coordinates has to be introduced to provide an explicit dependence on the volume in the second integrals. This set of coordinates is defined by

$$\alpha_i = L^{-1} \mathbf{R}_i \quad (4.5)$$

where L is the edge of the cubic simulation box in which all the particles are contained. The range of the coordinates $\{\alpha^N\}$ goes from zero to one.

If the $\{\alpha^N\}$ is substituted in Eq. 4.4, one obtains

$$\langle A \rangle = \frac{\int_0^\infty dv \exp(-\beta pv) v^N \int_w A([L\alpha]^N, v) \exp[-\beta U_N([L\alpha]^N, v)] d\alpha^N}{\int_0^\infty dv \exp(-\beta pv) v^N \int_w \exp[-\beta U_N([L\alpha]^N, v)] d\alpha^N}, \quad (4.6)$$

where the integrals over $\{\alpha^N\}$ are restricted to an unitary cube w . In conformity with Eq. 4.6 the phase space of the system in the (NpT) ensemble has to be sampled by a MC simulation according to the probability

$$\exp(-\beta pv - \beta U_N + N \ln v) \quad (4.7)$$

Although the Metropolis importance sampling algorithm can be easily adapted to sample the phase space of a classical system in the (NpT)

ensemble,[69] the extension to the quantum-classical system is not conceptually straightforward.

Quite intuitively, one can say that the fluctuations in the volume of the simulation box do not produce modification in the electron wavefunction if the electron is localized in a region small compared to the size of the box. Indeed, only in this case the system satisfies the quantum mechanical virial theorem[10]

$$\langle KE \rangle = -\frac{1}{2}\langle PE \rangle, \quad (4.8)$$

where KE and PE stand respectively for kinetic and potential energy. It becomes evident that the isomorphic chain need not be affected by changes in the volume if $L \gg \lambda_T$.

To find some support to the last statement one must concentrate on the partition function of the mixed quantum-classical system in the (NpT) ensemble. To simplify the algebra of the calculations, the potential field produced by the N molecules and acting on the i -th electron bead with coordinate \mathbf{r}_i will be represented by $\phi(\mathbf{r}_i)$. Thus, from Eq. 4.6 and 3.17 the partition function of the electron moving in this potential field can be written as

$$Q(P, \beta) = \int_0^\infty dv \exp(-\beta pv) \int_v d\mathbf{r}_1 d\mathbf{r}_2 \cdots d\mathbf{r}_P \exp(-\beta S_{eff}), \quad (4.9)$$

where

$$S_{eff} = \frac{P}{2m\beta^2} \sum_{i=1}^P (\mathbf{r}_i - \mathbf{r}_{i+1})^2 + \frac{1}{P} \sum_{i=1}^P \phi(\mathbf{r}_i). \quad (4.10)$$

At this point, it is useful to introduce a new set of electron coordinates

relative to the center of mass of the beads, namely

$$\begin{aligned}
 \mathbf{r}_{cm} &= \frac{1}{P} \sum_i^P \mathbf{r}_i \\
 \mathbf{r}'_1 &= \mathbf{r}_1 - \mathbf{r}_{cm} \\
 \mathbf{r}'_2 &= \mathbf{r}_2 - \mathbf{r}_{cm} \\
 &\vdots \\
 \mathbf{r}'_{P-1} &= \mathbf{r}_{P-1} - \mathbf{r}_{cm} \\
 \mathbf{r}'_P &= \mathbf{r}_P - \mathbf{r}_{cm}.
 \end{aligned} \tag{4.11}$$

Instead of integrating over the original P coordinates, one can now integrate over \mathbf{r}_{cm} and $\mathbf{r}'_1, \mathbf{r}'_2, \dots, \mathbf{r}'_{P-1}$ (note that \mathbf{r}'_P is linearly dependent on the $P-1$ bead coordinates and the center of mass, i.e., $\mathbf{r}'_P = -\sum_i^P \mathbf{r}'_i$). It follows that Eq. 4.9 can be rewritten

$$\begin{aligned}
 Q(P, \beta) &= \int_0^\infty dv \exp(-\beta pv) \int_v d\mathbf{r}_{cm} d\mathbf{r}'_1 d\mathbf{r}'_2 \cdots d\mathbf{r}'_{P-1} \\
 &\times \exp[-\beta S_{eff}(\mathbf{r}'^{P-1}, \mathbf{r}_{cm})].
 \end{aligned} \tag{4.12}$$

When the electron is localized in a cavity inside the solvent, the integrals over $\mathbf{r}'_1, \mathbf{r}'_2, \dots, \mathbf{r}'_{P-1}$ in Eq. 4.12 decay very rapidly outside this region. Consequently, when the dimensions of the electron necklace are small compared to the simulation box, these integrals need not be extended to the entire volume, but only to a restricted region of space enclosing the cavity. Thus, the partition function is now given by

$$\begin{aligned}
 Q(P, \beta) &= \int_0^\infty dv \exp(-\beta pv) \int_v d\mathbf{r}_{cm} \int_{v'} d\mathbf{r}'_1 d\mathbf{r}'_2 \cdots d\mathbf{r}'_{P-1} \\
 &\times \exp[-\beta S_{eff}(\mathbf{r}'^{P-1}, \mathbf{r}_{cm})].
 \end{aligned} \tag{4.13}$$

Here the dimension of v' are in the order of the electron wavefunction and $v' < v$. The integral over the center of mass of the electronic charge, namely \mathbf{r}_{cm} , must be extended to the simulation box volume, v .

Using volume scaled coordinates, the partition function in Eq. 4.13 can now be rearranged in the same fashion as for classical systems, but now the only coordinate to be scaled by the volume is $\mathbf{r}_{cm} = L \cdot \alpha_{cm}$. Thus

$$Q(P, \beta) = \int_0^\infty dv \exp(-\beta p v) v \int_w d\alpha_{cm} \int_{v'} d\mathbf{r}'_1 d\mathbf{r}'_2 \cdots d\mathbf{r}'_{P-1} \\ \times \exp[-\beta S_{eff}(\mathbf{r}'^{P-1}, L\alpha_{cm})], \quad (4.14)$$

where w is the unitary box. Combining Eqs. 4.14 and 4.7, it is now possible to write down the probability distribution from which to sample in a PIMC simulation at constant pressure

$$\Pi = \exp(-\beta p v - \beta(S_{eff} + U_N) + (N+1)\ln v). \quad (4.15)$$

In conclusion, the partition function in Eq. 4.14 and the probability density in Eq. 4.15 imply that each time the volume is changed only the coordinates of the molecules and electron polymer center of mass are to be scaled with it, while the position of each individual bead relative to \mathbf{r}_{cm} is kept fixed.

4.3 Simulation Details and Results

It is advantageous to the general discussion to report in some detail the results from the constant volume simulation. Such a calculation was repeated in this thesis in order to produce an equilibrated electron-ammonia

configuration which in turn was used as a starting point in the constant pressure calculation.

4.3.1 Simulations in the (NvT) Ensemble

Simulation of the Fluid Initially, a classical MC simulation of the liquid at constant volume was carried out in order to obtain an equilibrated configuration of ammonia molecules in which to introduce the electron. The simulation was performed at the same conditions of temperature and density as in Refs. [5] and [65]. To summarize, $T = 260$ K, $N = 250$, $V = 25.3 \text{ cm}^3 \text{ mol}^{-1}$. Cubic periodic boundary conditions were applied to the molecules center of mass in the simulation box to eliminate surface effects. At the beginning of the simulation, the ammonia molecules were arranged on a body center cubic lattice and given random orientation.

In this classical simulation a MC pass was defined as a sequence of trial moves of randomly chosen ammonia molecules. The length of this sequence equalled the number of molecules in the simulation box. Each move of an ammonia molecule involved translation of the molecular center of mass and rotation of the molecular inertial frame using quaternions.

The maximum allowed move for the coordinates was set to 0.1 \AA for the molecular center of mass and to 0.01 for the quaternions.[57] With such choices the overall acceptance rate was about 40 % for all the simulations.

After 2000 passes of equilibration, in which the potential energy settled to a steady value, averages were accumulated for 5000 more passes. In

the simulation conditions the ammonia was liquid. The calculated average potential energy and pair correlation function are in agreement with the previous MD and MC calculations done with the same model potential. In Fig. 4.1 the calculated and experimental nitrogen-nitrogen pair correlation function are compared. These functions show that the simple point charge potential is able to reproduce correctly the structural features of the liquid ammonia. From the integration of the calculated nitrogen-nitrogen correlation function it was found that each ammonia molecule is surrounded by 12 nearest neighbours.

Solvated Electron The number of beads in the primary and secondary chains used to simulate the electron were respectively $P_a = 128$ and $P_b = 8$ with a total discretization $P = P_a P_b = 1024$. Each time an attempted move of the primary chain was performed 25 molecules were moved as well. A PIMC pass consisted of the attempted move of all the primary chain beads and of $25 \times P_a$ ammonia molecules. The maximum allowed displacement of the primary chain beads was set to 0.1 \AA in order to achieve an acceptance rate for the polymer motion of about 30 %. The change in coordinates of a primary bead involved the recalculation of the secondary chain contributions from the two links connecting the two adjacent beads. One hundred secondary chains were included in the direct sampling. The ellipsoidal map around each link was defined by a first axis which coincides with the link and a second axis of 1.3 \AA .

A compact isomorphic electron polymer was inserted in an equili-

brated liquid ammonia configuration. Initially, the beads of the primary chain were randomly arranged to give a correlation length $\mathcal{R}(\beta/2) = 2$ Å. The molecules were moved to rearrange themselves around the electron chain for 100 passes. Then the concurrent sampling of the molecules and isomorphous polymer was initiated:

Initially, the simulation was carried out for 500 passes to equilibrate the system. During this period the electron expanded its size to reach a correlation length of 4.0 Å; its potential energy decreased to $-120 k_B T$ from $-30 k_B T$. The configurational energy of the liquid defined in Eq. 3.17 stabilized around $-18.40 \text{ KJ mol}^{-1}$, 0.40 KJ higher than the energy of the pure liquid.

Subsequently, the simulation was run on for 1000 more passes and averages accumulated. Partial averages of the potential and kinetic energies were recorded to monitor the convergence of the simulation. At the end of the run the energies oscillated steadily around the mean values.

The results of the simulation were similar to those in Ref. [65]. The electron was localized in a solvent cavity and its correlation length was $\mathcal{R}(\beta/2) = 4.01 \pm 0.02$ Å. In Fig. 4.2 the electron center of mass-ammonia pair correlation functions are reported. The scarcity of structural features in the two functions is primarily due to the quantum nature of the electron. This in turn is in agreement with the highly structured shape of the pair correlation functions of classical ion in polar solvents. As shown in a paper by Schnitker et al.[13] on an excess electron solvated in water, an increase

in discretization produces the disappearance of strong correlation between electron and molecules.

In Fig. 4.2 the (cm-N) curve is the more structured of the two. It presents a first peak at 3.9 Å and a weak second peak at 6.9 Å. By integration over r from the origin to the first minimum at 5.6 Å, it was found that there are 15 ammonia molecules in the first solvation sheath of the electron. In contrast the (cm-H) curve shows only one weak peak at 3.9 Å as (cm-N). The number of hydrogens in the first electron solvation shell, calculated from (cm-H) is consistent with the preceding result.

It must be pointed out that the electron c.m.-ammonia pair correlation functions calculated in Ref. [5] with a purely coulombic pseudopotential differ from the ones in this thesis for the position of the peaks which are closer to the origin (first peak at 2.9 Å, second at 5.5 Å) and for the number of ammonia molecules coordinated to the electron, 9 opposed to 15. This seems to indicate that the effect of the Shaw type pseudopotential is to produce an electron less localized inside the cavity and more diffuse onto the molecules of the first solvation sheath.

The electron dipole correlation function is plotted in Fig. 4.3. The ammonia molecules in the vicinity of the electron are on average bond oriented toward the electron center of mass. This is shown by the peak in the dipole correlation function at $\cos \theta = 0.65$ associated with an angle of 130 degree, close to 112 the angle between the oriented molecular axis and the NH bonds. Only the ammonia molecules within $r = 5.0$ Å from the

electron center of mass were included in the calculation of the curve. This cut-off in the $P_{cm}(\theta)$ defines the electron first solvation shell.

4.3.2 Simulations in the (NpT) Ensemble

In both the classical and quantum MC calculations performed in this study the volume was sampled by varying the cubic box edge L according to

$$L' = L + \xi_L l_0, \quad (4.16)$$

where ξ_L is a random number between 0 and 1 and l_0 is the maximum allowed change in L . In both the types of simulations a change in L was attempted after the position of the particles in the box had changed significantly.

Liquid Ammonia at Constant Pressure At first, a simulation of the pure fluid at $T = 260K$, $N = 250$ and at a pressure such as to reproduce the liquid ammonia molar volume of $25.3 \text{ cm}^3 \text{ mol}^{-1}$ was carried out. A classical MC pass consisted of the attempted move of 25 times the totality of the molecules and once the box edge L . The maximum displacements for the molecular coordinates were kept at the same value set in the preceeding calculation at constant volume while l_0 in Eq. 4.16 was chosen equal to 0.45 \AA to give a volume acceptance rate of 35 %. The calculation was started from an equilibrated configuration of ammonia molecules obtained at constant volume. It was found, after several attempts, that a pressure of

500 bars was needed to secure a molar volume of $25.26 \pm 0.02 \text{ cm}^3 \text{ mol}^{-1}$. The error was estimated in the usual way by looking at the subaverages.

After about 3000 MC passes the simulation converged following a standard equilibration run of 1000 passes. As was expected, the $g_{N-N}(r)$ did not show any significant variation with respect to the constant volume calculation. In addition, the fluid potential energy was very close to the preceeding calculation, $-18.82 \text{ KJ mol}^{-1}$ compared with $-18.80 \text{ KJ mol}^{-1}$

Solvated Electron at Constant Pressure The quantum simulation was initiated from a configuration taken from the constant volume calculation. A MC pass involved the attempted move of all the beads in the electron polymer chain along with 25 times the totality of the molecules and once the box edge L . The maximum cell move was the same as in the simulation of the pure fluid and brought a similar acceptance rate. For few hundred passes the molecules and the box were allowed to equilibrate at $p = 500$ bars around the beads which were left untouched. Subsequently the full sampling of the electron path, ammonia molecules and volume was started.

The convergence of the PIMC simulation was monitored by examining the box edge and the system total energy every few hundreds passes. These variables were found to be sufficiently stationary after a total of 1700 passes. In Fig. 4.4 four volume subaverages at different passes of the simulation are plotted. The average volume of the simulation box was 10622

$\pm 5 \text{ \AA}^3$.

At the end of the run the structure of the solvated electron was examined and compared to the results obtained in the previous calculation at constant volume. The electron wavefunction is slightly more expanded while the structure of the molecules around the electron does not change significantly. The complex time correlation functions $\mathcal{R}(t - t')$ for the two calculations are plotted in Fig. 4.5 The correlation length at constant pressure is 4.15 \AA which compare with 4.01 \AA of the other calculation. In Fig. 4.6 the (cm-H) and (cm-N) pair correlation functions are reported. There are no significant differences between these curves and the ones at constant volume in Fig. 4.2.

4.3.3 Partial Volume of Electron Solvation

Finally, from the results of the above sections one can calculate the relative expansion of the liquid produced by the electron. The calculated expansion of the box is

$$\Delta V_{box}(calc) = 119 \pm 10 \text{ \AA}^3. \quad (4.17)$$

The experimental molar volume of the solvated electron is affected by a large uncertainty. In fact, it is derived from the partial molar volume of very dilute metal-ammonia solution and an evaluation of the volume change produced by the metal cation in solution. At present the commonly accepted experimental estimate of the electron molar volume is [70]

$$\Delta V(exp) = 100 \text{ cm}^3 \text{ mol}^{-1}, \quad (4.18)$$

which compares to the result from this simulation

$$\Delta V(\text{calc}) = 71 \pm 6 \text{ cm}^3 \text{ mol}^{-1}, \quad (4.19)$$

derived from Eq. 4.17.

With the high uncertainty of the experimental molar volume borne in mind and in spite of the unsophisticated model potential for the electron-ammonia interactions, the agreement between experiment and calculation is satisfactory. However, a more sophisticated pseudopotential, perhaps including polarization, could very likely improve this agreement.

Another factor that could affect the simulation's result is the handling of long range electrostatic interactions by a spherical cut-off. However, due to the electron spatial localization in the solvent, this aspect is thought to be of minor importance with regard to the relative volume expansion.

For later reference, it must be pointed out that the quantum simulation at constant pressure described in this chapter was about 4 times more time consuming than the one at constant volume, totalling 12 hours of Cyber 205 CPU time.

Figure 4.1:

Nitrogen-nitrogen pair correlation function calculated (continuous line) and from x-ray diffraction (dashed line).

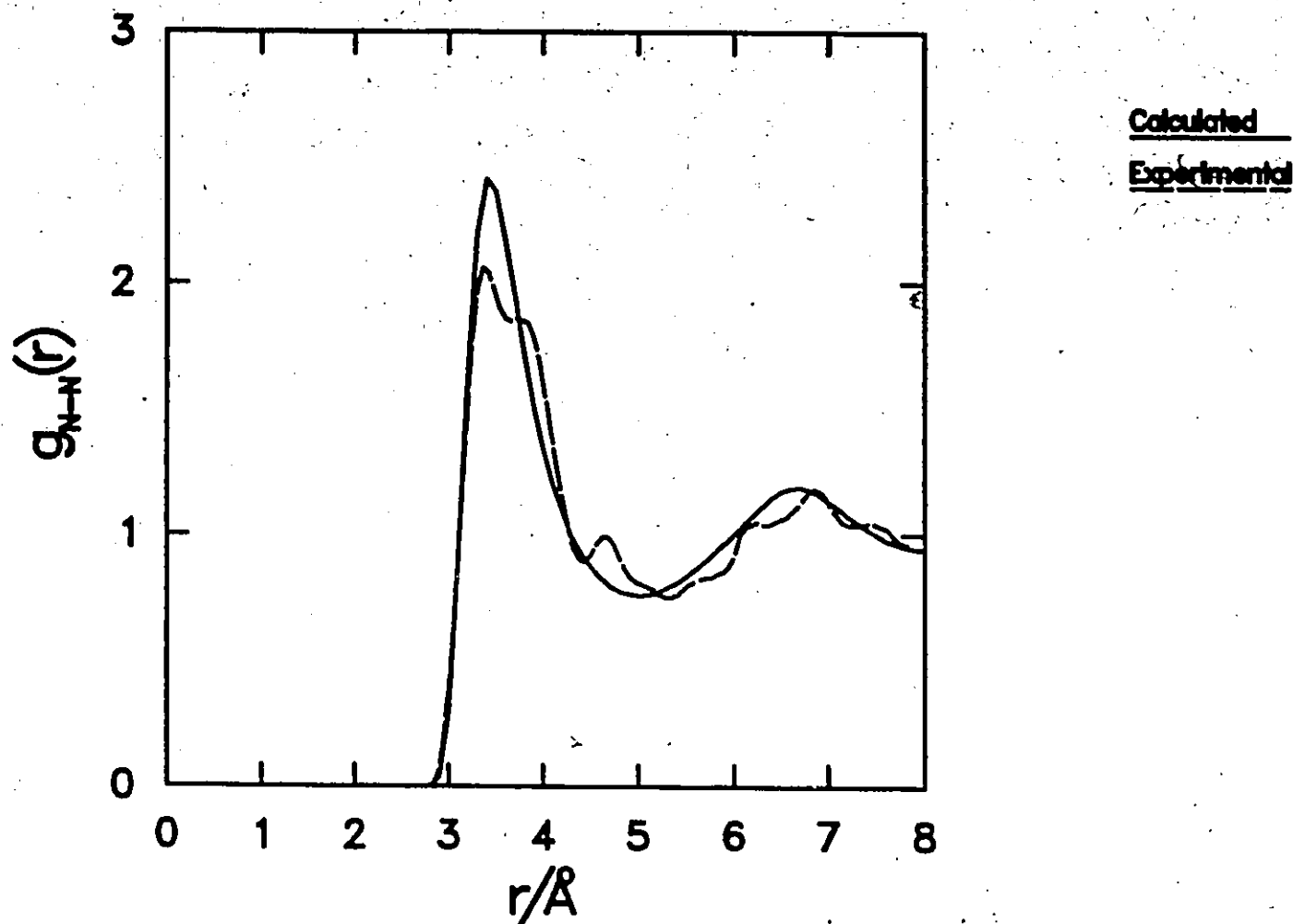


Figure 4.2:

From top to bottom, (cm-H) and (cm-N) pair distribution functions for an excess electron in liquid ammonia at constant volume.

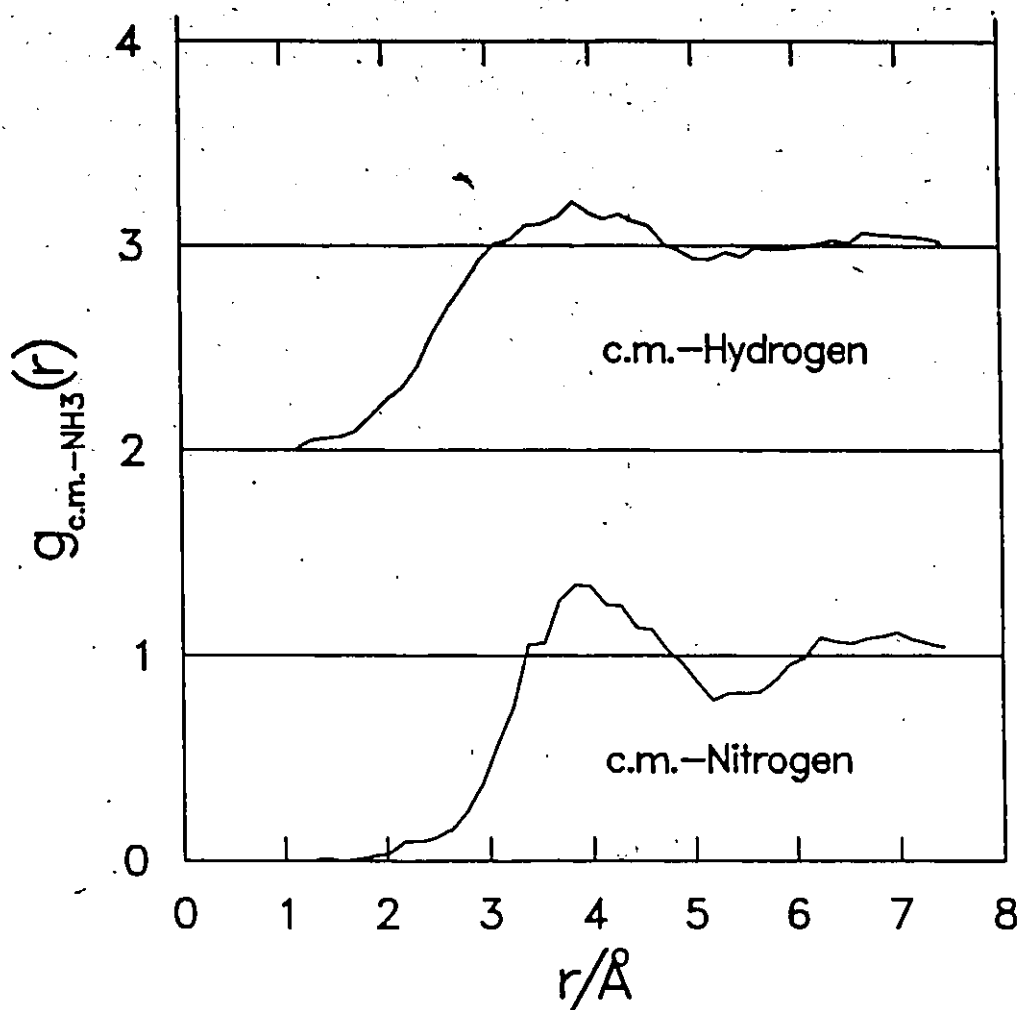


Figure 4.3:

Dipole correlation function for the electron center of mass.

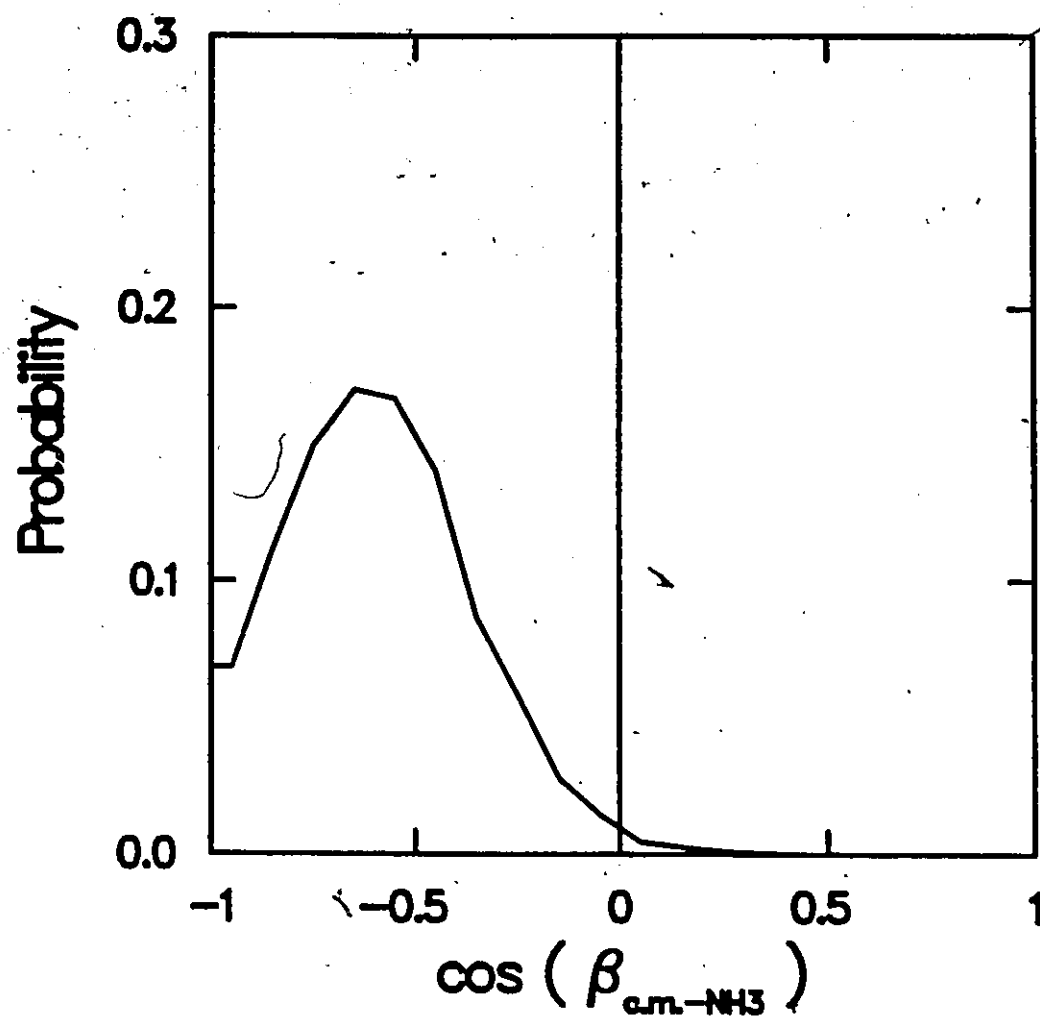


Figure 4.4:

Subaverages of the simulation box edge length, c , at different MC passes.

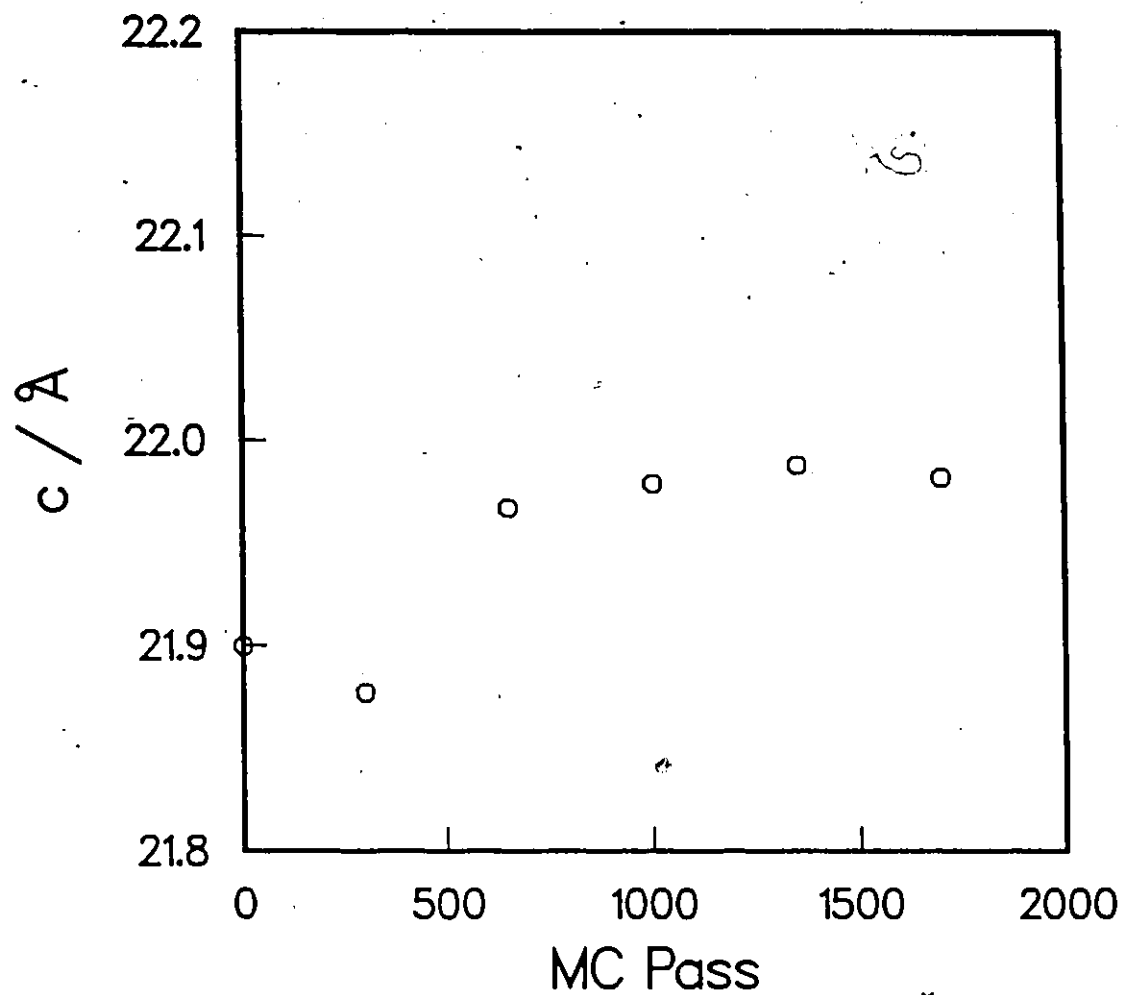


Figure 4.5:

Complex time correlation function for the solvated electron at constant pressure and at constant volume in liquid ammonia.

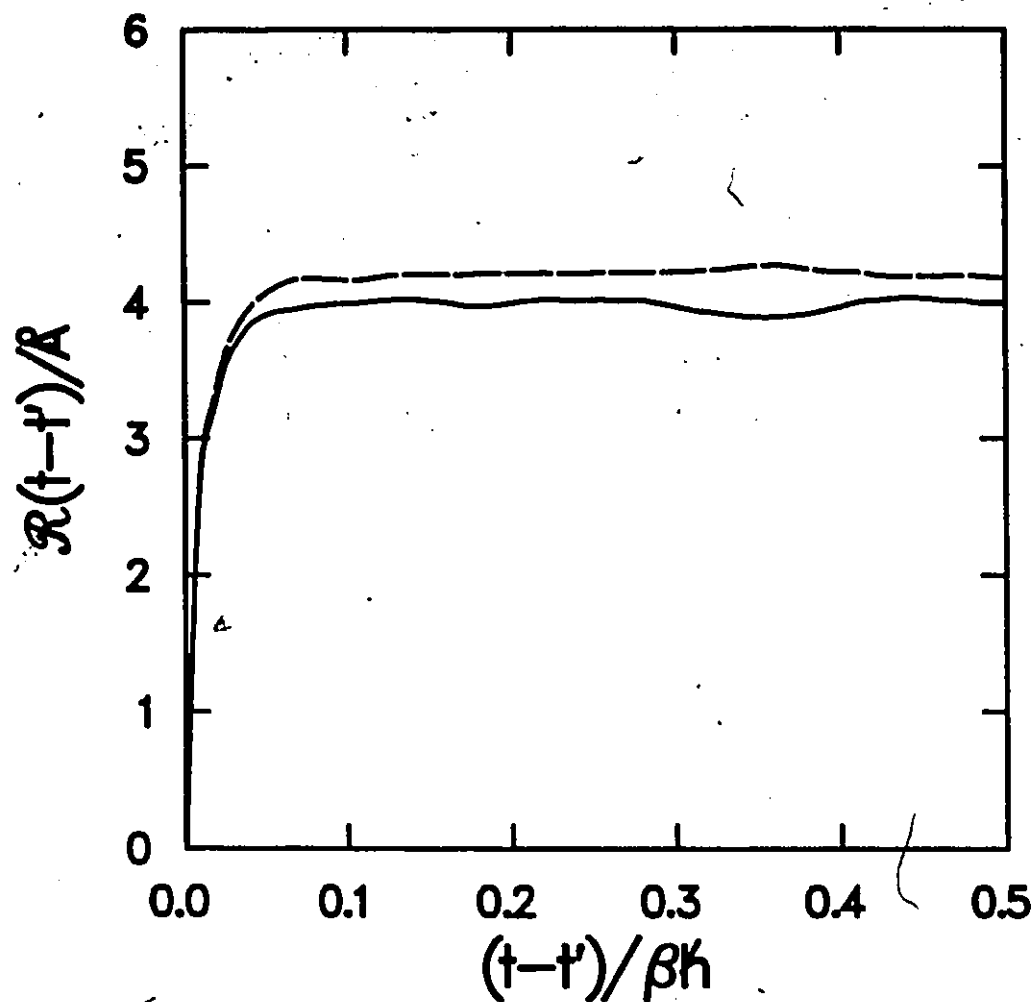
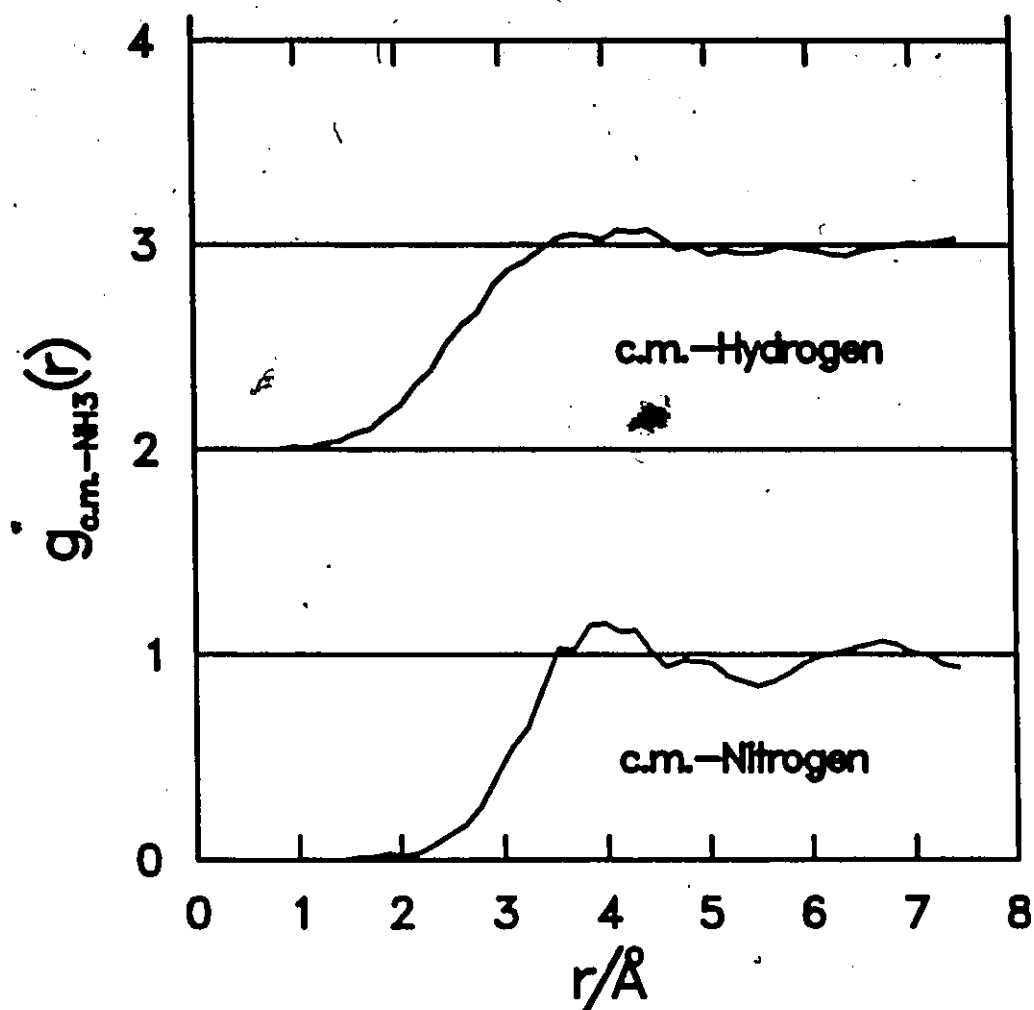


Figure 4.6:

Distribution functions at constant pressure for the solvent hydrogen and nitrogen atoms with respect to the electron center of mass.



Chapter 5

Free Energy of Electron Solvation in Liquid Ammonia

5.1 Free Energy from MC Simulations

The partition function and the free energy of a system composed of N interacting classical particles can be calculated by observing [71,72] that

$$\frac{v^N}{Q} = \frac{\int \exp(-\beta U_N) \exp(+\beta U_N) d\mathbf{R}^N}{\int \exp(-\beta U_N) d\mathbf{R}^N}, \quad (5.1)$$

and

$$Q = v^N \langle \exp(\beta U_N) \rangle^{-1}. \quad (5.2)$$

In principle, the above canonical average can be estimated by a conventional MC simulation. [71,73] Unfortunately, since $\exp(\beta U_N)$ increases very rapidly with an increase in U_N , a Metropolis MC calculation, which samples

the most physically important regions of the phase space, will not be able to give appropriate weight to those regions of high configurational energy (U_N) not physically likely to be reached. For the usual statistical systems, this limitation makes impossible the evaluation of the free energy from Eq. 5.2.

Notwithstanding this fact, in the past few years more successful free energy methods have been devised. All these methods calculate the difference in free energy between a reference state of known free energy and the state of interest. For example, the *thermodynamic integration method*[74,75] requires that the two systems be connected by a reversible path, defined by some continuous parameter. Generally, this involves carrying out a MC simulation for each point of a chosen grid along the path. On the other hand, methods such as the *energy distribution technique*[76,77,78] and the *acceptance ratio method*[79,80,78] are able, in principle, to estimate the free energy difference without using intermediate stages. Nevertheless, calculations in the past have shown that multistaging is always a necessity when studying systems of physical interest.[76,77,78] It is instructive at this point to elucidate the differences amongst the above free energy methods.

i The *acceptance ratio method* was first introduced by Bennet.[79] It exploits the following property of the Metropolis sampling function

$$\frac{M(x)}{M(-x)} = \exp(-x), \quad (5.3)$$

where $M(x) = \min[1, \exp(-x)]$. In the importance sampling algorithm each move is accepted and rejected according to $M(\beta U_N)$. If U_N^0 and U_N^1 are respectively the potential functions that describe the reference system and the system of interest, then the following relation is satisfied

$$\frac{M[\beta(U_N^0 - U_N^1)]}{M[\beta(U_N^1 - U_N^0)]} = \exp[\beta(U_N^1 - U_N^0)]. \quad (5.4)$$

This can be conveniently rearranged into

$$M[\beta(U_N^0 - U_N^1)] \exp[-\beta(U_N^1)] = M[\beta(U_N^1 - U_N^0)] \exp[-\beta(U_N^0)]. \quad (5.5)$$

The above equation can be exploited to calculate the ratio Q_0/Q_1 between the partition functions of the two systems. By dividing both sides of Eq. 5.5 by $Q_1 Q_0$ and integrating over the configurational space of the two systems, one obtains

$$\frac{1}{Q_0} \frac{\int M[\beta(U_N^0 - U_N^1)] \exp[-\beta(U_N^1)] d\mathbf{R}^N}{Q_1} = \frac{1}{Q_1} \frac{\int M[\beta(U_N^1 - U_N^0)] \exp[-\beta(U_N^0)] d\mathbf{R}^N}{Q_0}, \quad (5.6)$$

which implies

$$\frac{Q_1}{Q_0} = \frac{\left\langle M[\beta(U_N^1 - U_N^0)] \right\rangle_0}{\left\langle M[\beta(U_N^0 - U_N^1)] \right\rangle_1}. \quad (5.7)$$

The route to estimate the two canonical averages on the right hand side of Eq. 5.7 is to conduct two MC simulations, one for each system, and calculate the total acceptance rate in both ensembles of the move that switches

the two potential functions. The two averages must be large enough to be successfully evaluated by a MC calculation. This is not the case when the two potential functions are very far apart.

Unfortunately, in the totality of free energy problems that have been studied in the past with this method, the phase spaces of the two systems never overlapped sufficiently to allow the evaluation of Eq. 5.7 in one stage. The solution to this problem is to single out intermediate potential functions between U_N^0 and U_N^1 and calculate 5.7 in different stages.

ii Calculations in the past have shown that the evaluation of Eq. 5.7 using multistaging requires a very lengthy sampling. The same type of problem arises when the *energy distribution method* is used. This method calculates the ratio Q_0/Q_1 according to

$$\frac{Q_0}{Q_1} = e^{\beta \Delta} \frac{h_0(\Delta)}{h_1(\Delta)}, \quad (5.8)$$

where

$$\begin{aligned} h_0 &= \langle \delta(U_N^0 - U_N^1 - \Delta) \rangle_0 \\ h_1 &= \langle \delta(U_N^0 - U_N^1 - \Delta) \rangle_1. \end{aligned} \quad (5.9)$$

When $h_0(\Delta) = h_1(\Delta)$, from Eqs. 5.8 and 5.9

$$\Delta = A_1 - A_0. \quad (5.10)$$

As happened in the acceptance ratio method, a poor overlap between the two systems configurational spaces leads to difficulties in the evaluation

of Eq. 5.8. These problems can be overcome by resorting to multistage sampling as it is done in the *acceptance ratio method*.

iii The *thermodynamic integration method* calculates the difference in free energies between two systems using the identities

$$\begin{aligned} A_1 - A_0 &= \int_{A_0}^{A_1} \langle dA \rangle \\ &= \int_{\lambda_0}^{\lambda_1} \left\langle \frac{\partial A}{\partial \lambda} \right\rangle d\lambda, \end{aligned} \quad (5.11)$$

where λ is a parameter that defines a reversible path between the systems described respectively by A_1 and A_0 . The canonical average in Eq. 5.11 can be evaluated by a standard MC simulation. Usually, the convergence of the free energy derivatives is good. The *thermodynamic integration method* integrates numerically $\langle \partial A / \partial \lambda \rangle$ with respect to λ evaluating the thermal average on a grid of λ values between λ_0 to λ_1 . If $\langle \partial A / \partial \lambda \rangle$ is a smooth function of λ , only a few points might be needed to evaluate the integral. Phase transitions along the reversible path may influence the convergence of the free energy derivative and increase the error.

Free energy calculations performed in the past using the *acceptance ratio* and the *energy distribution* methods have required lengthy sampling to obtain reasonable convergence of the required averages and appreciable accuracy in the final results. It is now clear that, if the initial and final states are very far apart from each other, the thermodynamic integration technique provides the route, less demanding in computer resources, to

calculate the free energy. If, instead, two states overlap sufficiently the two other techniques may be less wasteful of computer time.

5.2 Application to the Electron in Liquid Ammonia

The Helmholtz free energy of electron solvation in liquid ammonia may be interpreted as the free energy necessary to charge up an electron immersed in the liquid from charge zero to full charge. This is the solvated electron analog of the Debye charging trick used in the electrolyte theory.

In the initial state at zero charge the electron can be considered free since there is no interaction with the molecules of the solvent. The fully charged electron, instead, is solvated by the ammonia molecules and is self-trapped in a cavity produced in the liquid. The two states are sufficiently different from each other that the free energy difference is anticipated to be efficiently estimated by the *thermodynamic integration* method.

The parameter λ , over which the integration is to be carried out, is the charge of the electron. Equation 5.11 can be rewritten as

$$A_1 - A_0 = \int_0^1 \left\langle \frac{\partial A}{\partial q} \right\rangle dq, \quad (5.12)$$

where A_0 and A_1 are the free energies respectively of the electron immersed in liquid ammonia at zero charge and at full charge. The integral in Eq. 5.12 is calculated by choosing an appropriate grid of charge values and evaluating

the statistical average $\langle \partial A / \partial q \rangle$ at this mesh of points.

The derivative of the free energy with respect to the charge can be explicitly derived in the canonical ensemble by acting on

$$A = -\frac{1}{\beta} \log Q. \quad (5.13)$$

One obtains

$$\frac{\partial A}{\partial q} = -\frac{1}{\beta Q} \frac{\partial Q}{\partial q}. \quad (5.14)$$

In the case of the solvated electron, one uses the isomorphic path integral partition function in Eq. 3.17.

The electron-ammonia pseudopotential used in this thesis represents each solvent molecule as a collection of charge sites.[81] Thus, the interaction potential between the electron at \mathbf{r}_i and the solvent molecules is given by

$$\begin{aligned} V(\mathbf{r}_i) &= \sum_{j=1}^N \sum_{s=1}^{n_s} \frac{q q_{js}}{|\mathbf{r}_i - \mathbf{R}_{js}|} \\ &= q \mathcal{V}(\mathbf{r}_i), \end{aligned} \quad (5.15)$$

where N is the number of molecules, n_s is the number of charge sites on each molecule, q_{js} and \mathbf{R}_{js} are respectively the charge and the position of the s -th site in the j -th molecule. From Eq. 5.14 and 3.17 it is straightforward to derive the following expression for $\langle \partial A / \partial q \rangle$

$$\begin{aligned} \left\langle \frac{\partial A}{\partial q} \right\rangle &= \frac{1}{Q(N, P, \beta)} \left(\frac{mP}{2\pi\beta} \right)^{3P/2} \left(\frac{MP}{2\pi\beta} \right)^{3N/2} \\ &\times \int \prod_{i=1}^N d\mathbf{R}_i \prod_{s=1}^P d\mathbf{r}_s V_{ep} \exp \left[-\beta (V_{e-N} + V_{N-N}) \right], \end{aligned} \quad (5.16)$$

where

$$V_{ep} = \frac{1}{P} \sum_{i=1}^P \nu(\mathbf{r}_i), \quad (5.17)$$

is the total potential acting on the electron. The configurational integral on the right hand side in Eq. 5.16 is nothing but the thermal average of V_{ep} in the canonical ensemble. Thus, writing $dq = e d\gamma$, where $1 \geq \gamma \geq 0$, Eq. 5.12 can be rewritten as

$$A_1 - A_0 = \int_0^1 e \langle V_{ep} \rangle d\gamma. \quad (5.18)$$

The equilibrium average $\langle V_{ep} \rangle$ can be evaluated by a MC simulation for every value of γ . The calculation of the difference in free energy amounts to the numerical integration of $\langle V_{ep} \rangle$ over γ with an appropriate choice of mesh points.

5.3 Simulation Details

All the parameters of the PIMC simulations were set as in the previous calculations described in Chapter 4.

A series of MC simulations were carried out by decreasing the charge of the electron from full to zero charge. The initial electron-ammonia coordinates used to start a new calculation were produced in the preceeding run involving a higher electron charge. The discharging process created a progressive delocalization of the electron associated with an increase of the isomorphic polymer average diameter. The system at full charge was prepared according to the procedure described in the previous chapter.

Typically, a run was performed by initially equilibrating the system for 500 passes. The averages were then accumulated for a number of passes sufficient to make certain the overall convergence of the calculation. As in the previous chapter, the convergence of the calculation was checked by looking at the subaverages about every 400 passes and comparing them to the ones obtained for the previous segments. Only in one calculation involving the electron charged at $0.5 e^-$ the error on the potential and kinetic energies was large. Typically, for all the other electron charges the relative error on the potential $\langle V_{ep} \rangle$ was around 4 % and about 2500 passes were required to ensure convergence.

5.4 Results

5.4.1 The Discharge Process

Going from full charge to zero charge the electron evolved from being trapped in a cavity in the solvent (localized state), to being extended to large regions (delocalized state). This "phase transition", which took place when the charge reached $0.5 e^-$, caused the disappearance of the cavity. Consequently, the short range correlation between the electron and the ammonia molecules was lost. At $0.5 e^-$ the equilibration of the system was very difficult; the value of $\langle V_{ep} \rangle$ oscillated greatly and exhibited poor convergence.

It was mentioned in section 3.6 that the complex time correlation

function, $\mathcal{R}(t - t')$, can be used to distinguish between localized and delocalized electron states. Thus, the response of the electron to the variation of its charge is clearly visible in the shape of this correlation function. In Fig. 5.1 the $\mathcal{R}(t - t')$'s for some of the simulations are plotted. From the gap in correlation length between charge $0.5 e^-$ and $0.4 e^-$ ($\mathcal{R}(\beta\hbar/2)$) one infers that the electron remains in a compact state until it reaches $0.5 e^-$ where it undergoes a transition to more extended states. A perhaps clearer picture of the electron behaviour when its charge is decreased from full charge to zero charge is given in Fig. 5.2 where $\mathcal{R}(\beta\hbar/2)$ is plotted versus the electron charge. At charge $0.5 e^-$ the electron is in a peculiar state, in between localization and delocalization.

To confirm this interpretation, in Fig. 5.3 the electron c.m.-nitrogen pair correlation functions for charge $0.25 e^-$, $0.50 e^-$, $0.9 e^-$ are reported. At charge $0.9 e^-$ the $g_{cm-N}(r)$ is equal to zero when $r < 2 \text{ \AA}$, showing the presence of an exclusion volume for the ammonia molecules. On the contrary, at charge $0.25 e^-$ the $g_{cm-N}(r)$ is zero only at the origin; the electron is in an extend state, the cavity has disappeared. When the charge is $0.5 e^-$ the situation is intermediate; $g_{cm-N}(r)$ becomes zero around 0.5 \AA . A pictorial representation of the electron at charge $0.25 e^-$, $0.5 e^-$ and $0.9 e^-$ is given respectively in Figs. 5.4, 5.5 and 5.6 where representative instantaneous configurations for the electron primary chain in each of the cases are plotted. All three pictures are drawn to the same length scale, therefore the difference in size of the primary chains are meaningful.

Further calculations were carried out to test the reliability of the results obtained for $\langle V_{ep} \rangle$ and the possibility of hysteresis. At first, utilizing the electron-ammonia coordinate at charge $0.1 e^-$ as a starting configuration the electron was charged up to a charge of $0.25 e^-$ and, subsequently, to $0.4 e^-$. In the end, a final run was performed at charge $0.1 e^-$ starting the simulation from an equilibrated configuration of the pure liquid and adding an electron at charge $0.1 e^-$ in a fully extended state. No substantial hysteresis was found for $\langle V_{ep} \rangle$ in the results. This is shown in Fig. 5.7 where $\langle V_{ep} \rangle$ for all the simulations versus the charge on the electron is plotted. The results of these simulations relative to the $\mathcal{R}(\beta\hbar/2)$ show, instead, the large uncertainty on the dimension of the electron in extended states at lower charges (see Fig. 5.2).

5.4.2 Free Energy of Solvation

The integral of $\langle V_{ep} \rangle$ plotted in Fig. 5.7 was evaluated using a cubic spline interpolation method. The Helmholtz free energy of electron solvation was found to be

$$A_1 - A_0 = -11.5 \pm 1 k_B T. \quad (5.19)$$

The error on this value was due mainly to the uncertainty in the potential function at charge $0.5 e^-$. It was estimated by recalculating the integral at the upper and lower bound of $\langle V_{ep} \rangle$ at charge $0.5 e^-$. It was found that the error due to the other regions was comparatively small.

The total energy of electron solvation, ΔE is given by the sum of

the electron total energy, E_T , and the reorganization energy of the fluid, E_R . Namely

$$\Delta E = E_T + E_R. \quad (5.20)$$

E_T was directly derived from the run at full charge, while the calculation of E_R required an additional MC simulation of the ammonia pure fluid, ΔE was estimated to be

$$\Delta E = -28.3 \pm 1 k_B T. \quad (5.21)$$

Finally, the entropy of solvation is

$$\Delta S = -16.8 \pm 2 k_B. \quad (5.22)$$

Unfortunately, this value of the entropy does not agree with the experimental $\Delta S = 18 k_B$. [22] It must be pointed out, however, that the experimental determination of the entropy was conducted at constant pressure [22,21] while this calculation was carried out at constant volume.

Instead of embarking on a new series of constant pressure calculations using the technique described in the previous chapter, it was chosen to correct the experimental constant pressure value of the entropy by the appropriate factor.¹ The entropy at constant volume and constant pressure are related by the following expression

$$\Delta S_v = \Delta S_p - \Delta S_{\Delta v}, \quad (5.23)$$

¹It must be remembered that a PIMC simulation at constant pressure is on average 4 times more time consuming than at constant volume.

where ΔS_v is the entropy of solvation at constant volume, ΔS_p is the entropy change at constant pressure and $\Delta S_{\Delta v}$ is the entropy change when the liquid expands by one solvated-electron molar volume.

The physical meaning of the correction $\Delta S_{\Delta v}$ can be understood from the thermodynamic cycle in Fig. 5.8. Here $\Delta S(p, v)$ is the solvation entropy at a constant volume v and at average pressure p . The pressure at which the experimental entropy is available is $p = 1 \text{ bar}$, v is the volume at which the PIMC simulation has been performed. Moreover, Δv is the volume expansion produced by the electron, $p + \Delta p$ is the pressure of the constant volume calculation. It is clear that $\Delta S(p, v + \Delta v)$ and $\Delta S(p + \Delta p, v)$ correspond respectively to ΔS_p and ΔS_v in Eq. 5.23. For this diagram to be useful one has to assume that $\overline{AB} = \overline{CD} = \Delta S_{\Delta v}$ and that the effect of changing the pressure at constant volume on the entropy of solvation is negligible. Therefore

$$\Delta S(p + \Delta p, v) \simeq \Delta S(p, v), \quad (5.24)$$

and

$$\begin{aligned} \Delta S(p, v) &= \Delta S(p, v + \Delta v) - \overline{AB} \\ &\simeq \Delta S(p, v + \Delta v) - \Delta S_{\Delta v} \end{aligned} \quad (5.25)$$

With this assumption in mind, the correction to the experimental ΔS_v can be estimated to first order in ΔV by using the thermodynamic relation

$$\Delta S_{\Delta v} = \left(\frac{\partial P}{\partial T} \right) \Delta V. \quad (5.26)$$

$(\partial P/\partial T)$ can be estimated from the equation of state for fluid ammonia,[82,83] its numerical value is 22.7 bar K^{-1} . The experimental partial molar volume of electron solvation is estimated at $100 \text{ cm}^3 \text{ mol}^{-1}$ [70] By using the experimental entropy at constant pressure $\Delta S_p(\text{exp.}) = 18 k_B$ and Eq. 5.23 the experimental ΔS_v is

$$\Delta S_v(\text{exp.}) = -9.3 k_B. \quad (5.27)$$

The calculated entropy change ($\Delta S_v(\text{calc.}) = -16.8 \pm 2 k_B$) is then in fair agreement with the experimental value.

5.5 Discussion

This study has shown that the entropy of electron solvation at constant volume is negative. This finding is consistent with the results of the preceeding chapter and previous studies[5,65] that a localized electron favours local ordering, at least, in the molecules of its first solvation shell. The positive entropy measured experimentally is mostly due to the volume expansion produced by the electron in the solvent. The entropy change calculated in this simulation was in acceptable agreement with the experiment.

It was also found that discharging the electron produced a transition from localized states near full charge to delocalized states near zero charge. This transition occurred around charge $0.5 e^-$.

To conclude this chapter, it must be said that the remaining dis-

agreement between experiment and calculation is likely to be related to the simple pseudopotential model used in this study. Since delocalized states occur only at small electron charge the existence of long range electrostatic forces is not likely to have a large effect on the calculated entropy.

Figure 5.1:

Complex time correlation functions for the electron-ammonia system calculated for various values c of electron charge. From top to bottom $c = 0.0, 0.1, 0.25, 0.4, 0.5, 0.6, 0.75, 0.9$ and $1.0e^-$.

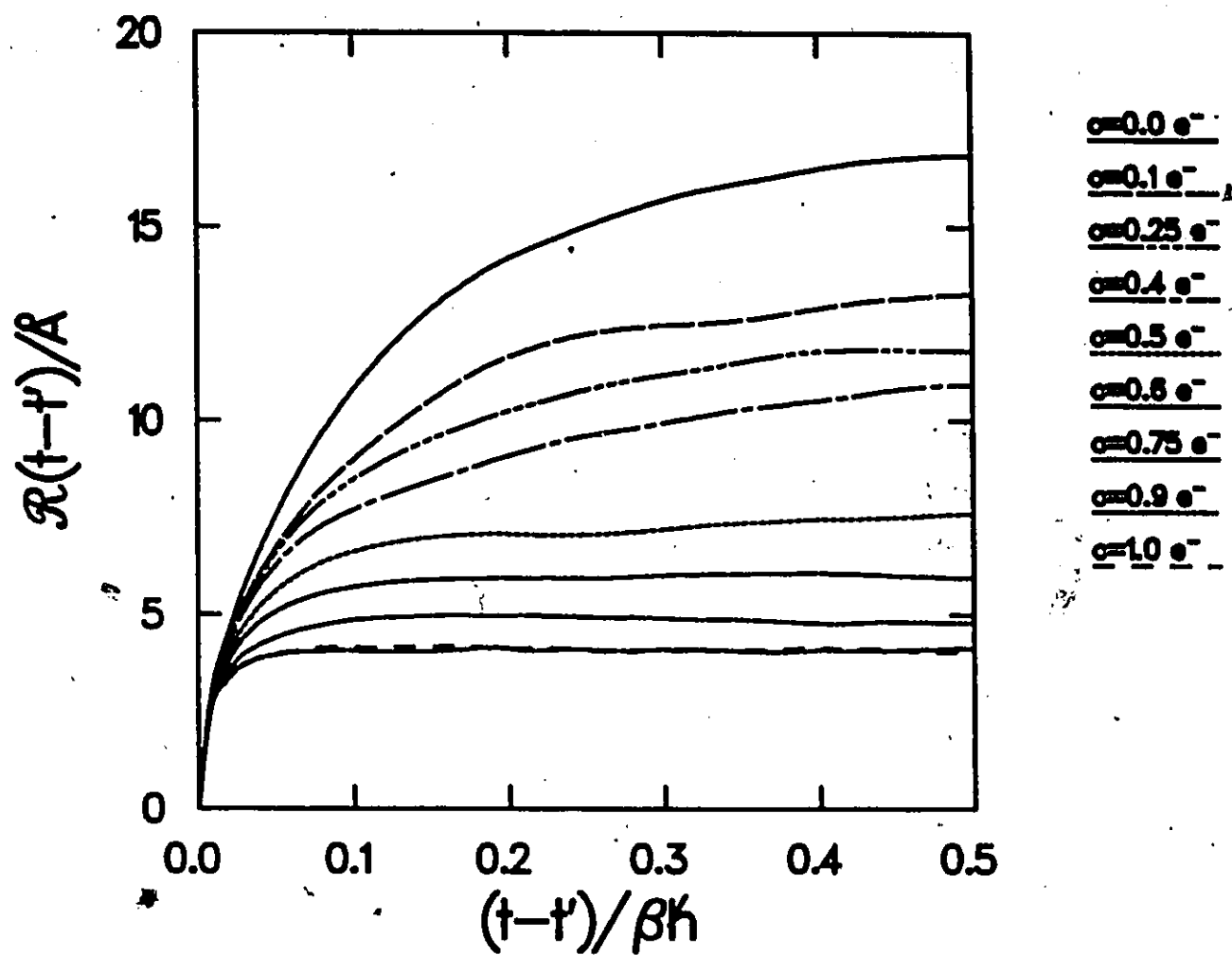


Figure 5.2:

Asymptotic values of the complex time correlation function the electron-ammonia system for the values of the electron charge given Fig. 5.1. The circles are the results for the sequential discharging of the electron, the triangles from charging up runs starting from $c = 0.1$, and the square is an independent run at $c = 0.1$ which started from an extended (free) state.

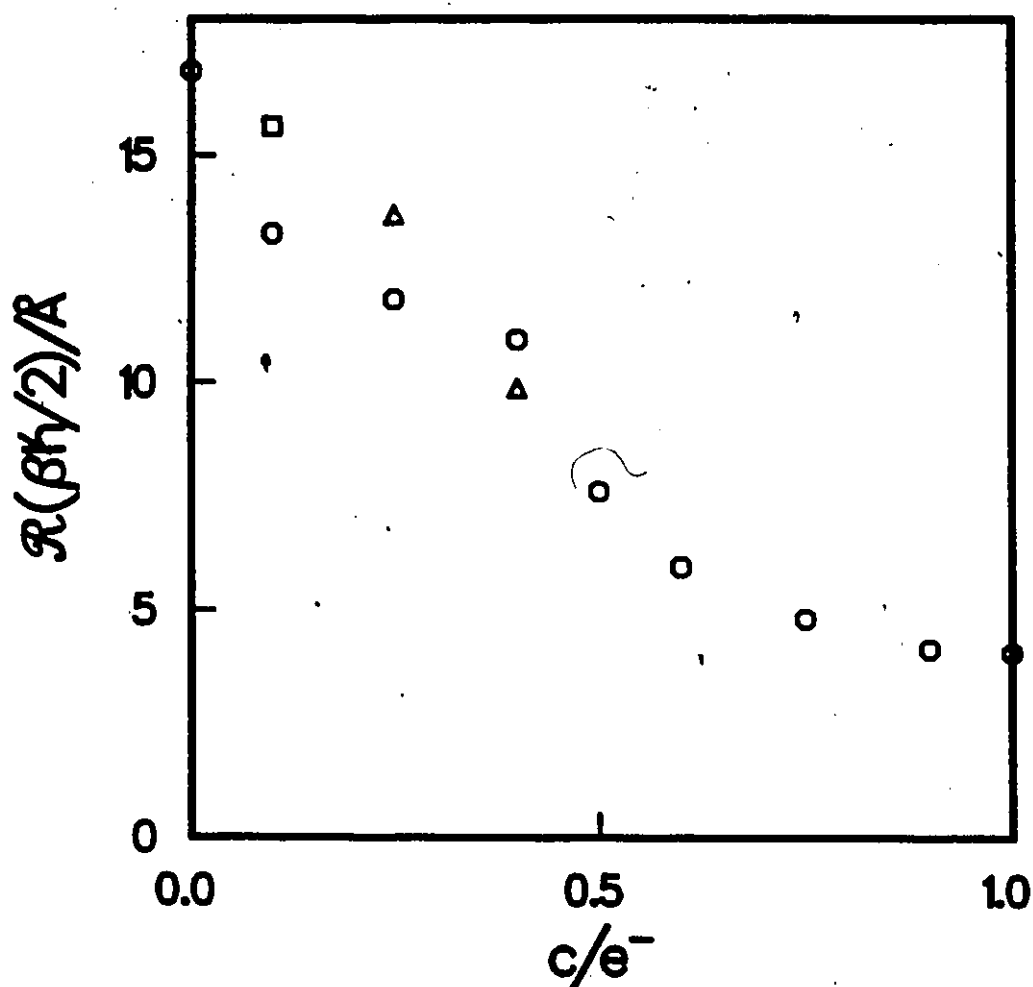


Figure 5.3:

Electron (center-of-mass)-nitrogen correlation functions for three values of electron charge. The disappearance of the cavity should be noted.

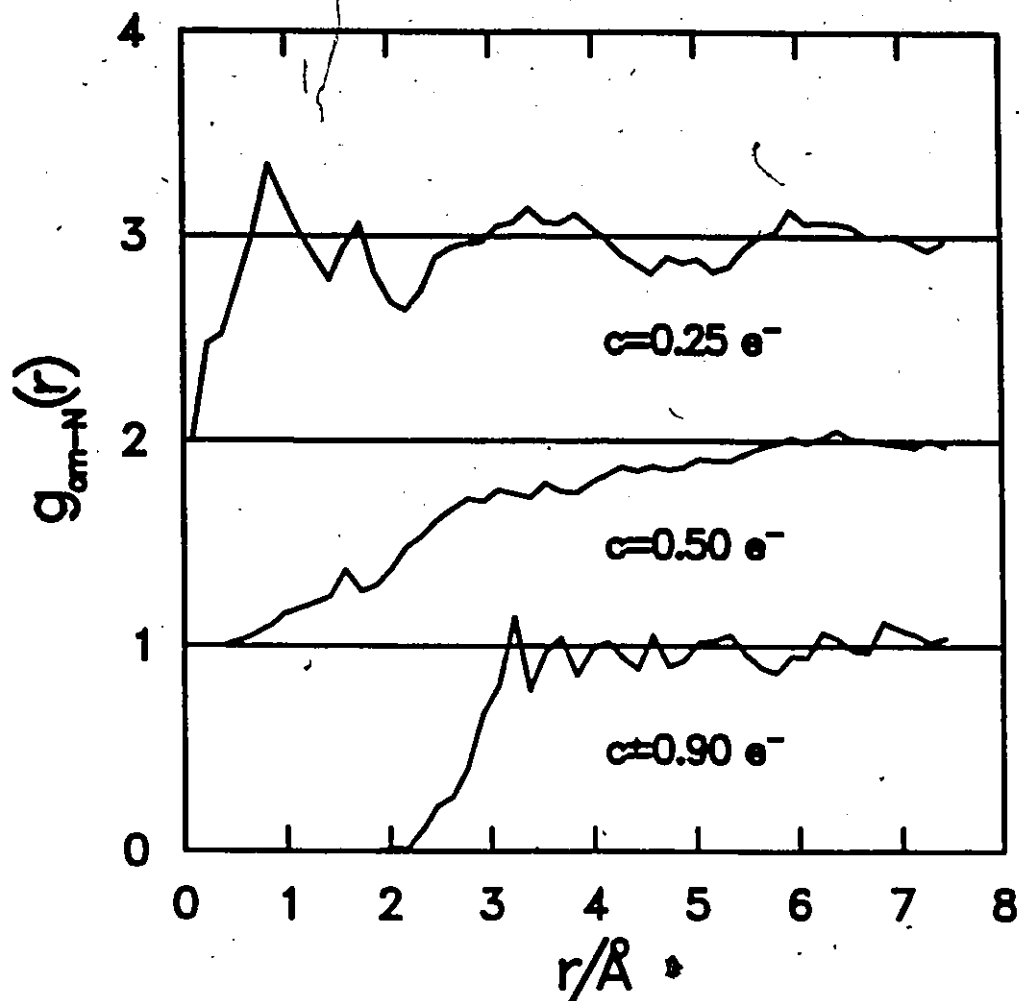


Figure 5.4:

Instantaneous configuration of the electron and solvent when the electron charge is $c = 0.9e^-$. Only the P_z primary chain particles comprising the isomorphous electro polymer are shown (small dots). The spacing between the large circles is 25.5 Å.

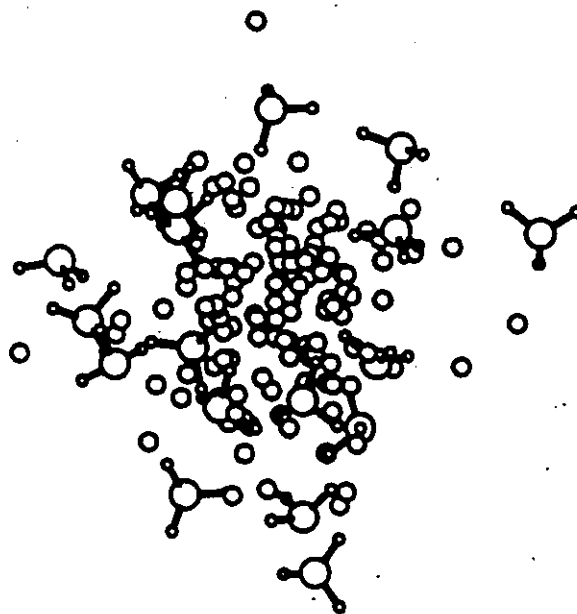


Figure 5.5:

Instantaneous configuration of the electron and solvent when the electron charge is $c = 0.5e^-$ drawn on the same scale as Fig. 5.4.

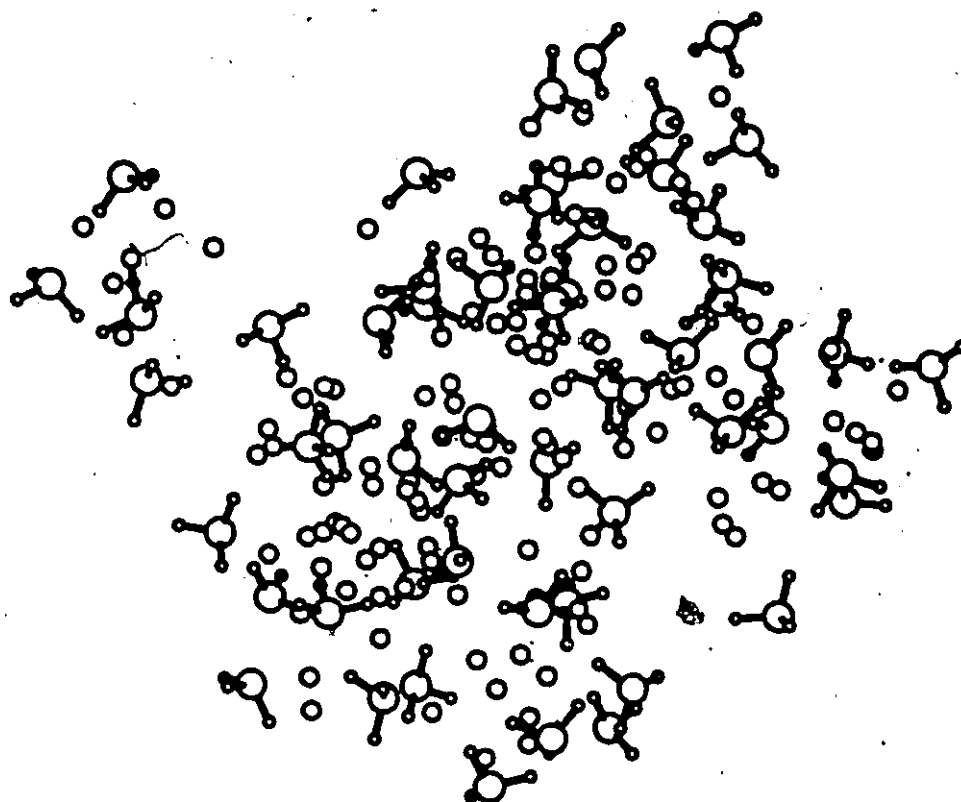


Figure 5.6:

Instantaneous configuration of the electron and solvent when the electron charge is $c = 0.25e^-$ drawn on the same scale as Fig. 5.4 and 5.5.

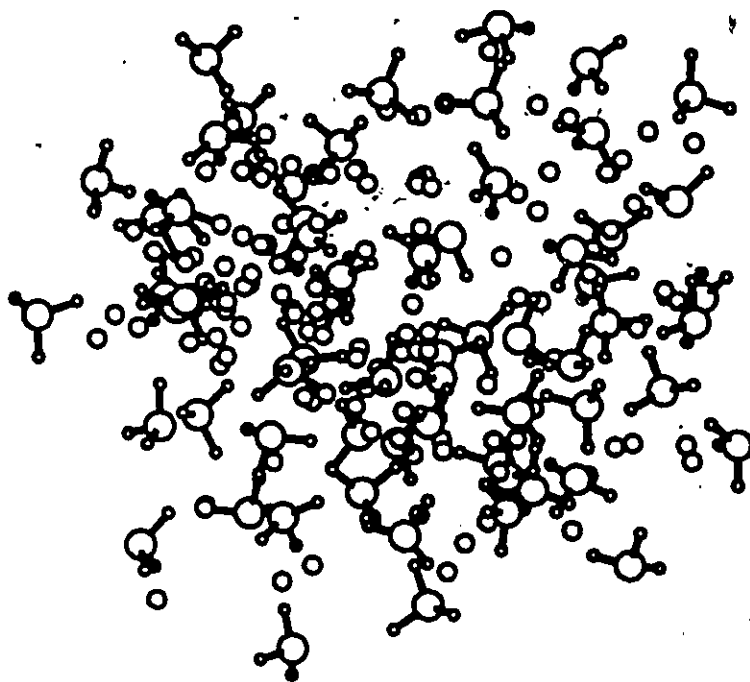


Figure 5.7:

The electron-solvent potential V_{ep} as a function of the electron charge. The symbols have the same meaning as in Fig. 5.2.

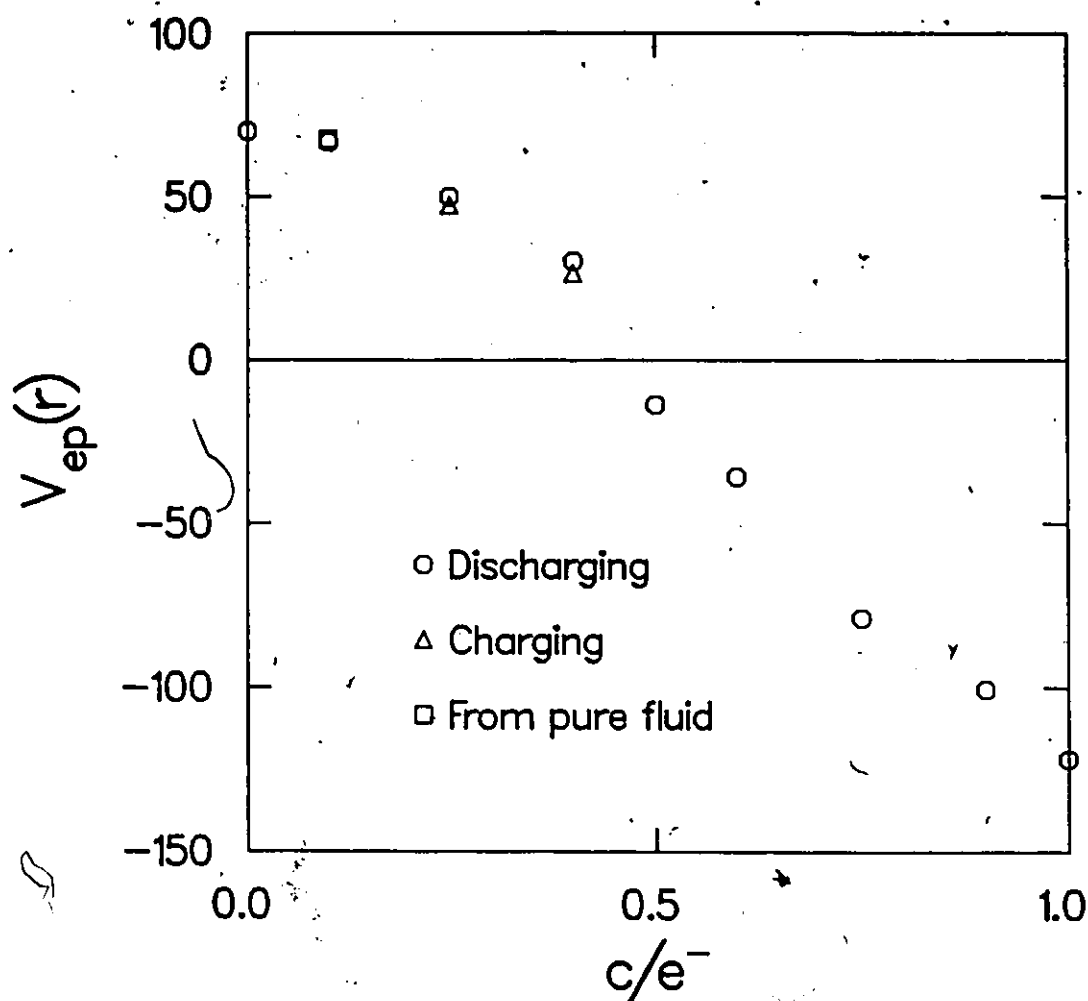
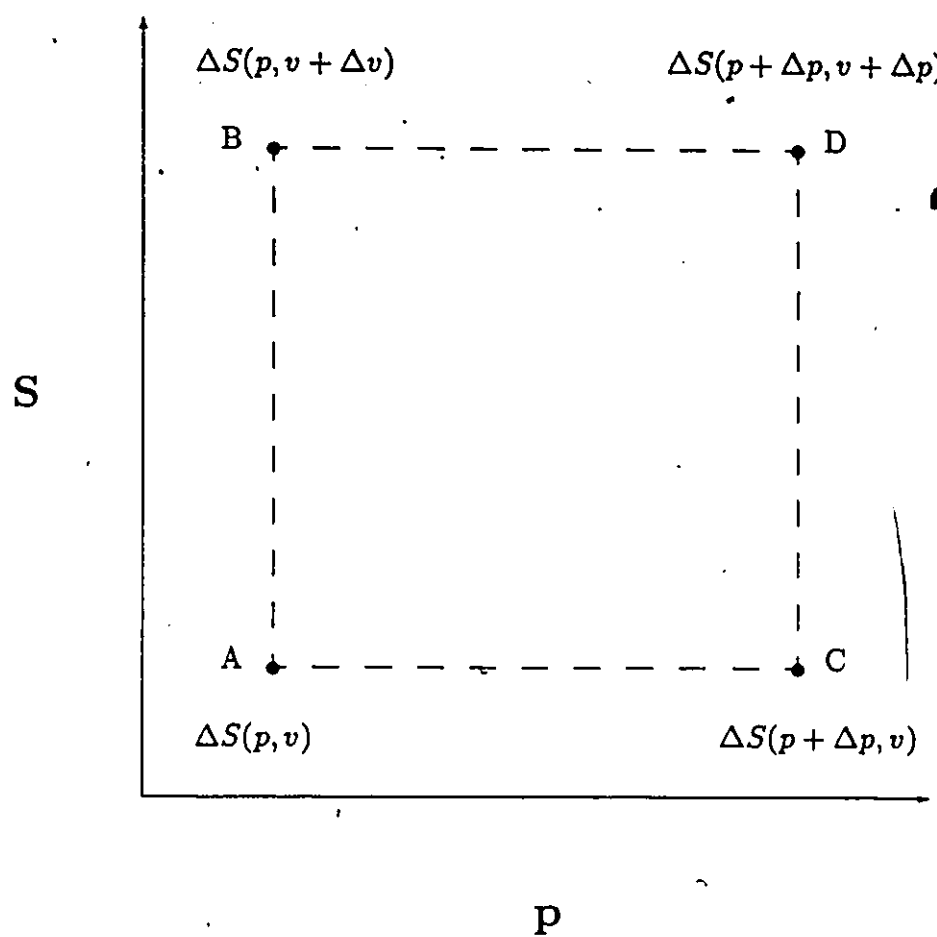


Figure 5.8: Entropy cycle



Chapter 6

Ionization of Alkali Atoms in Ammonia : Li, Na, Cs

In the past alkali metal-ammonia solutions have been the subject of intensive investigations.[84,70,22] The focus of most of these studies has been the transition from non-metallic to metallic properties which the metal-ammonia solutions experience at very low concentration of the metal. As an example of this peculiar behaviour, in Fig. 6.1 the molar conductivity Λ of the sodium-ammonia system is plotted versus the sodium mole fraction.[22] It is evident from the graph that a transition to a more conducting state occurs at mole fractions $x(\text{Na}) > 0.02$. Most alkali metal-ammonia solution transport properties show a remarkably small dependence on the type of ion present and conductivity curves similar to the one in Fig. 6.1 are found for the other metals of the series.[84]

Metallic behaviour of the concentrated metal-ammonia solutions is further indicated by their bronze colour and metallic reflectivity. At lower concentrations, instead, the solutions show a dark blue colour.

To be more specific, according to the classification scheme for liquid, electronically conducting materials introduced by Allgaier[85] the alkali metal-ammonia solutions are class B liquids. They have an intermediate behaviour between good metallic liquids (class A) and electrolytes (class C). It is particularly noticeable that the temperature coefficient $\gamma = \sigma^{-1} d\sigma/dT$ (σ specific conductivity) is positive (as in semiconductors) at low concentrations and becomes negative for all the alkali metals at a mole fraction of about 0.2.[86]

All the experimental evidence discussed above indicates that there are two distinct electronic states existing in different ranges of concentration. The solvated electron state as discussed in Chapter 4 is prevalent at low concentrations, while delocalized states are responsible for the metallic conductivity at higher metal-ammonia ratios. From the positive sign of γ , it can be inferred that at low concentrations the conduction occurs through thermal activation of the electron carriers which jump to the conduction band.

In the past simple models of metal-ammonia solution have been developed to explain the electronic conductivity at the high concentration regime. These models were mostly an extension of the standard treatment of ionic electrolytes.[87,88] The electrons were considered nearly-free

ing in an average potential field created by the solvated positive ions and ammonia molecules. Unfortunately, these types of models cannot include effects due to local fluctuations in the electron-ion and electron-molecule potential which are more important in a liquid than in a solid. Such effects can be taken care of by utilizing simulation techniques.

Recently, a dilute lithium-ammonia solution has been studied by simulating the lithium valence electron with the PIMC method.[16] Although this simulation technique cannot be used to simulate a metal-ammonia solutions in the high concentration regime (it is unable to handle conveniently delocalized states and more than one electron), this approach is useful if the goal of the investigation is to better understand the effects of the solvent in the ionization process.

A few problems have to be faced in order to simulate alkali atoms in ammonia. In the first place, the soft core Shaw type pseudopotential used in Ref. [16] may not be suitable for heavier alkali metals where the repulsion between the atom core and the valence electron is more pronounced. Secondly, a suitable intermolecular potential between the alkali positive ion and ammonia is not available in the literature except for the Li-ammonia interaction.

This chapter is arranged as follows. In section 6.1 results of the classical simulation of the Li, Na and Cs ions in ammonia and details of the ion-ammonia intermolecular potential are given. In section 6.2 the PIMC simulations of the three atoms in ammonia are presented and the

effect of different electron-ion pseudopotentials is discussed.

6.1 Li^+ , Na^+ and Cs^+ in Liquid Ammonia

6.1.1 Ion-ammonia Potentials

In the past, most of the theoretical studies on ionic solutions has involved water as the solvent. Alkali ions in water have been studied by molecular dynamics and Monte Carlo techniques and interaction potential for these systems are readily available in literature. Unfortunately, there is almost a complete absence of these studies for liquid ammonia. At present only a MC simulation of a Li^+ ion solvated in ammonia has been reported in literature which presented a simple model potential for the ion-ammonia interaction.[16,89] The same model will be used in this thesis for Li^+ , Na^+ and Cs^+ solvated in ammonia.

The authors in Refs. [16,89] devised their potential in part from a 6-31G* level SCF calculation.[90] This article examined dimers of 20 first and second-row bases, which included ammonia, with H^+ , Li^+ and Na^+ . The total energy and the equilibrium distance and geometry of the complexes were given. It was shown that the intermolecular interaction between ammonia and alkali ions is dominated by electrostatic ion-dipole and polarization contributions. Ion-base interaction energies and equilibrium distances for heavier alkali ions (K^+ , Rb^+ and Cs^+) were then extrapolated.

On this basis the model potential in Ref. [16] consisted of Coulom-

bic and dispersion contributions. The electrostatic part involved the interaction between the unitary positive charge on the cation and four charges sites distributed on the ammonia molecule. The magnitude and position of the four charges were taken as in the electrostatic SPC model potential for ammonia and described in Chapter 4. A Lennard-Jones potential between the nitrogen and the cation handled the short-range contributions. In Refs. [16,89] the parameters of the Lennard-Jones potential were fitted to the dimer energy and equilibrium distance given by the SCF calculation. The same strategy is followed in this thesis to determine Lennard-Jones parameters for sodium and caesium interacting with ammonia. In table 6.1 the fitted potential parameters for the three cations are listed.

6.1.2 Classical MC Calculations

Simulation Details Classical MC simulations were performed on a system composed of 250 ammonia molecules and an alkali ion at a molar volume $V = 26.5 \text{ cm}^3 \text{ mol}^{-1}$ and temperature $T = 260 \text{ K}$. The ammonia molecules were moved according to the standard MC procedure described in Chapter 3 while the alkali ion was kept fixed in the center of the box. As usual, the acceptance rate was maintained around 40%. A MC pass was defined in accordance to section 4.3.1. Typically, the simulations were run for 5000 passes following a period of 2000 passes of equilibration, during which the ammonia molecules adapted to the presence of the ion.

Structure The structure of the ammonia molecules around an ion X is described by the two pair correlation functions $g_{XN}(r)$ and $g_{XH}(r)$, where $X = \text{Li}^+$, Na^+ and Cs^+ . Further information on the orientational order around the ion can be gathered from the dipole correlation function which was defined in section 3.6.

The functions $g_{XH}(r)$ and $g_{XN}(r)$ for the three ions are plotted in Figs. 6.2-6.3. The positions at which the first peaks occur are reported in table 6.2. The separation between the nitrogen and the ions are very close to the value of the parameter σ in the respective Lennard-Jones potentials. In Fig. 6.4 the dipole correlation functions are reported.

The results in Figs. 6.2 and 6.3 show that in the $g_{XN}(r)$'s the first peak is always very strong signalling the expected very pronounced coordination between the ion and the molecules in the first sheath. The height of the peak decreases going from lithium to caesium. For lithium and sodium this peak falls to zero while for caesium it reaches a small minimum value. The ammonia molecules of the second solvation shell are less correlated to the ion. Sodium experiences the sharpest second peaks.

The average angle θ between the molecular axis and the axis that unites the ion with the nitrogen of the first nearest neighbours can be derived from the positions of the first peaks in both $g_{XN}(r)$ and $g_{XH}(r)$. The results are listed in table 6.2. The deviation from $\theta = 0$ predicted by the *ab initio* calculations is very small for the two smallest cations, but more marked for caesium. More than one configuration contributes to the

main peak in $g_{CSN}(r)$ as shown by its sizable width. These deviations are an effect of the other nearby solvent molecules.

In addition, the broader peak of the caesium dipole distribution function in Fig. 6.4 shows that the molecules of its first solvation sheath experience on average more orientations compared to those of lithium and sodium.

The coordination number, n_N , is usually defined as the mean number of molecules in the ion first solvation shell. The separation $r \doteq r_{min}$ at which the function $g_{XN}(r)$ reaches its first minimum defines the spatial extension of this first shell. Only Li^+ and Na^+ have a clear plateau in their correlation functions while Cs^+ has a less shallow minimum. Therefore the value of n_N is better defined for the two former than for the latter. The coordination numbers for the three cations are listed in table 6.2. Their values are in agreement with chemical experience and neutron diffraction experiments.[91] It must be added that in the case of Cs^+ the number of hydrogens in the first shell is not equal to $3 \times n_N$ as in the other cases (see table 6.2). This indicates that few of the ammonia molecules of the second shell are able to penetrate in the first shell.

Results pertaining to the equilibrium energetics of the ions solvated in liquid ammonia are given in table 6.3. It is observed that the three ions have a negative solvation energy. The major contribution to the ionic energy is supplied by the electrostatic component. Going from the smaller ion to the larger, the contribution from the atom-atom interactions increases

noticeably.

The solvation of an ion is accompanied by some change in the intermolecular structure of the fluid compared with the pure sample. The reorganization energy, which quantifies this change, is calculated in table 6.3 relative to the energy of the pure liquid obtained in Chapter 4. It shows that Cs^+ exerts the smallest effect on the liquid configurational energy.

6.2 Alkali Atoms in Ammonia

6.2.1 The Pseudopotential Problem

In previous path integral computer simulations the ion-electron interactions have been handled by using a Shaw type pseudopotential described in Chapter 3 (see Eq. 4.3). The locality of this pseudopotential is essential to its use in a PIMC calculations. The value of the parameter R_c in Eq. 4.3 for each of the alkali metals can be calculated by fitting to the experimental first ionization energies (Li, 5.39 eV; Na 5.14 eV; Cs 3.89 eV). [68]

However, the simplicity of this pseudopotential (only one parameter) is also its major limitation. The constant negative potential energy for $r \leq R_c$ produces an unphysically high electron density inside the ion core due to a valence s electron. This problem was not important in early band structure calculations where soft core pseudopotentials were mostly used. Given the nearly free-electron nature of the Bloch energy bands of most of the non-transition metals, pseudopotential models were chosen to give a

quick damping of the form factor V_K for large $K \geq 2K_F$. [68,92,47]

Hard core ion-electron pseudopotentials have been used in the past mainly in the study of the structural properties of elemental metals and binary compounds. Andreoni et al. [93] recently proposed a simple model for this type of pseudopotentials. Andreoni's pseudopotential is l dependent (non-local) and can be written as

$$V_l(r) = -\frac{Ze}{r} + W_l(r), \quad (6.1)$$

where Z is the valence core charge ($Z = 1$ for alkali metals), $W_l(r)$ is a short range potential

$$W_l(r) = A_l \frac{\exp(-\gamma_l r)}{r^2}. \quad (6.2)$$

A_l and γ_l are the parameters that describe the interaction of the valence electron with core electrons. $W_l(r)$ contains contribution from short-range orthogonality, electrostatic and exchange interactions. The interaction is positive if some of the core electrons have the same angular momentum as the valence electron. In this case $W_l(r)$ is dominated by the repulsive orthogonalization term. Instead, when the valence electron is in a state with angular momentum different from those of the core electrons, the potential incorporates only the electrostatic and exchange contributions being the valence and core electrons already orthogonal. The l dependent parameters of the Andreoni hard-core model potential are fitted to the Hartree-Fock (HF) energies and valence HF wave functions from infinity to the outer node. The non-locality of this potential model does not prevent

its use in a PIMC simulation. In fact, it may be inferred that the valence electron ground state of an alkali metal in liquid ammonia is mainly an s type state. Therefore it is reasonable to use in the ion-electron interaction only the potential parameters corresponding to $l = 0$. Both, soft-core (SC) and hard-core (HC) potentials have been used in this thesis. In table 6.4 the parameters of both pseudopotentials for Li, Na and Cs are presented.

6.2.2 The Li Atom in Liquid Ammonia

A previous PIMC calculation[16] has shown that the Li atom in ammonia is unstable and forms a contact ion pair in which the valence electron charge is polarized by the surrounding molecules. No spontaneous ionization was observed. The soft-core potential given in table 6.2 was used in this study.

The Li atom was subsequently ionized by a series of calculations in which the center of mass was constrained to increasing distances from the ion. In this way the activation energy of the ionization process was estimated. Unfortunately, since MC simulation cannot directly calculate the chemical potential, it was not clear if the entropic contribution could stabilize the ionized form with respect to the contact ion pair.

In this thesis the results from the HC potential will be discussed with respect to those obtained with the SC potential used in Ref. [16]. Since in that study most of the structural information on the ion-electron contact pair solvated in ammonia was not reported, the same calculation had been repeated.

Details of the Simulations

The PIMC calculation of an atom in ammonia was carried out at the same conditions of temperature, density and size of the simulation box as in the classical simulations discussed previously. To be more specific $T = 260$ K, $N = 250$ and $V = 26.5 \text{ cm}^3 \text{ mol}^{-1}$. With respect to the previous calculations of an excess electron in liquid ammonia, all the simulation parameters (such as electron discretization, potential cut-offs, definition of MC pass, etc.) remained unchanged.

Before the simulation was initiated the discretization of the electron ($P = P_a P_b = 1024$, $N_f = 100$) was checked against the reproducibility of the atomic spectroscopic term value. The calculated PIMC electron total energy for the isolated atom matched the experimental value within a few percent.

The initialization of the atom-ammonia system followed the lines of previous solvated electron simulations described in Chapters 4 and 5. A configuration taken from the calculations of the classical Li^+ ion was used as a starting point. The electron was inserted on the Li^+ in a compact state with $\mathcal{R}(\beta/2) \simeq 2 \text{ \AA}$. When the HC potential was used the beads of the primary chains were introduced just outside the core region, where the pseudopotential was strongly positive.

Both the simulations with a SC and HC pseudopotential were conducted following the same lines. Initially, the electron was allowed to adapt to the ion-ammonia potential field by moving the primary chain beads for

100 passes while the coordinates of the molecules were kept unchanged. The contemporaneous sampling of molecules and electron phase space followed. After 500 passes needed to equilibrate the solvent molecules around the Li atom, 2000 more passes of data acquisition and averaging were required to reach an acceptable stability of the energies.

Results

a. **Electron Wavefunction** At the end of the SC and HC simulations the electron was found in a compact state bound to the Li^+ . The complex time correlation functions are shown in Fig. 6.5. It is clear in this figure that the HC pseudopotential produces a larger spatial extension of the electron beads. The electron correlation lengths were found to be 2.34 Å and 3.21 Å respectively for the SC and HC calculations. These values compare with 4.02 Å of the solvated electron.

The two calculations found the Li atom in a dipolar state in which the electron center of mass was separated from the center of the ion by a certain distance ξ . The HC pseudopotential produced the largest atomic polarization with $\xi = 1.5 \text{ Å}$. This separation was $\xi = 0.54 \text{ Å}$ for the SC pseudopotential. If the center of the electronic charge is approximated by the center of mass of the beads the dipole moments resulting in the SC and HC calculations are respectively 2.6 D and 7.2 D.

The polarized Li atom obtained in the two simulations has been interpreted in the past as due to a dipolar excitonic state.[94] Accordingly,

the dipole moment of Li is a hybrid state formed by the superposition of $2s$ and $2p$ states. Simple arguments, based on the continuum dielectric theory, showed that the resulting polarization induced in the polar fluid is likely to stabilize this state against the energy increase produced by the hybridization.

Additional information about the size and, to a lesser extent, the shape of the electron wavefunctions can be gathered from the electron- Li^+ charge site pair correlation function. In Fig 6.6 the two functions relative to the SC and HC calculations are compared. It is clear from these curves that the HC model produces a much deeper penetration of the electron cloud into the Li solvation shells. As expected, the inner core becomes a region precluded to the electron. The peaks in the functions plotted in Fig. 6.6 indicate maxima in the electron wavefunction at the corresponding radial distances. The change in pseudopotentials does not seem to have a large effect on the position of these peaks.

b. Liquid Structure around the Li Atom The structure of the liquid ammonia in the region surrounding the Li atom (Li^+ plus electron) is best characterized by the Li^+ -ammonia and electron cm-ammonia pair correlation functions. In Figs. 6.7-6.10 these correlation functions, resulting from the SC and HC calculations, are plotted.

The large polarization of the Li atom caused by the HC pseudopotential is the cause of the intense first peak in the $g_{\text{Li}^+ \text{N}}(r)$ (comparable to

the one calculated from the simulation of the classical ion, see Fig. 6.2) which in turn is associated with a considerable ordering of the liquid in the vicinity of the ion. Much less intense (about one half) is the corresponding peak in the SC calculation. This can be explained by noticing that the orientation of the ammonia molecules in the Li first solvation shell favoured by the electron beads is opposed by the Li^+ and viceversa. These competing steric effects are curtailed when the ion and the electron beads are farther apart. Moreover, the presence of the electron on the Li^+ induces a decrease in the Li^+ coordination number. The SC and HC calculations yield respectively $n_N = 2$ and $n_N = 3$ which compares with $n_N = 4$ given by the calculation of the classical ion.

The integration of the two $r^2 g_{\text{Li}^+ \text{H}}(r)$'s in Fig. 6.8 shows that while the HC calculation gives a number of hydrogens in the Li^+ first shell very close to $3 \times n_N$, the SC simulation reveals a sizable penetration between first and second solvation shell. In the latter case the first coordinated hydrogens are 11 compared to the expected 7. The average angles θ defined in section 6.1.2 calculated with the two pseudopotentials are not significantly different from those of the classical ion.

The $g_{\text{cm}-\text{N}}(r)$'s and $g_{\text{cm}-\text{H}}(r)$'s in Figs. 6.9 and 6.10 show sharp and intense peaks in contrast with the results for the solvated electron. The less polarized Li atom obtained by the SC simulation yielded a $g_{\text{cm}-\text{N}}(r)$ which repeated most of the features of the corresponding correlation function for Li^+ . The same trend was observed for the $g_{\text{cm}-\text{H}}(r)$, but to a smaller extent.

These findings are to be related to the rather short distance separating the contact ion pair and to the small electron average diameter. As expected, the larger correlation length and polarization of the Li atom produced by the HC pseudopotential decreased the structural characteristics of the relative (cm-N) and (cm-H) correlation functions. This is particularly visible in the $g_{cm-H}(r)$. The coordination numbers found for the electron and Li^+ in the SC simulation were identical. Two ammonia molecules on average were coordinated to the electron. In the HC calculation, instead, the electron coordination number was about 4.

Further information on the orientational ordering of the ammonia molecules coordinated to the electron and Li^+ can be derived from the respective dipole correlation functions plotted in Figs. 6.11 and 6.12. Only the contributions from solvent molecules within 4 Å from the Li^+ or electron center of mass were included in the computation of these correlation functions. In both calculations, the ammonia molecules around the electron are seen to be influenced by the nearby Li^+ , this being the main cause of the sharp peak between 0.7 and 1.0 in Fig. 6.11. The weaker tail around -0.5 is instead due to a fraction of solvent molecules bond oriented towards the electron. The dipole correlation functions for Li^+ in Fig. 6.12 exhibit intense peaks at 1.0 corresponding to the dipole ordered $\theta = 0$. Only in the curve obtained from the SC calculation a weak tail for negative $\cos \theta$'s is visible.

Finally, a pictorial representation of the contact ion pair formed

upon immersion of the Li atom into liquid ammonia is given in Figs. 6.13 and 6.14. Here two instantaneous configurations representative, respectively, of the SC and HC calculations, are plotted.

6.2.3 Cs and Na in Liquid Ammonia

The PIMC simulations in the previous sections did not predict a spontaneous ionization of the Li atom in liquid ammonia. Although there is no direct experimental evidence to support these findings, it should be noticed that neutral Li may be stabilized at low temperature in solid ammonia.[95] In contrast, in the case of Na and heavier alkali metals experiments clearly indicate that they are ionized in liquid ammonia. The main objective of the following PIMC study has been to investigate whether or not the spontaneous ionization of Cs and Na can be observed in the simulations.

The physical conditions, the simulation parameters and the initialization procedures used in the following PIMC calculations on Cs and Na were identical to those previously specified for the Li calculations in section 6.1.2.

The Dipolar Cs Atom

In the case of Li the SC pseudopotential does not obstruct the excess electron to enter inside the ion core. This effect is expected to be even more marked for a larger ion where its bigger ionic radius prevents the ammonia molecules of the first solvation shell from getting closer to the excess

electron. In order to verify this supposition a simulation of the Cs atom using the SC potential in table 6.4 was performed. It was found that the SC pseudopotential promoted the formation of a contact ion pair $\text{Cs}^+\text{-e}^-$. The electron necklace localized at about 0.81 Å from the ion. This produces a dipole moment on the Cs of approximately 3.9 D. In Fig. 6.15 an instantaneous configuration from the PIMC simulation is presented.

The localized nature of the electron state is clearly seen in Fig. 6.16 where the $\mathcal{R}(t - t')$ is plotted. Its average correlation length, $\mathcal{R}(\hbar\beta/2) = 2.61$ Å, is very close to that given by the SC calculation on Li. The electron necklace exhibits a limited penetration in the first solvent sheath as shown by the drop to zero at 4.0 Å of the chain radial correlation function in Fig. 6.17.

The $(\text{Cs}^+\text{-N})$ and $(\text{Cs}^+\text{-H})$ pair correlation functions are plotted in Fig. 6.18. Here it is visible a decrease in intensity with respect to the results for the classical ion (compare with Figs. 7.3-4) due to electron screening. The $g_{\text{Cs}^+\text{-H}}(r)$ reveals a splitting in the first peak produced by two inequivalent hydrogens of the first solvent sheath. The angles θ corresponding to these peaks are -39° and $+37^\circ$. This splitting is responsible for the broad peak around $\cos\theta \simeq 0.8$ in the Cs-ammonia dipole correlation function plotted in Fig. 6.19. The cut-off for this function was set to 5 Å. The same function shows maxima for negative values of the X axis due to the ammonia molecules coordinated to the electron. The dipole correlation function relative to the center of mass of the electron plotted in Fig. 6.19 shows

similar characteristics. The coordination number of Cs is 10, unchanged from the results of the classical ion (see table 6.2).

The results for the (cm-N) and (cm-H) correlation functions plotted in Fig. 6.20 are not very different from those obtained in the Li simulation. Both of them have the same main peaks as those for the Cs^+ , but broader and less defined. The $g_{\text{cm-H}}(r)$ exhibits only a broad first peak: no splitting is found.

The conclusion from these results is that the SC pseudopotential does produce an unphysical localization of the electron necklace inside the Cs core. On this basis, it seems hopeless to expect a different behavior in liquid ammonia of the other alkali atoms, if a SC pseudopotential is used. Anticipating the findings of the next section, the HC pseudopotential is able, instead, to promote the spontaneous ionization of these atoms in liquid ammonia.

Ionization of Cs and Na

Since the contribution to the pseudopotential from the repulsive core is very marked in Na and Cs, the initialization of the respective simulations was carried out in a very cautious manner. The frozen electron necklace was inserted in the region outside the ion core and the solvent molecules were equilibrated for 200 passes. Then the polymer beads and molecules were allowed to relax.

For both atoms, the electron immediately expanded into the solvent

molecules and started to drift away from the ion. Such an ionization process occurred through the initial formation of an extended electron state which, after about 1000 passes, peaked to a correlation length of 15 Å and 12 Å respectively for Na and Cs. After 3000 more passes for Cs and 4000 more for Na, the process culminated in the creation of a solvated cation and a solvated electron. This mechanism of ionization involving a transient quasifree electron state is in agreement with what has been previously found in Ref. [16] regarding the induced ionization of Li in ammonia. As an examples of this intermediate stage, an instantaneous configuration taken from the Na calculation after 2000 passes is plotted in Fig. 6.21.

Three electron-Cs⁺ charge site correlation functions calculated at different stages of the simulation are presented in Fig. 6.22. This picture shows the maximum of the electron density drifting away from the Cs⁺ and localizing at about 11 Å from it. Similar results were obtained for Na, in this case the electron localized at about 14 Å from the Na⁺.

In conclusion, it must be pointed out that the HC model used in this chapter seems to be basically sound. In fact, in agreement with the experimental evidence it predicts the spontaneous ionization of Na and Cs in liquid ammonia.

Table 6.1: Ion-Ammonia Lennard-Jones Parameters

	Li ⁺	Na ⁺	Cs ⁺
ϵ (KJ mol ⁻¹)	5.5	7.0	14.0
σ (Å)	2.07	2.20	2.90

Table 6.2: Structural Data

	$r(\text{I-N})$ (Å)	$r(\text{I-H})$ (Å)	θ (degree)	n_N	n_H
Li ⁺	2.05	2.62	3	4	12'
Na ⁺	2.25	2.77	1	5	15
Cs ⁺	3.15	3.37	18	10	35

Table 6.3: Energetics of Ionic Solvation

	$\langle E_R \rangle$	$\langle E_C \rangle$	$\langle E_D \rangle$	$\langle E_T \rangle$	$\langle \Delta E_S \rangle$
Li ⁺	1.19	-3.44	0.01	-3.43	-2.24 \pm 0.01
Na ⁺	1.24	-3.29	-0.08	-3.37	-2.13 \pm 0.01
Cs ⁺	1.00	-2.30	-0.61	-2.91	-1.91 \pm 0.01

$\langle E_R \rangle$ is the reorganization energy of the liquid, $\langle E_C \rangle$, $\langle E_D \rangle$ and $\langle E_T \rangle$ are respectively the Coulombic, Lennard-Jones and total energies of the ion. $\langle \Delta E_S \rangle$ is the solvation energy. Energies are in KJ mol⁻¹.

Table 6.4: Parameters of the soft and hard core pseudopotentials

	R_c	A_0	γ_0
Li^+	2.885	2233	6
Na^+	3.482	6820	6
Cs^+	4.887	1.309×10^6	6

R_c is defined in Eq. 4.3, while A_0 and γ_0 are defined in Eq. 6.2. All data are in atomic units.

Figure 6.1:

Molar conductivity Λ of sodium ammonia solutions at $T = 240$ K and $p = 1$ bar.

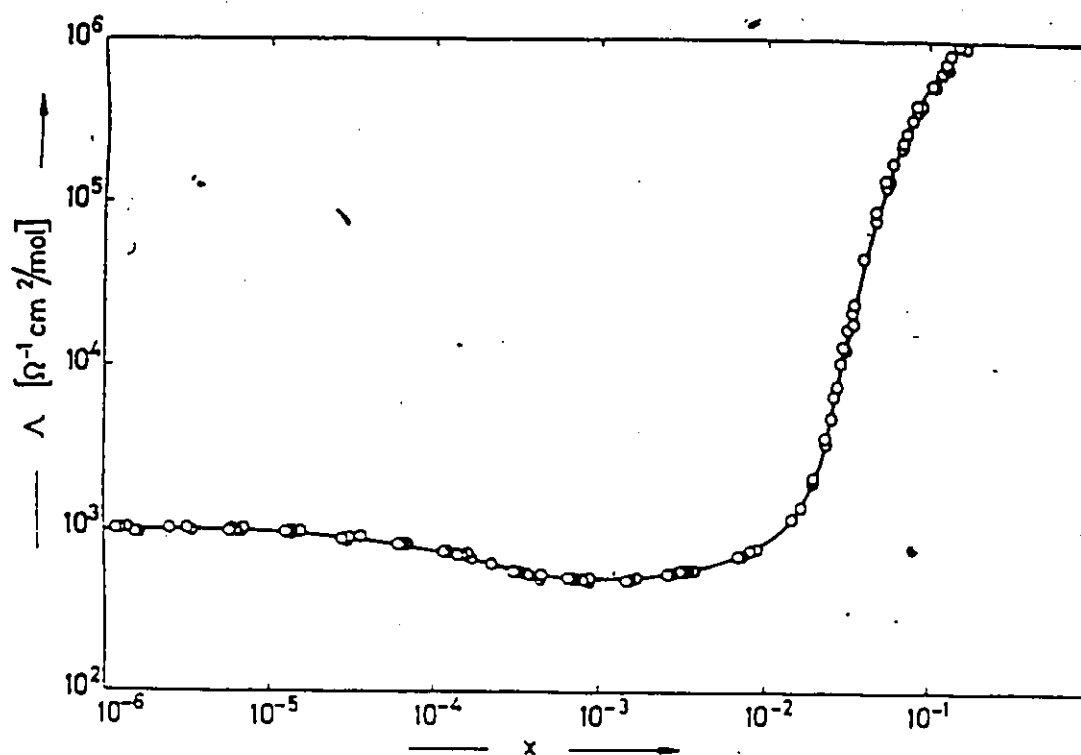


Figure 6.2:

Distribution functions for the solvent nitrogen atoms with respect to Li^+ , Na^+ and Cs^+ .

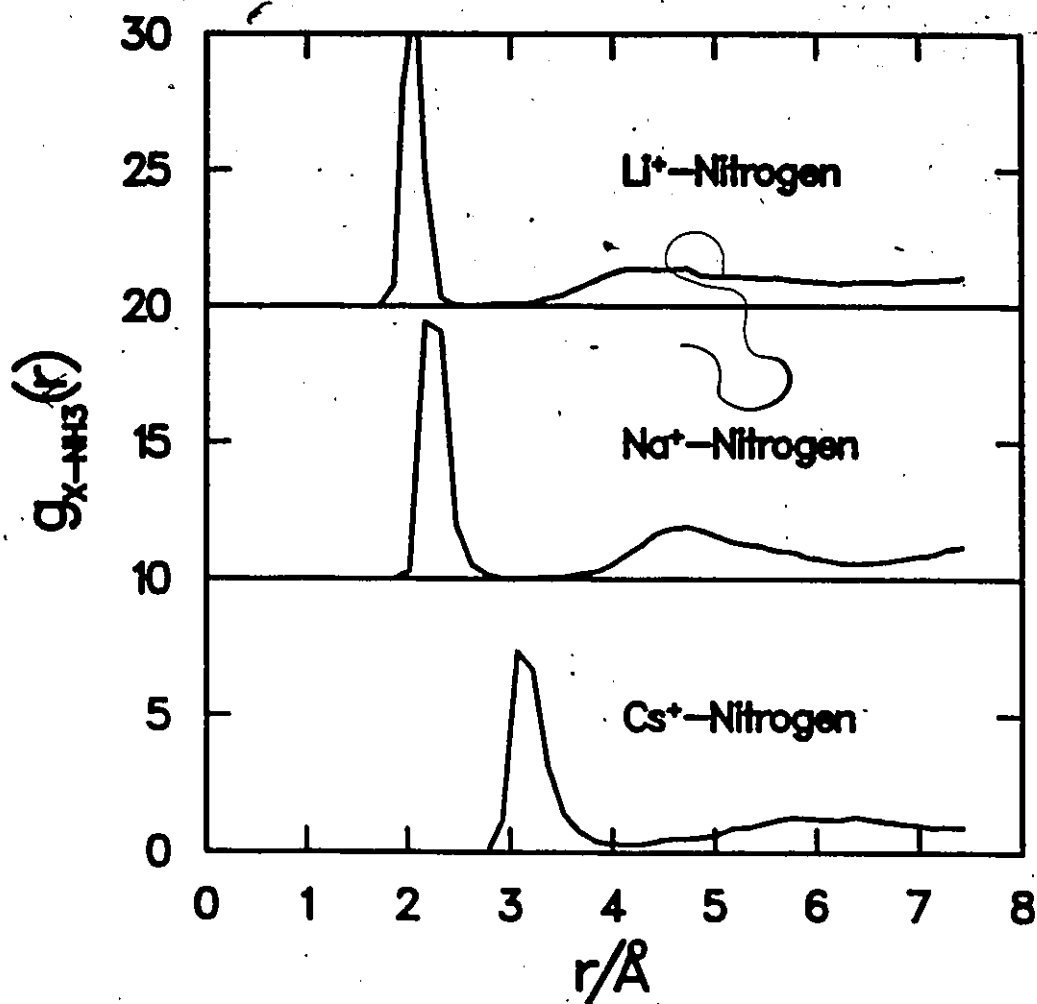


Figure 6.3:

Distribution functions for the solvent hydrogen atoms with respect to Li^+ , Na^+ and Cs^+ .

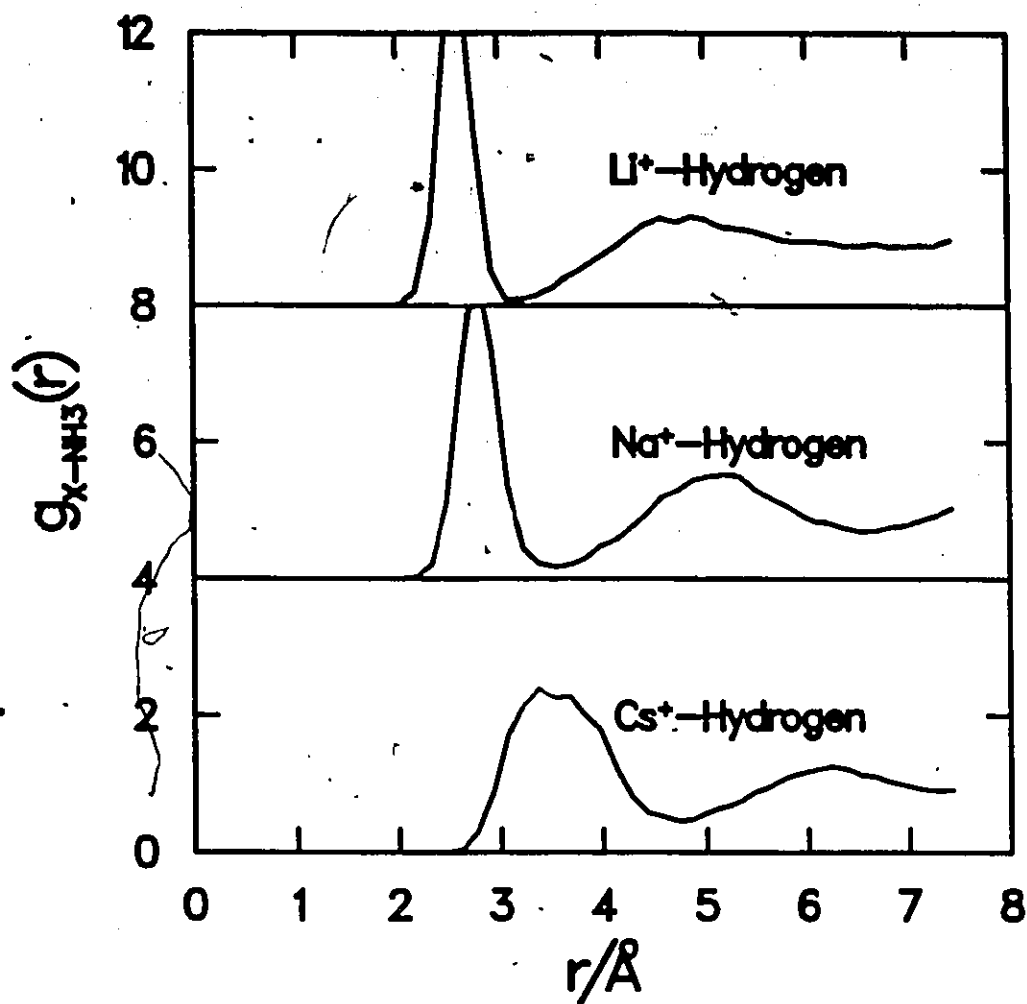


Figure 6.4:

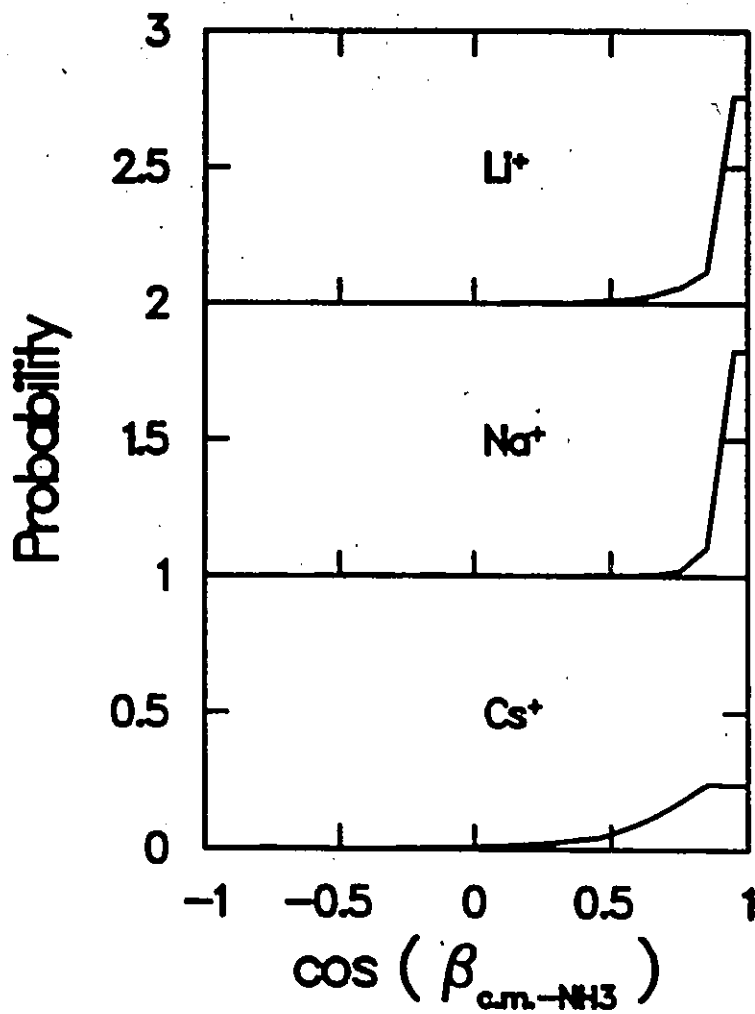
Dipole correlation functions for Li^+ , Na^+ and Cs^+ .

Figure 6.5:

Complex time correlation functions for the electron bound to Li^+ obtained using the Li soft core and hard core pseudopotentials.

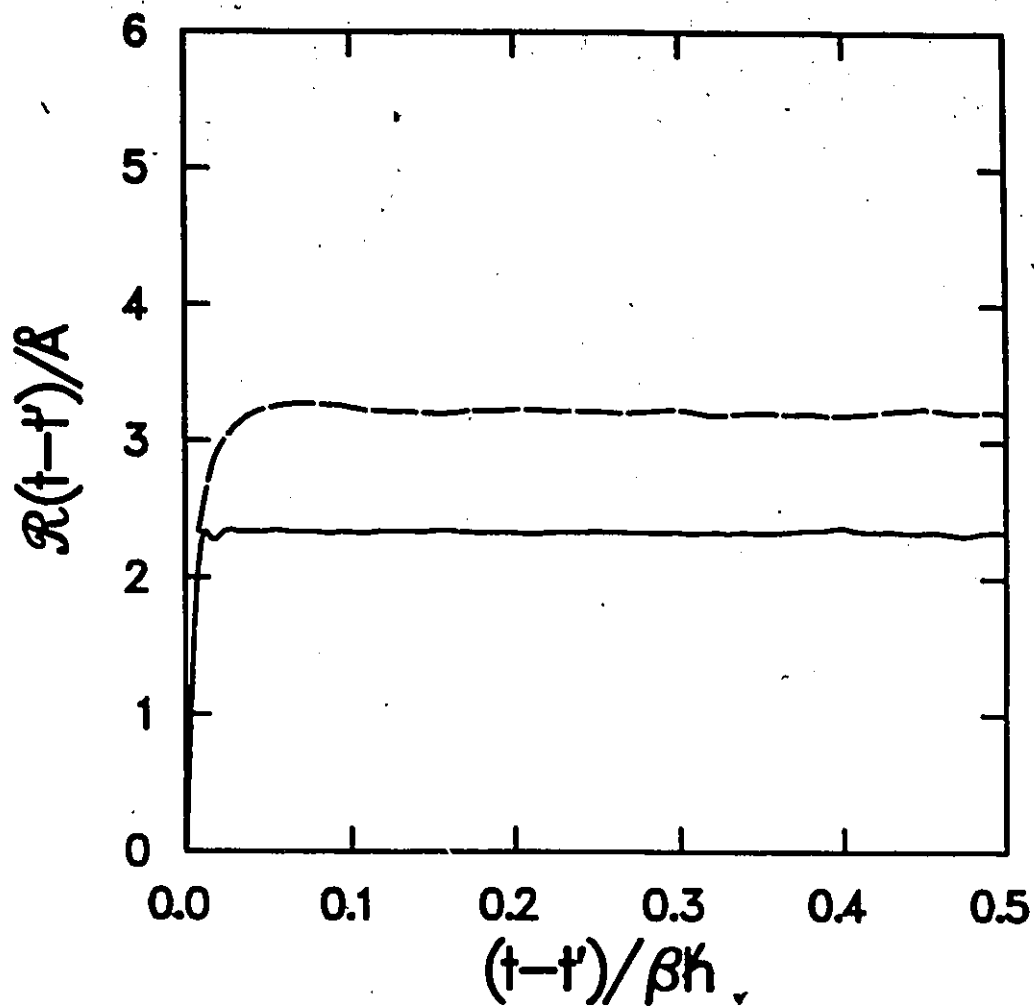


Figure 6.6:

Electron- Li^+ charge site correlation functions obtained from the PIMC calculation carried out using the Li soft core and hard core pseudopotentials.

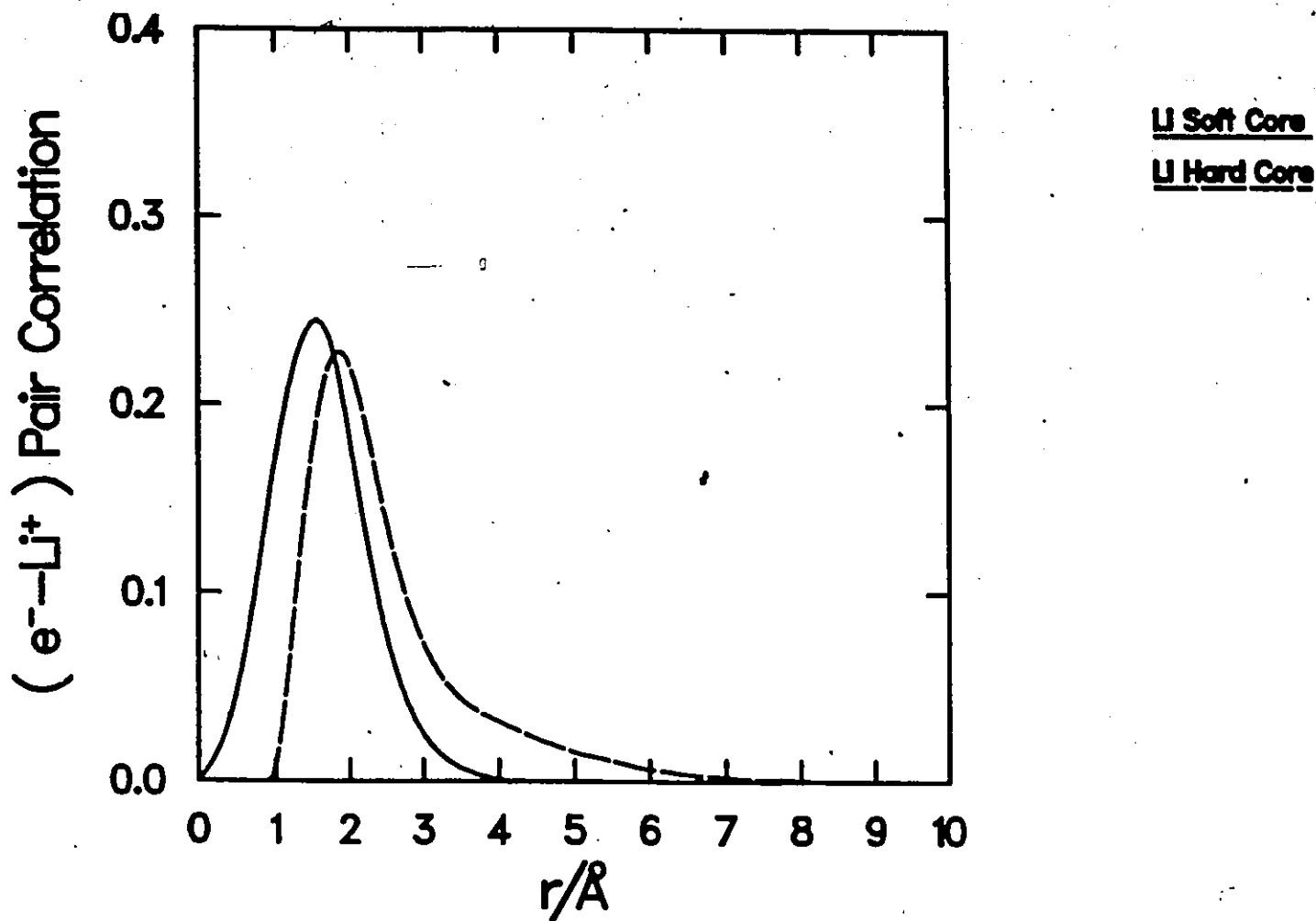


Figure 6.7:

(Li-N) pair correlation functions for Li in liquid ammonia obtained using the Li soft core and hard core pseudopotentials.

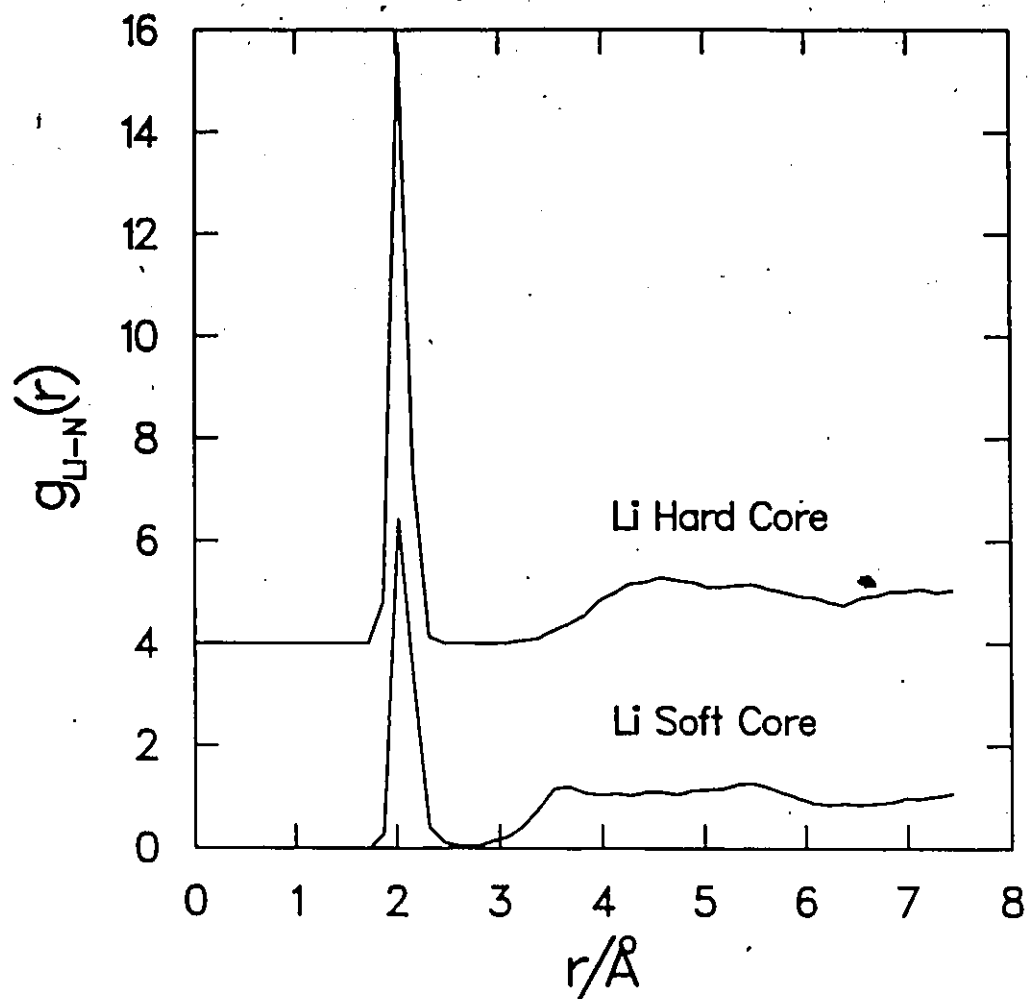


Figure 6.8:

(Li-H) pair correlation functions for Li in liquid ammonia obtained using the Li soft core and hard core pseudopotentials.

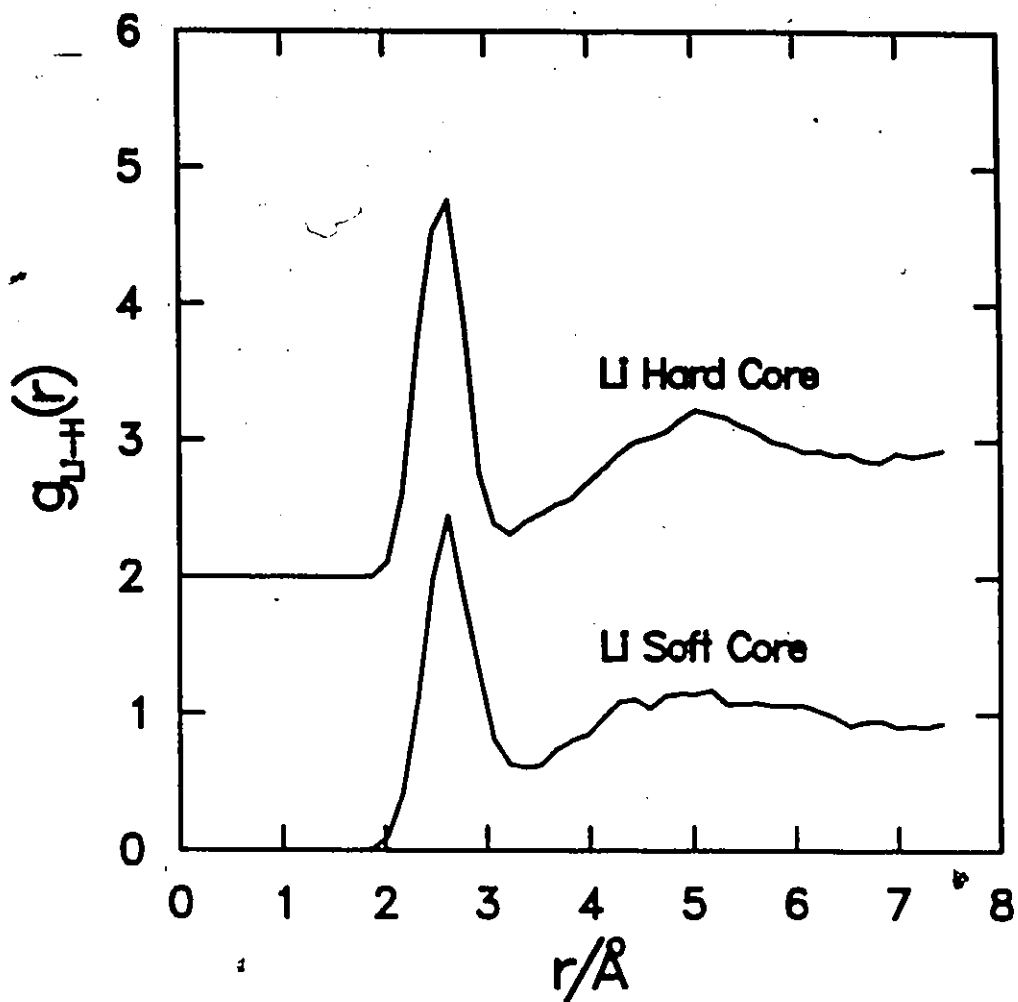


Figure 6.9:

Pair radial correlation functions for nitrogen atoms with respect to the electron center of mass obtained using the Li soft core and hard core pseudopotentials.

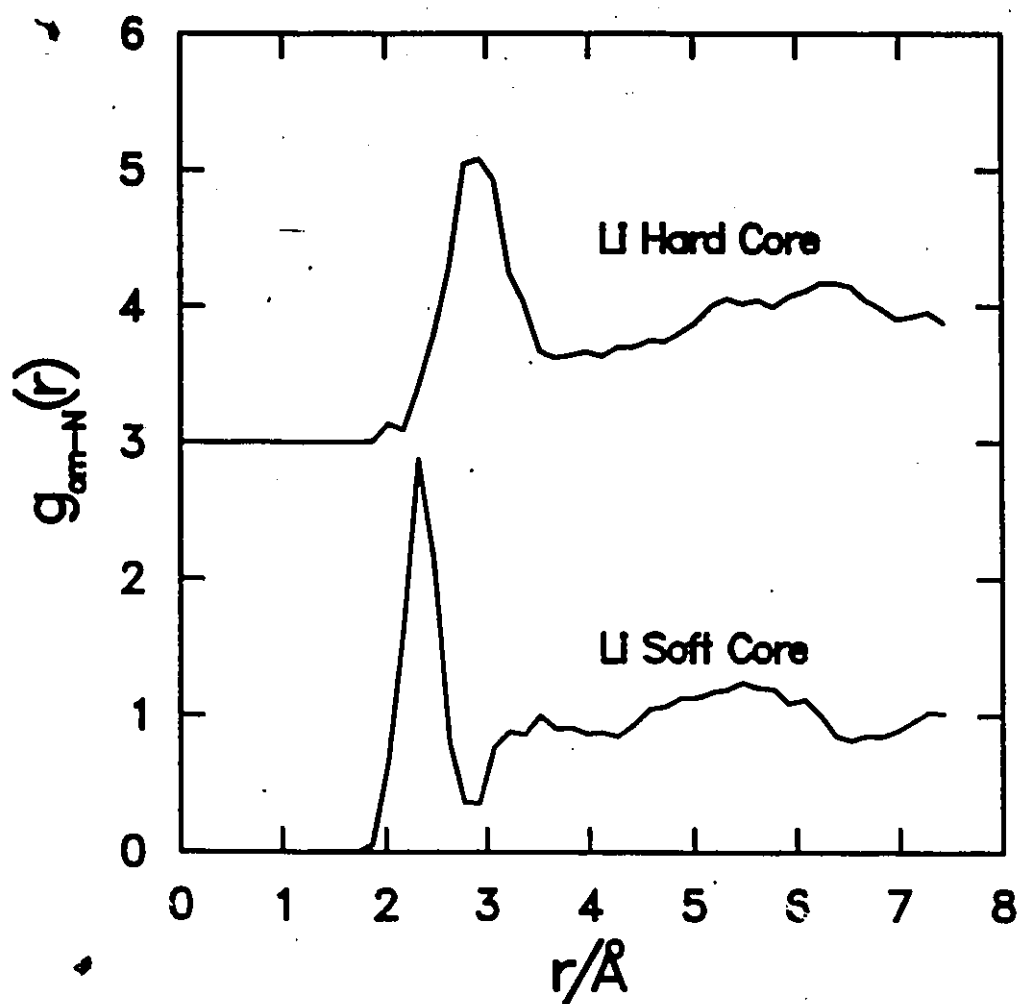


Figure 6.10:

Pair radial correlation functions for hydrogen atoms with respect to the electron center of mass obtained using the Li soft core and hard core pseudopotentials.

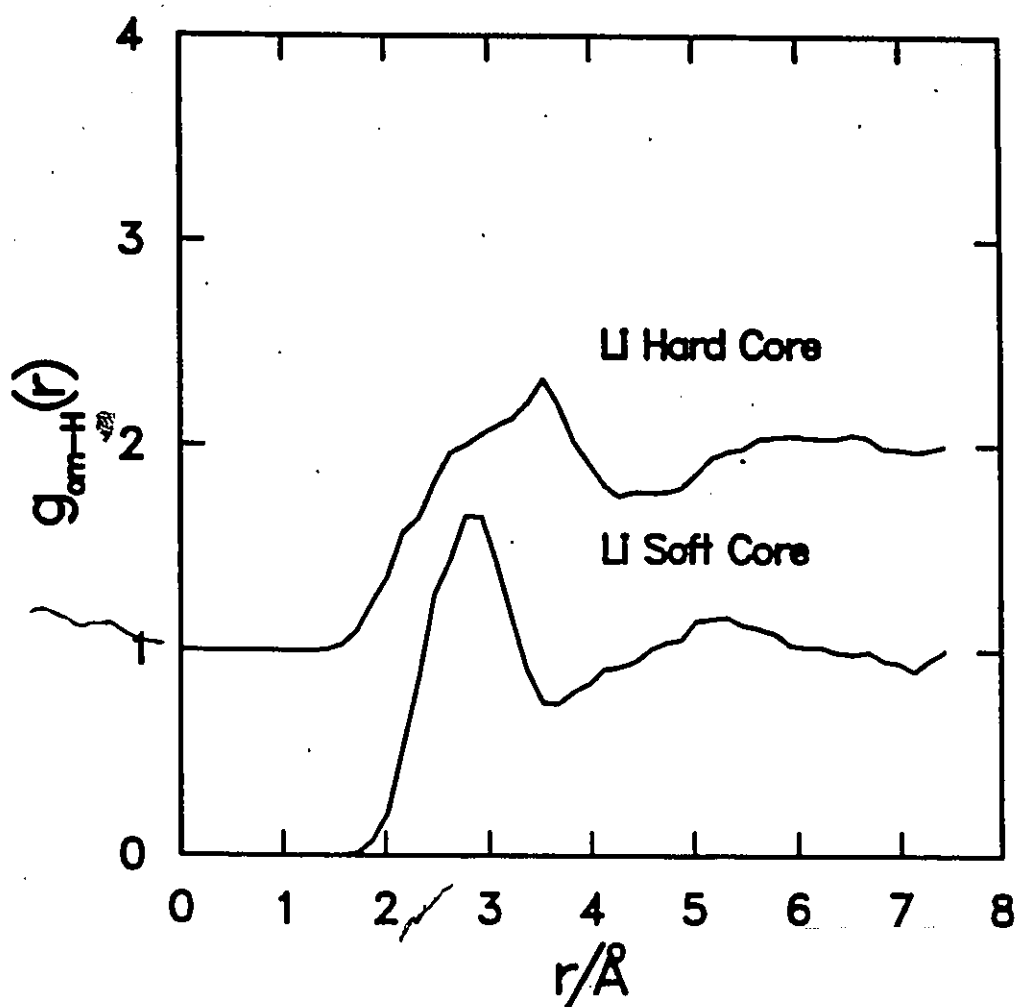


Figure 6.11:

Electron-ammonia dipole correlation functions obtained using the Li soft core and hard core pseudopotentials.

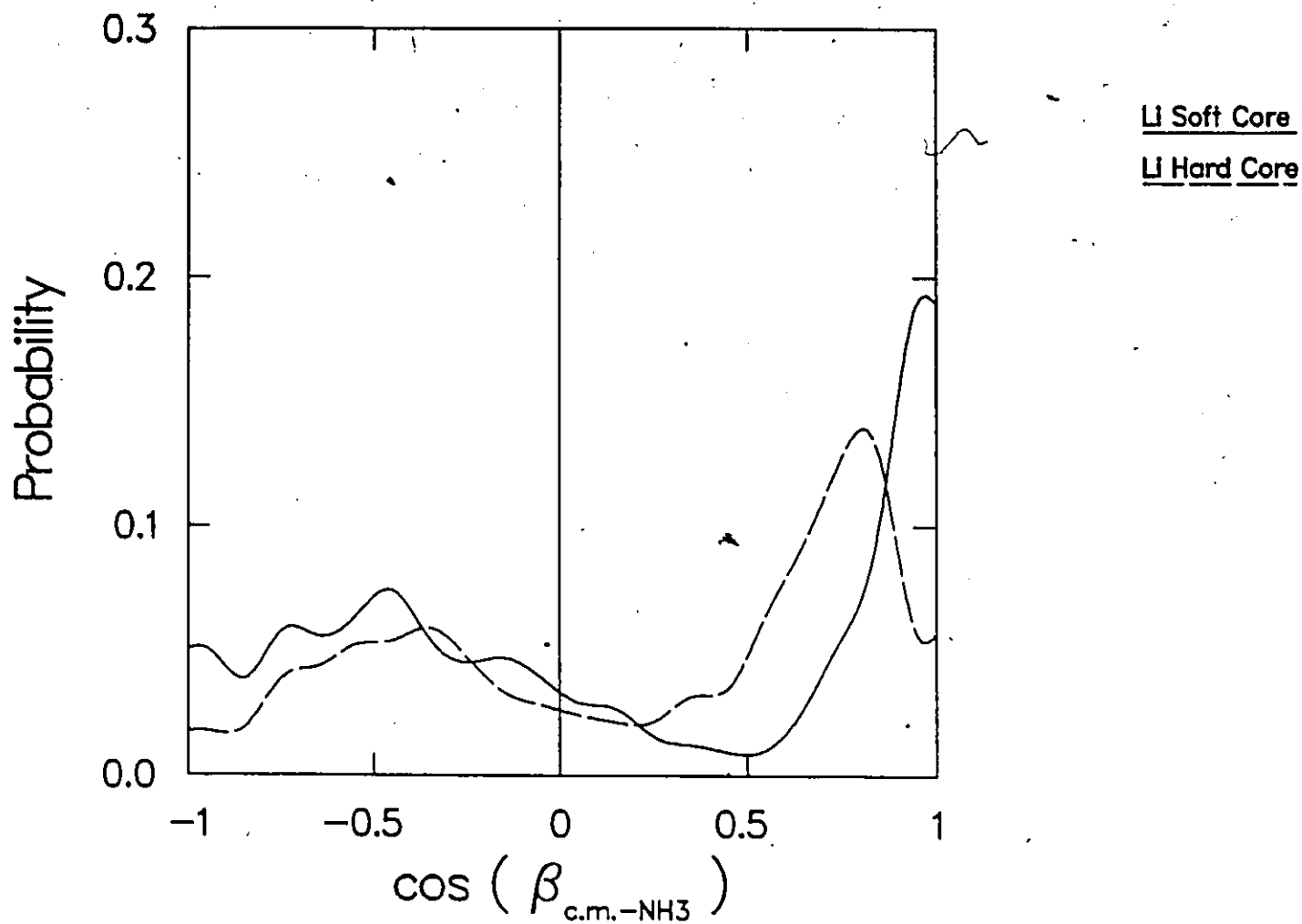


Figure 6.12:

(Li⁺-NH₃) dipole correlation functions obtained using the Li soft core and hard core pseudopotentials.

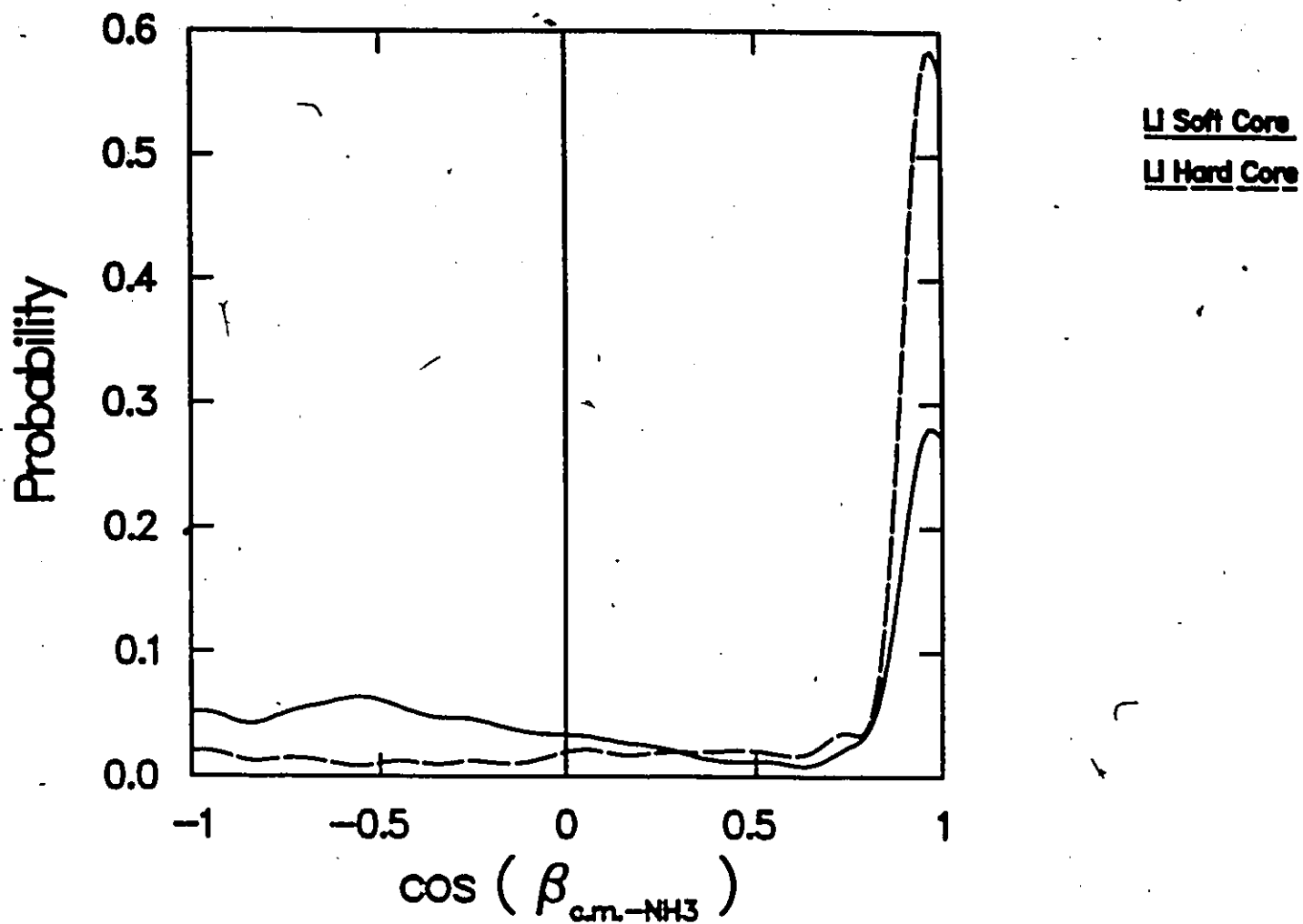


Figure 6.13:

Instantaneous configuration for the contact ion pair ($\text{Li}^+ - \text{e}^-$) from the Li soft core simulation. For graphic reasons, only one out of four primary chain beads is plotted. The Li ion is shaded. The corners of the box are 11.4 Å.

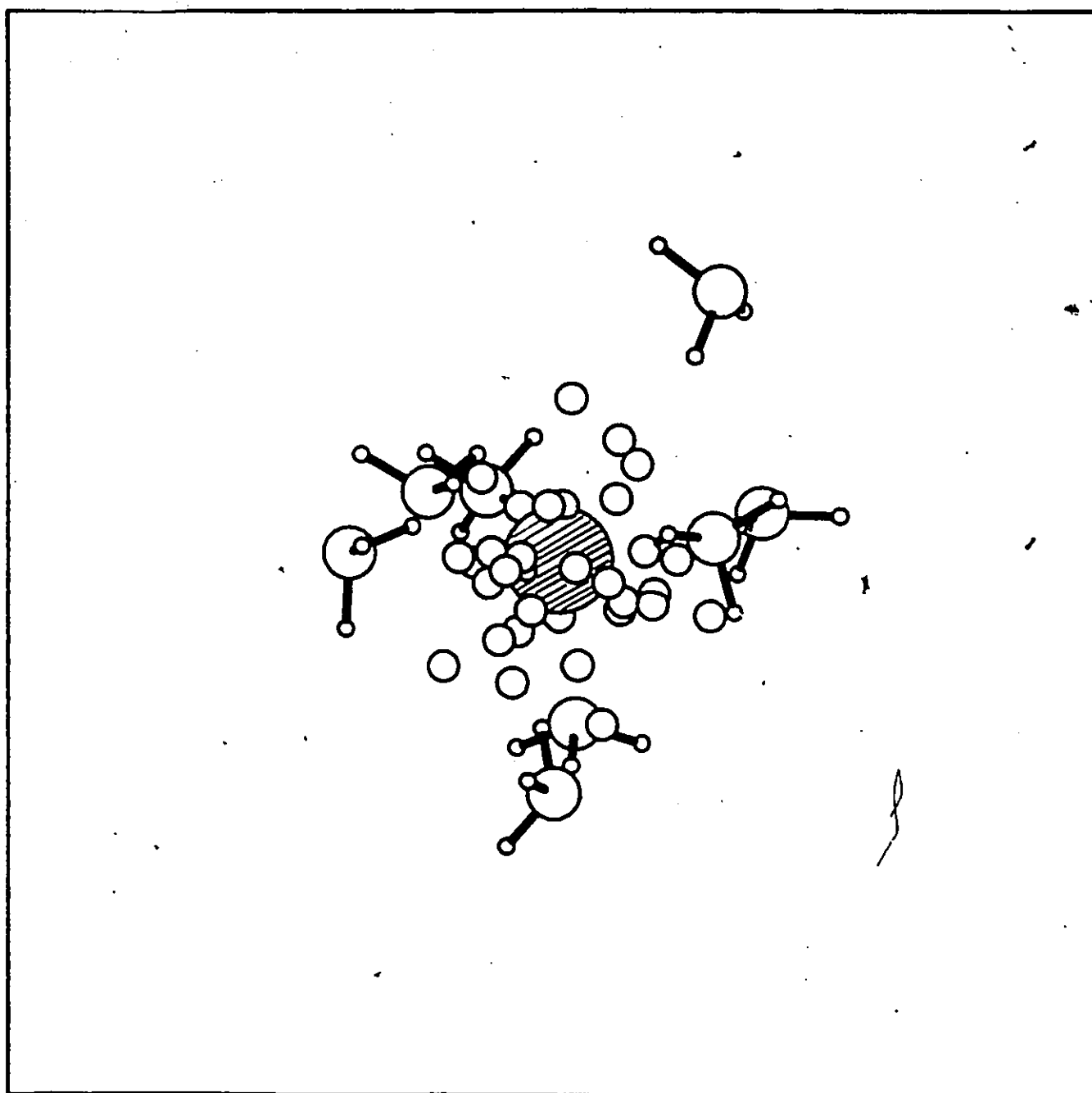


Figure 6.14:

Instantaneous configuration for the contact ion pair ($\text{Li}^+ \cdot \text{e}^-$) from the hard core Li simulation. For graphic reasons, only one out of two primary chain beads is plotted. The Li ion is shaded. The corners of the box are 16.4 Å.

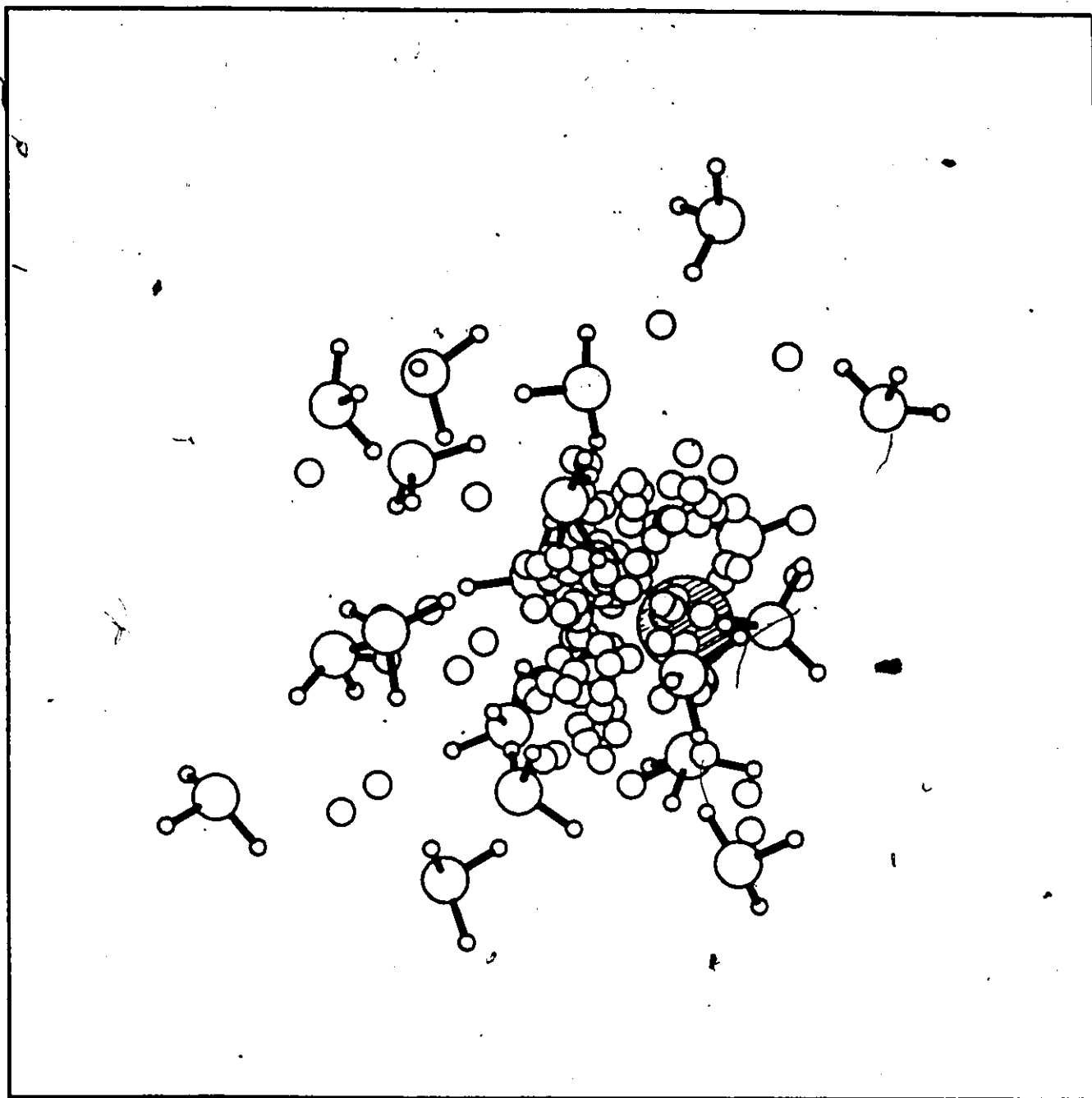


Figure 6.15:

Instantaneous configuration for the contact ion pair ($\text{Cs}^+ \cdot \text{e}^-$) from the soft core Cs simulation. For graphic reasons, only one out of four primary chain beads is plotted. The Cs ion is shaded. The corners of the box are 11.4 Å.

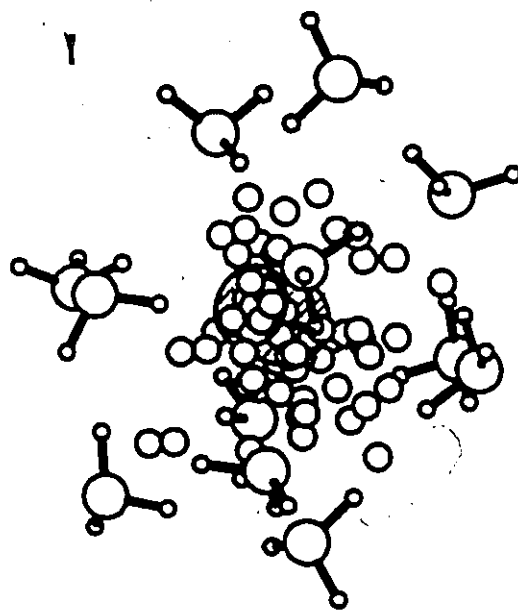


Figure 6.16:

Complex time correlation function of the electron bound to Cs^+ obtained using the Cs soft core pseudopotential.

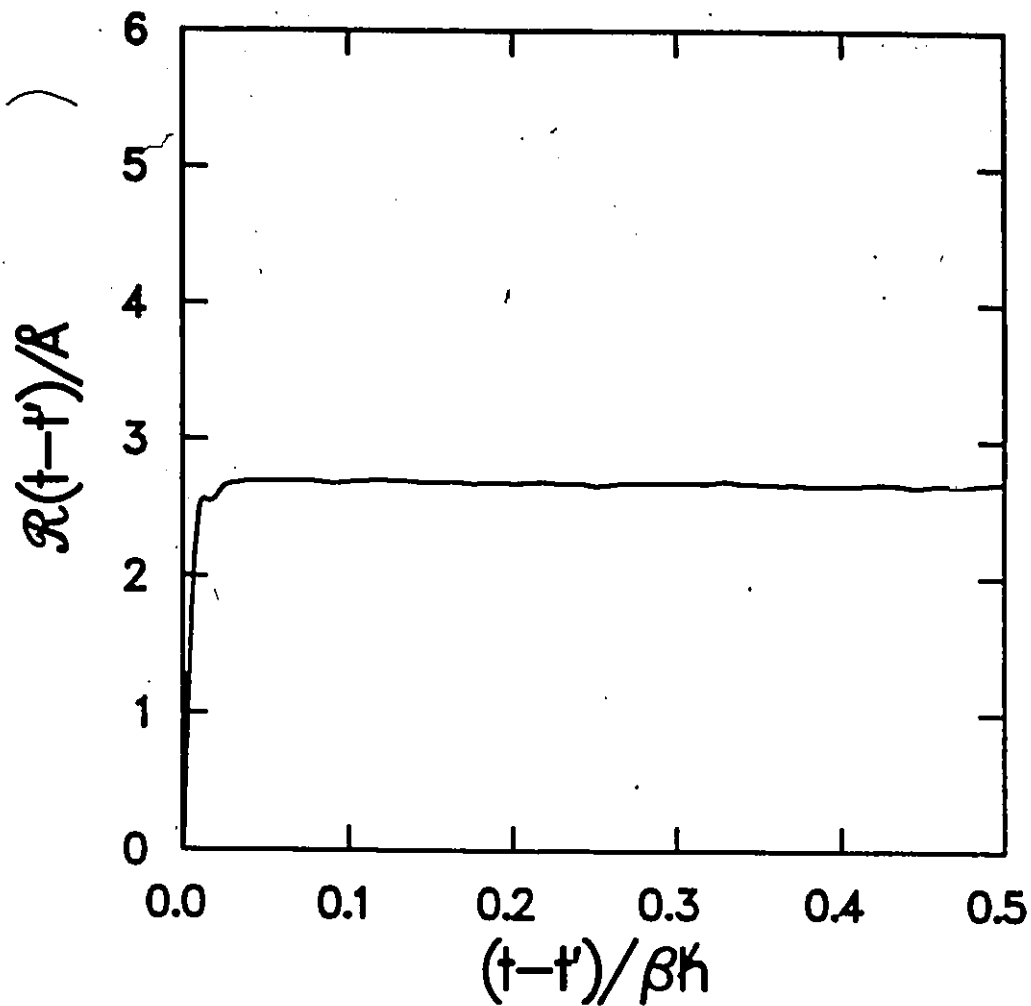


Figure 6.17:

Chain radial correlation function of the electron polymer with respect to the Cs ion calculated using the Cs soft core pseudopotential.

Fig. 6.18 Cs-Site Chain Correlation Function

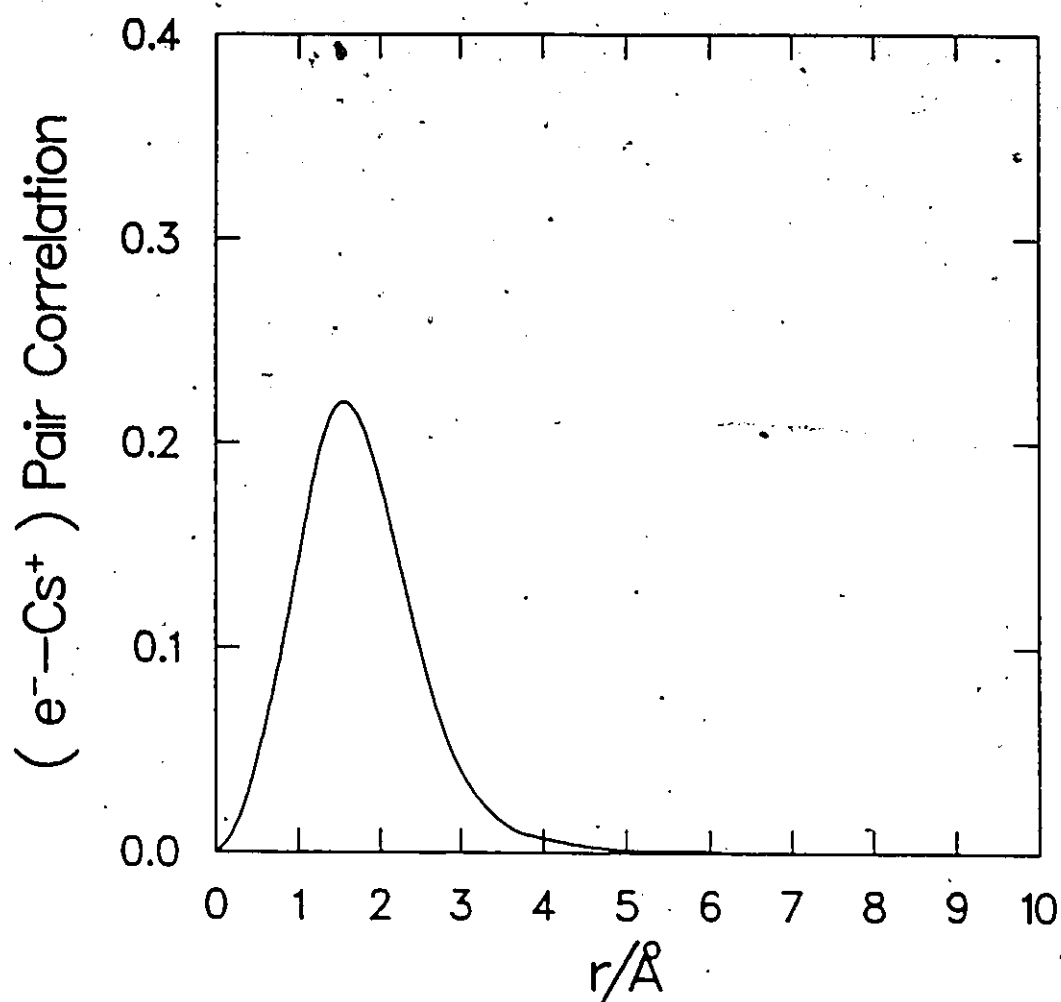


Figure 6.18:

Distribution functions for the solvent nitrogen and hydrogen atoms with respect to the Cs ion using the Cs soft core pseudopotential.

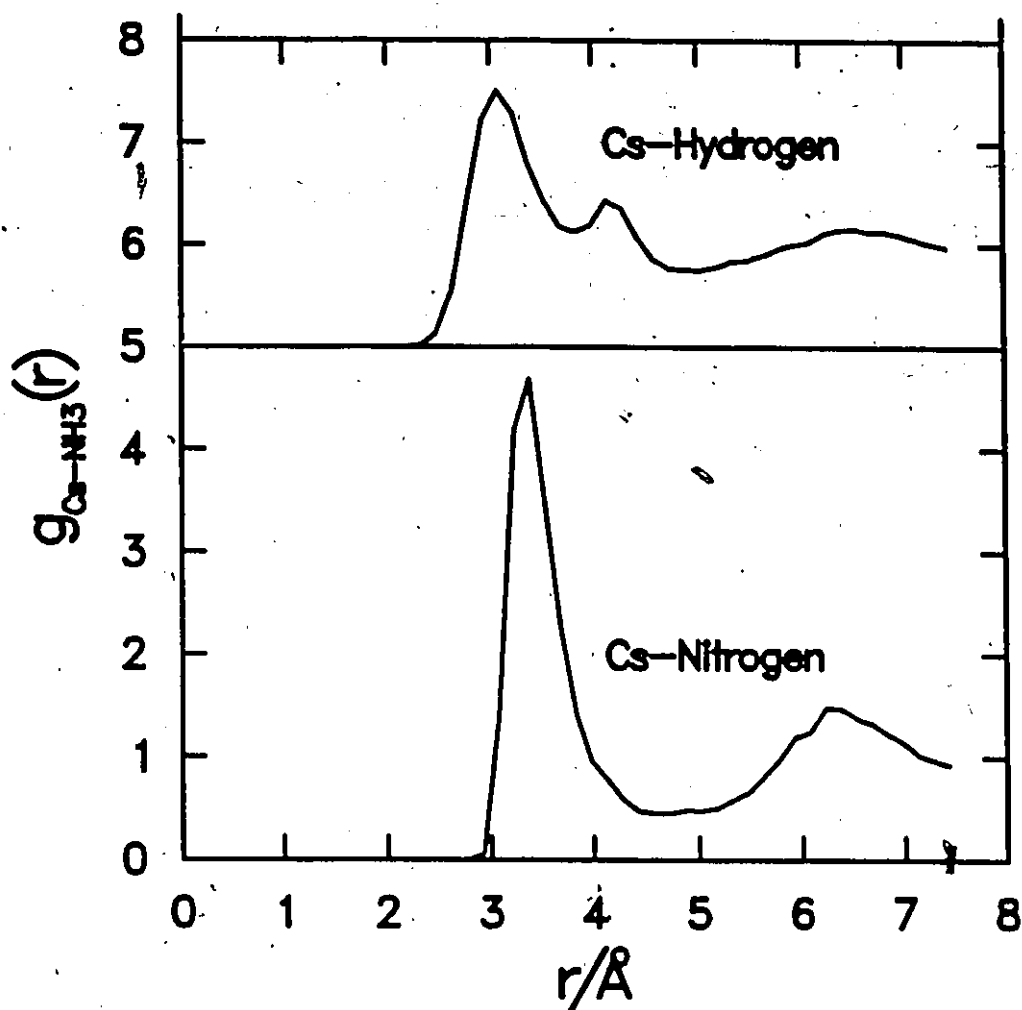


Figure 6.19:

Cs-ammonia dipole correlation function from the SC Cs simulation.

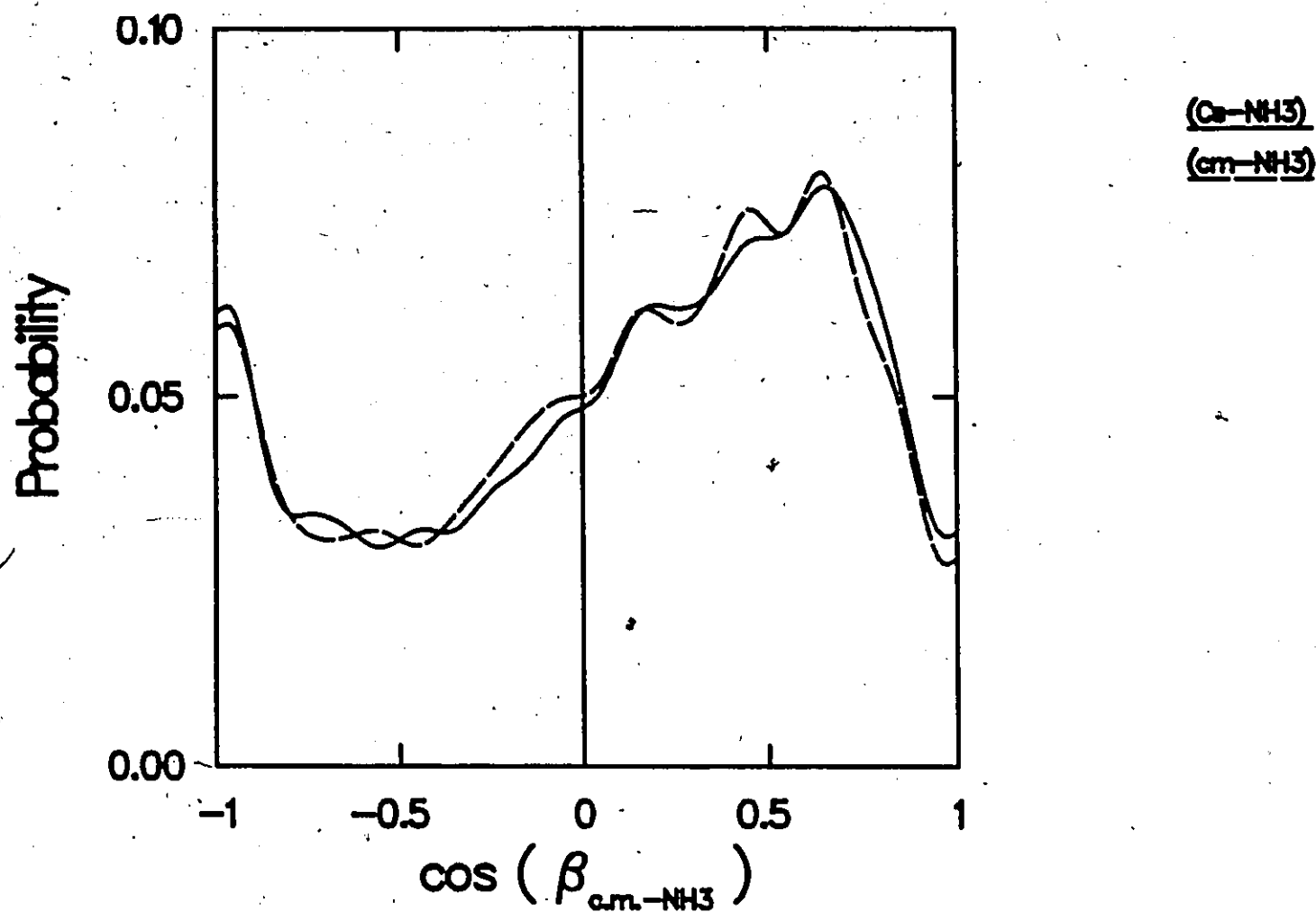


Figure 6.20:

Distribution functions for the solvent nitrogen (N) and hydrogen (H) atoms with respect to the electron center of mass using the Cs soft core pseudopotential.

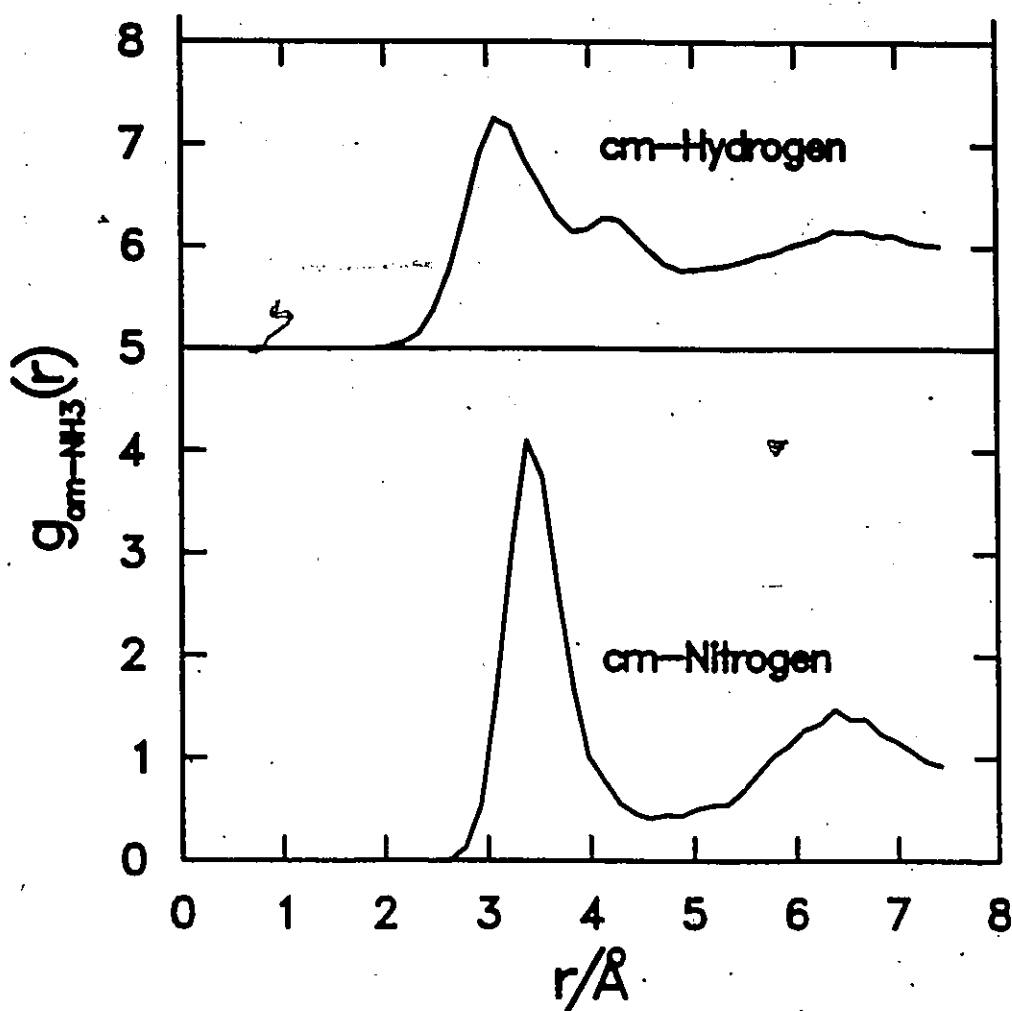


Figure 6.21:

Instantaneous configuration for the contact ion pair ($\text{Na}^+ \cdot \text{e}^-$) from the Na hard core simulation. Only the primary chain beads are plotted. The Na ion is shaded. The corners of the box are 32.2 Å.

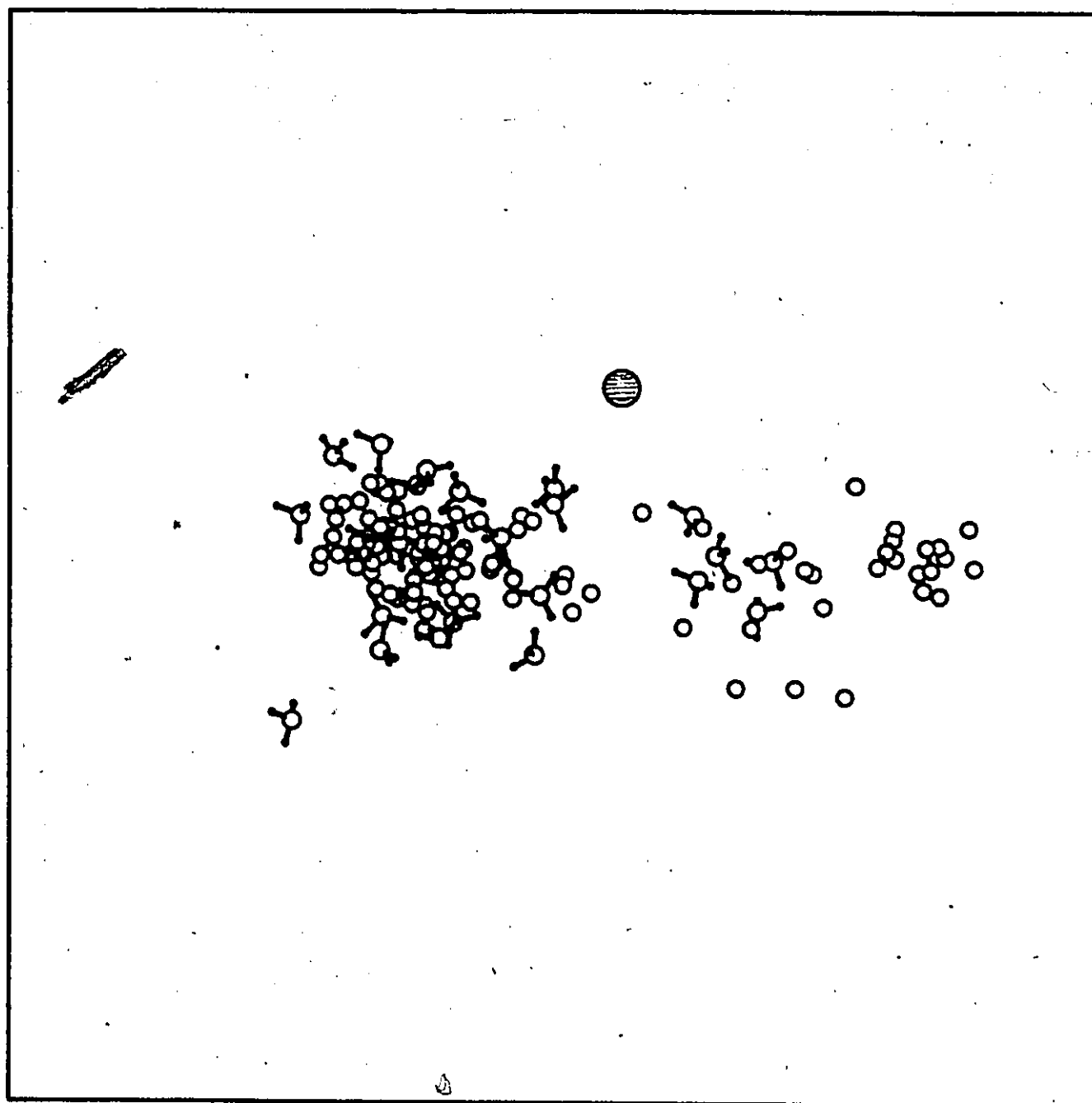
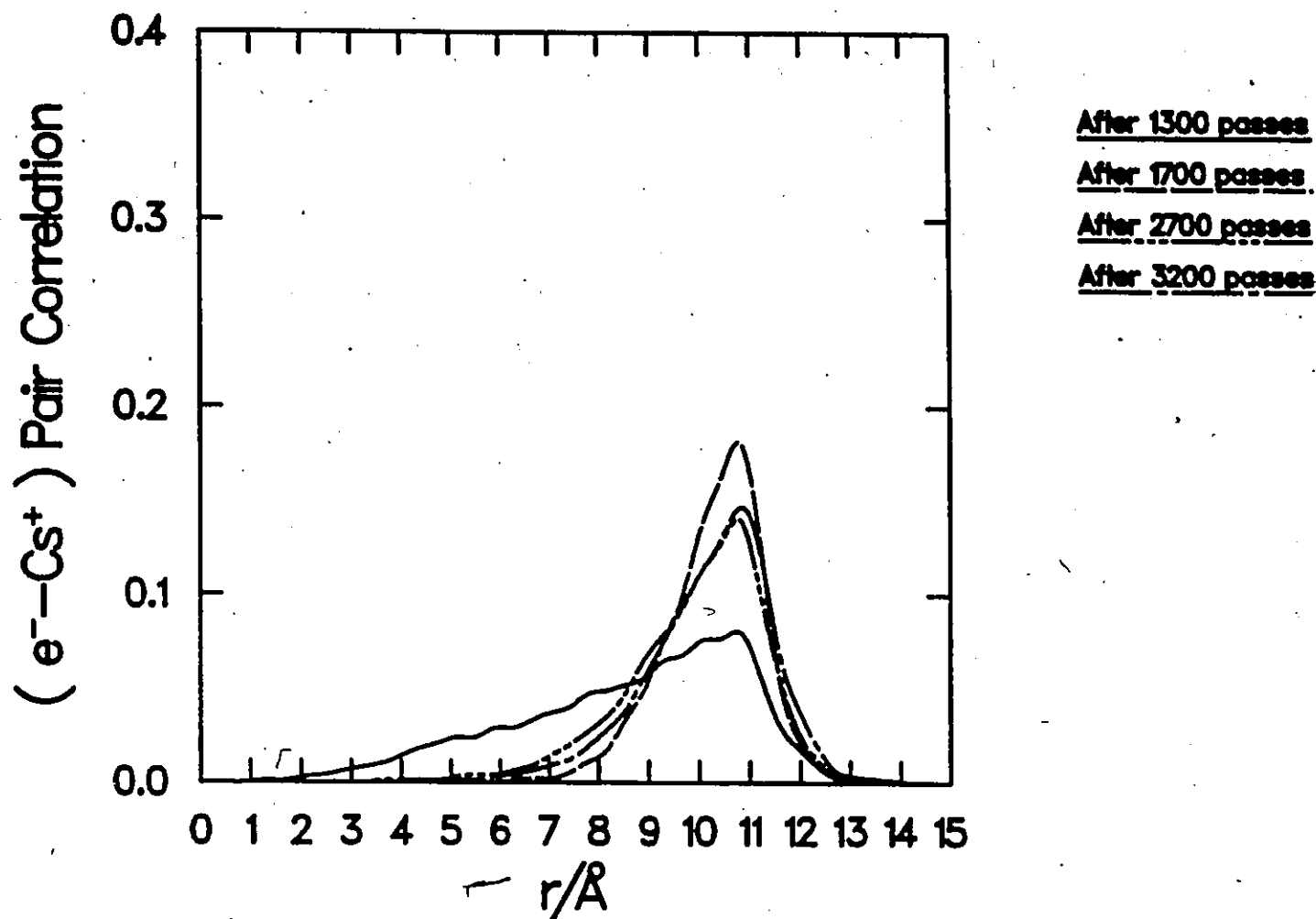


Figure 6.22:

Electron-Cs ion charge site correlation function at different stages of the simulation carried out using the Cs hard core pseudopotential.



Chapter 7

Electron Attachment to Ammonia Clusters

Negatively charged ammonia and water clusters have been recently discovered by injecting low-energy electrons into supersonic expansions of NH_3 and H_2O . [96,24,97,98,25] About 18 water and 30 ammonia are required to bind an electron. These new findings have stimulated many theoretical investigations regarding the mechanism of electron attachment to clusters.

Water clusters in particular have been the center of most of these studies. Most noticeably, a series of articles by Landman et al. [99,66,100,101,102] have appeared recently which used path integral molecular dynamics to explore $(\text{H}_2\text{O})_n^-$ for $n = (8-132)$. [66] This investigation agrees with the experimental evidence that electron attachment in water clusters is not energetically favoured for $n < 18$. Landman et al.

found that for intermediate sizes ($n = 18 - 32$) the electron is bound to the cluster through a surface state. Here a sufficiently large dipole moment of the cluster develops in order to create the bound state. In larger clusters, $n = 64, 128$, the formation of an internally bound electronic state is favoured over a surface state.

The electron affinity of small ammonia clusters has recently been discussed using a dielectric continuum model.[103] In this theory the electron moves in an average potential energy, which correspond to the bottom of the conduction band of the liquid ammonia, and in an additional attractive potential field due to the polarization induced on the ammonia molecules. This theory predicts the localization of the excess electron inside the cluster for $n > 30$. Such a result is in contrast with the mechanism of electron attachment through the surface state found for medium size water clusters. The calculations described in this chapter was undertaken in order to test this explanation of the experimental data.

7.1 Preparation of the clusters

7.1.1 Neutral Clusters

Calculations were carried out on 3 neutral clusters composed of 16, 36 and 54 ammonia molecules each. The initial configurations for the systems were chosen by randomly distributing the molecules around the center of a box with 30 Å edges, maintaining the cluster density close to that of the liquid.

Standard classical MC simulations were conducted for few hundreds passes, where a pass involves an attempted move of the center of mass and the orientation of all molecules in the cluster. The maximum displacement for the coordinates was adjusted to obtain an approximate acceptance rate between 30 – 40%. As in the other studies of this thesis, the orientations of the molecules were sampled using quaternions.

After this first initial equilibration stage, the simulations were run for an additional few thousand passes. During this period, information about the structure and pair correlation functions of the clusters were accumulated. In particular, it was important to know if the molecules in the clusters were in a frozen or liquid state. Each of the two possibilities implies a different strategy to be followed in order to determine the ground state energies.[66]

All through this initial stage of the simulations the evolution of the molecular center of mass mean square displacement, D^l , was followed. Its steady increase during the simulation showed that the cluster studied was liquid. D^l is defined by

$$D^l = \frac{1}{N} \left\langle \sum_{j=1}^N [R_j^l - R_j^0]^2 \right\rangle \quad (7.1)$$

where R_j^l is the position of the j -th molecule center of mass at the l -th MC pass and N is the number of molecules.

After the equilibration period the calculations were carried on in order to accumulate averages. Intermediate results were used to check for convergence during the runs. Generally, after $\simeq 30,000$ passes the

simulation converged in the sense that the total molecular potential energy reached a stable value.

7.1.2 Charged Clusters

The composite electron-cluster system was studied using the same simulation technique and similar interaction potentials as in the previous studies in this thesis. The number of beads in the primary chain and each secondary chain configuration were respectively $P_a = 256$ and $P_b = 8$. Accordingly, the total electron discretization was $P = P_a P_b = 2048$. The weight of a link connecting two adjacent beads of the primary chain were evaluated from the contributions of 100 distinct secondary chain configurations. Each MC pass involved the attempted move of all beads in the primary chain with the corresponding sampling of the secondary chains and, several times ($5 \div 10$), the totality of ammonia molecules.

For all the clusters, the simulations commenced from a localized internal electronic configurations. When the cluster showed an apparent stable trapped interior state, additional runs were performed starting from an exterior state for which the electron necklace was initially outside the cluster boundaries.

The starting configuration for the interior state was produced by running a classical MC simulation for the ammonia cluster and a negative ion of charge $1e^-$. A Lennard-Jones potential, with $\sigma = 2.0 \text{ \AA}$ and $\epsilon = 5.5 \text{ kJ mol}^{-1}$, for the nitrogen-ion interaction was employed. This potential

produces a cavity with a diameter of about 4 Å in the center of the cluster.

After few thousands MC passes of equilibration, the negative ion was replaced by a configuration of primary chain beads distributed according to a Gaussian of width 3 Å. For about 50 passes the electron was allowed to expand while the cluster molecules were held stationary. Next, the electron polymer was frozen and the molecules were moved for a few more passes (≈ 100). Finally, the simultaneous sampling of the electronic and molecular phase space was initiated.

The simulations were carried out until the size of the electron necklace appeared stable. Then averages were accumulated until the convergence of the electron plus cluster energy was achieved. Typical equilibration and acquisition periods were respectively 5000 – 9000 and 3000 passes. Long equilibration runs were needed for the $N = 16$ and 36 clusters because the starting configuration collapsed and the electron escaped from the interior of the cluster.

The exterior state was set up by choosing a configuration of electron beads from a Gaussian distribution with width ~ 3 Å and placing the necklace beside an equilibrated neutral cluster. The center of mass of the electron necklace was located at about 2 Å from the outermost ammonia molecule of the cluster. The composite system was then run for about 3000 passes for equilibration and about 2000 more to accumulate statistics.

7.2 Structural Properties

7.2.1 Neutral Clusters

At first, some preliminary calculations were performed on the three neutral clusters with $N = 16, 36$ and 54 at 200 K . In all three cases the ammonia molecules immediately started to escape from the clusters. This observation is perhaps not too surprising since the triple point of ammonia is 196 K . In order to see if the presence of an electron could enhance stability of such clusters, attempts were made to study the negatively charged cluster states starting from an interior as described above. In each case the ammonia clusters broke apart and hence were not stable at 200 K .

Next, the temperature was lowered to 100 K and the neutral clusters were studied again. This time they did not disintegrate but showed liquid-like behaviour in the sense that D^1 increased steadily during the simulations.

In Fig. 7.1 the nitrogen-nitrogen pair correlation function of the three neutral clusters is compared to that of the bulk liquid ammonia at 260 K and molar volume of $25.3\text{ cm}^3\text{ mol}^{-1}$. The narrowing and compression of the first neighbour peak in the cluster compared to the liquid is largely due to their lower temperature. With the decrease of N , there is a gradual disappearance of structure in the $g(r)$'s after the first peak.

7.2.2 Charged Clusters

The calculations for the two smaller negatively charged clusters at 100 K showed that they maintained liquid-like structure very similar to that of the neutral clusters. The reason is that, unlike for the larger $N = 54$ cluster, no stable interior solvated state is formed, when the simulation is started from an interior state prepared as described above. The cavity inside the $N = 16$ and $N = 36$ clusters, which initially contained the electron polymer, collapses and the electron escapes to the outside. Only for the $N = 54$ cluster did the electron polymer remain trapped for the entire length of the simulation.

A convenient way to characterize the various configurations of the electron necklace is to examine the complex time correlation function, $\mathcal{R}^2(t - t')$. It is important to remember (see Chapter 3) that the correlation length, namely $\mathcal{R}(\beta\hbar/2)$, is a direct measure of the mean square diameter and therefore the size of the electron. If this quantity is evaluated for the interior state in the $N = 54$ cluster it is found $\mathcal{R}(\beta\hbar/2) = 3.7 \text{ \AA}$ which compares with 4.1 \AA of the bulk liquid.

In contrast, the behavior of an electron interacting with the smaller clusters is very different. When $N = 16$ the electron is almost totally detached from the cluster, it becomes "diffuse" and its average diameter is comparable to that of a free electron. At 100 K $\lambda_T = (\hbar^2\beta/m_e)^{1/2} \simeq 30 \text{ \AA}$, which implies that $\mathcal{R}(\beta\hbar/2) \simeq 25 \text{ \AA}$. For $N = 36$, the electron escapes to form a more compact surface state in which the electron polymer has

$\mathcal{R}(\beta\hbar/2) \simeq 9 \text{ \AA}$, expands and is attached to the cluster surface.

To test the stability of the interior state found for the $N = 54$ cluster, it was necessary to run an extra simulation starting from a cavity of diameter 6 \AA and then running the system in the usual way. The larger initial cavity does not affect the final result ; the electron remains trapped and the molecules relax bringing the electron (and cavity) average diameter to the same value as in the previous calculation. The interior state found for the cluster with $N = 54$ shows strong similarities with the solvated electron state in the bulk. In Fig. 7.2 an instantaneous configuration sampled from the MC run is presented. Figure 7.3 presents the pair correlation functions for N and H atoms, with respect to the electron center of mass, in the cluster. These functions have to be compared with the ones in the bulk reported in Fig. 4.2. The former are more structured, most likely, because of the lower temperature. Nevertheless, the coordination number for both calculations is the same, around 12.

On the basis of the above calculation, one can conclude that the interior state for $N = 54$ is at least metastable. Previous work on electron attachment to H_2O clusters found that surface states were more favourable until $N \simeq 100$. [66] Accordingly, an additional run was performed for the same cluster, this starting from a exterior state. This simulation converges to a stable surface state similar to the one the negatively charged $N = 36$ cluster evolves to.

In Fig. 7.4 a pictorial representation of the surface states at $N =$

36, 54 and the diffuse state at $N = 16$ is given. The similarities of the surface states of clusters with $N = 36$ and 54 and their contrast with the $N = 16$ case are clearly seen in Fig. 7.5 where the respective complex time correlation functions are shown. The values of $\mathcal{R}(\hbar\beta/2)$ for the surface states (see Table 7.1) agree within statistical error: around 8.8 Å for $N = 36$ and 9.1 Å for $N = 54$.

The nature of the reconstruction of the ammonia cluster induced by an electron attached to the surface is also of interest. The orientational ordering of the solvent in the vicinity of the electron can be quantified by examining the corresponding dipole correlation function. The evaluation of this probability distribution function, which is shown in Fig. 7.6, includes only those molecules within a distance $|\mathbf{R}_i - \mathbf{r}_{em}| < 5$ Å from the center of mass of the electron. A truncation radius of this length effectively excludes all solvent beyond the first solvation sheath. From Fig. 7.6 it can be concluded that electron attachment to the surface of the cluster causes strong dipole ordering of the molecules in the cluster. This contrasts with the electron in bulk ammonia and in the interior state for $N = 54$, where bond order in the first solvation sheath is predominant. A similar effect was found in H_2O clusters.

The electron center of mass nitrogen distribution functions for the surface states are presented in Fig. 7.7. The density distribution shifts inward in the case of $N = 54$ in comparison to the $N = 36$ case.

7.3 Energetics of Electron Attachment

The electron solvation energy is defined as the sum of the binding energy and the reorganization energy of the cluster molecules, namely

$$\langle \Delta E \rangle = \langle E \rangle + \langle E_R \rangle, \quad (7.2)$$

where $\langle E_R \rangle$ is given by

$$\langle E_R \rangle = \langle U \rangle - \langle U_0 \rangle, \quad (7.3)$$

with $\langle U_0 \rangle$ and $\langle U \rangle$ being respectively the potential energies of the neutral and negatively charged cluster. $\langle E \rangle$ is defined as the sum of the electron kinetic and potential energies minus the free particle contribution, namely

$$\langle E \rangle = \langle K \rangle + \langle P \rangle - \frac{3}{2} k_B T. \quad (7.4)$$

In Table 7.1 the results concerning the equilibrium energetics of the neutral and charged clusters are presented. It is found an essentially free electron state for the ammonia cluster with $N = 16$, i.e., ΔE is zero within error bars. This suggests that an electron cannot be bound by so few ammonia molecules. For the exterior states occurring at $N = 36$ and $N = 54$, large negative solvation energies are found. This implies that electron attachment to small ammonia clusters occurs through surface states. That the reorganization energy $\langle E_R \rangle$ has a small negative value for the $N = 16$ and the $N = 36$ surface states is puzzling at first sight. A possible explanation is that the electron causes an enhanced alignment

of surface molecules in the cluster (recall Fig. 7.6) and hence reduces the ammonia clusters entropy.

The convergence of both the quantum and classical calculations was checked every few thousand passes by comparing subaverages. The estimated uncertainties on the intermolecular potential energies varied with the size (see Table 7.1). As expected, the relative error was higher for the smallest cluster. The error on the electron binding energy was less than on the molecular potential energy.




Table 7.1: Energetics of the Neutral and Charged Clusters.

$\langle P \rangle$ and $\langle K \rangle$ are the electron potential and kinetic energies. $\langle E \rangle$ is the electron binding energy defined in eq. 7.4. $\langle U_0 \rangle$ and $\langle U \rangle$ are the intermolecular potential energies of the neutral and charged clusters. $\langle E_R \rangle$ and $\langle \Delta E \rangle$ are the reorganization and the solvation energies (eq. 7.2 and 7.3).

Energies are in eV and length in Å.

N	$\langle T \rangle$	$\langle P \rangle$	$\langle E \rangle$	$\langle U_0 \rangle$	$\langle U \rangle$	$\langle E_R \rangle$	$\langle \Delta E \rangle$	$\mathcal{R}(\hbar\beta/2)$
16	0.013	- 0.002	-0.002	- 2.939	- 2.957	- 0.018	- 0.020 ± 0.042	30.1 ± 3
36	0.223	- 0.438	-0.228	- 7.216	- 7.276	- 0.060	- 0.288 ± 0.033	8.8 ± 1
54	1.072	- 2.261	-1.201	- 11.529	- 9.811	1.718	0.517 ± 0.018	3.7 ± 0.1
54s [†]	0.260	-0.550	-0.303	- 11.529	- 11.383	0.146	- 0.157 ± 0.024	9.1 ± 1

[†] Surface State

Figure 7.1:

Distribution functions for the nitrogen atoms. Results for bulk liquid ammonia at $T = 260K$ and $V = 25.3cm^3mol^{-1}$ and for the neutral ammonia clusters at $T = 100K$.

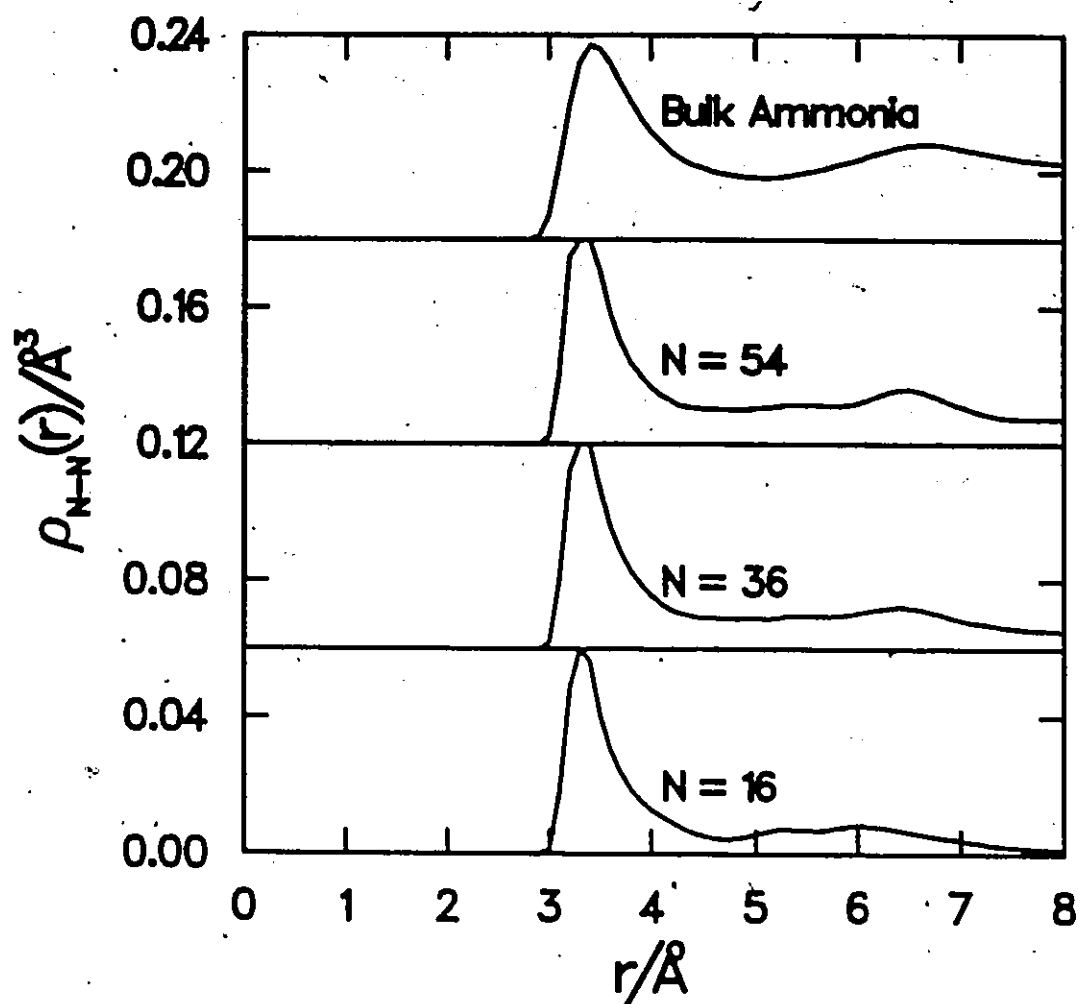


Figure 7.2:

Instantaneous configuration of an electron in an interior-solvated state for the $(NH_3)_{54}^-$ cluster. The corners of the cubic box are 30 Å. Only the bends of the primary chains are plotted (empty dots).

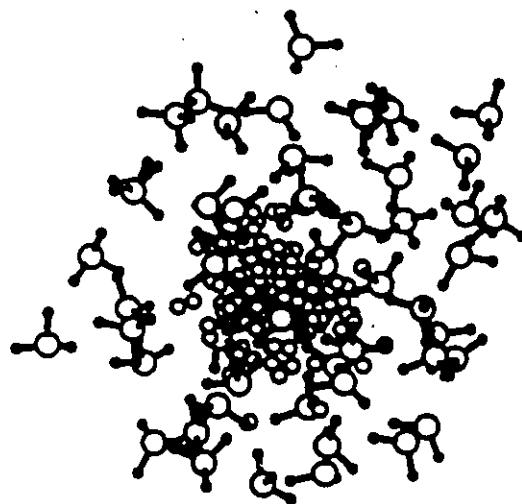


Figure 7.3:

Distribution functions for the solvent nitrogen (N) and hydrogen (H) atoms with respect to the center of mass of the electron charge density for the interior solvated state of a $(\text{NH}_3)_5^+$ cluster.

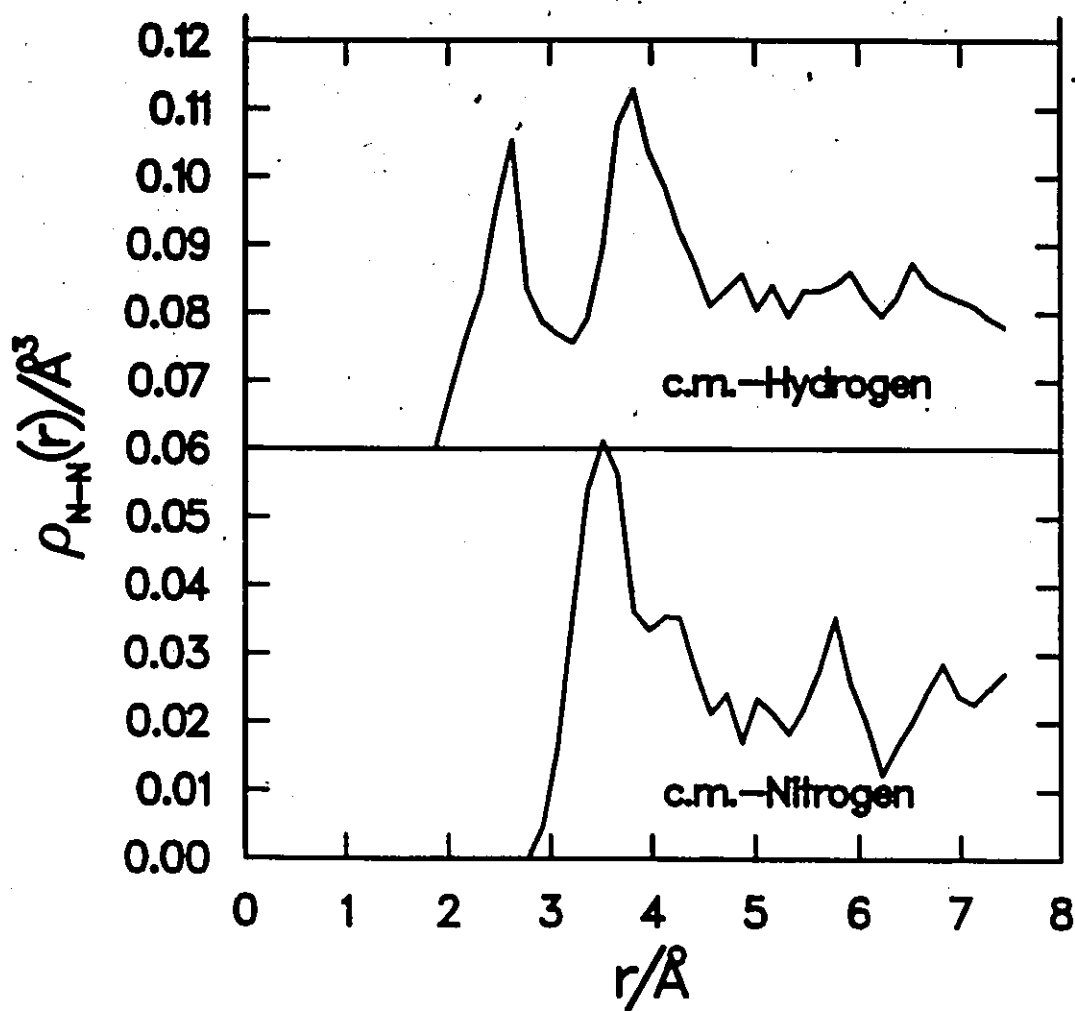
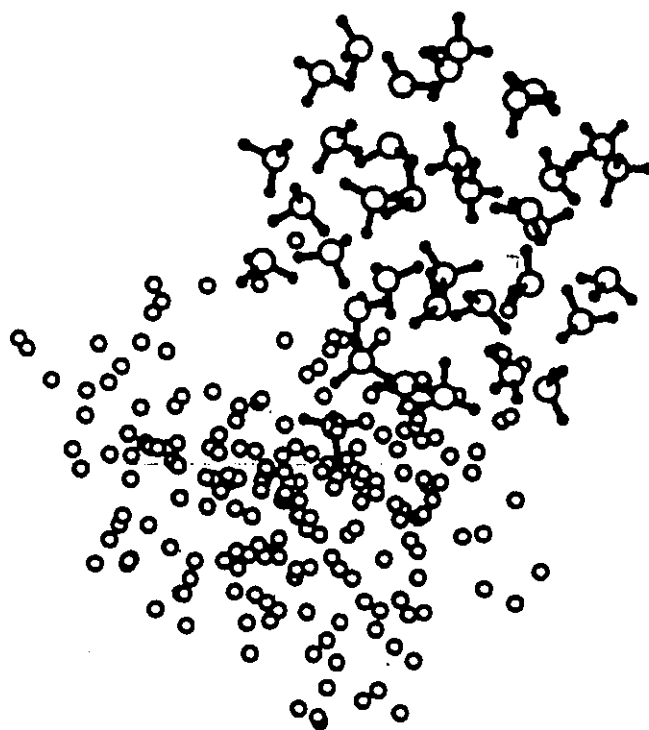
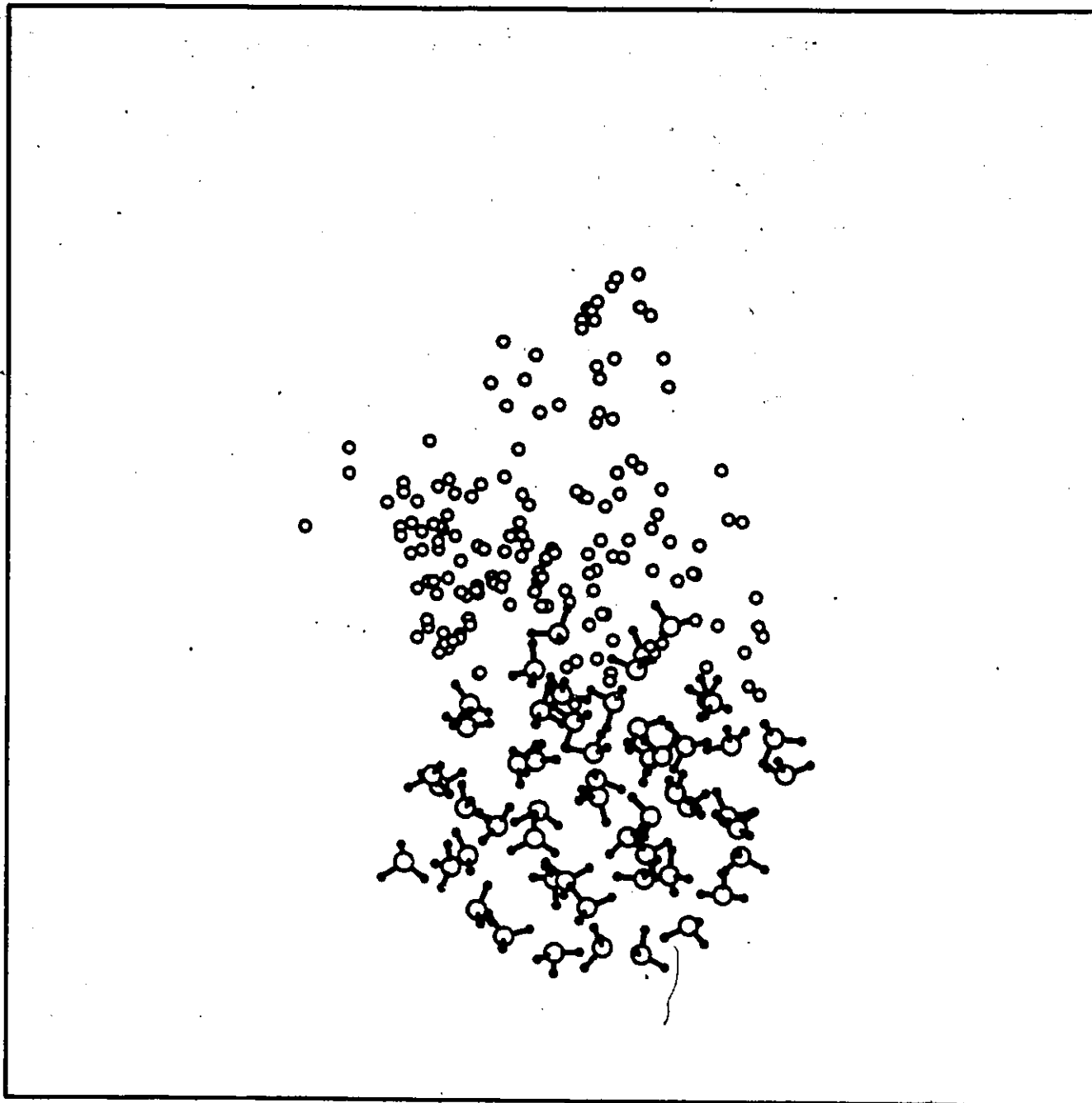


Figure 7.4:

Three instantaneous configurations at the end of the MC runs for the surface states for $(NH_3)_{36}^-$, $(NH_3)_{54}^-$ and the diffuse state for $(NH_3)_{16}^-$. The corners of the boxes are 30.0 Å for $(NH_3)_{36}^-$ and $(NH_3)_{54}^-$, and 55.0 Å for $(NH_3)_{16}^-$. Only the beads of the primary chains are plotted (empty dots).





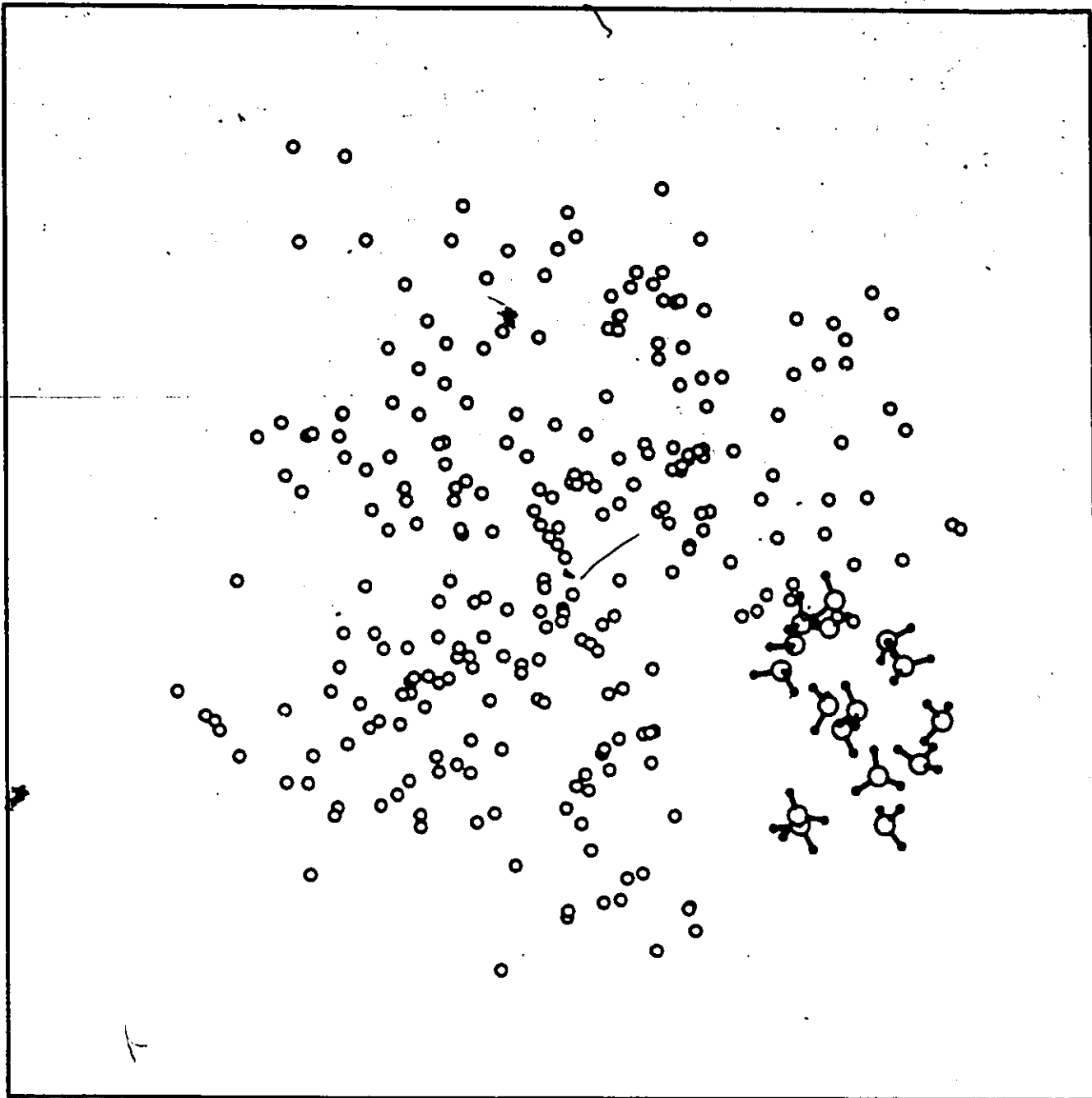


Figure 7.5:

Complex time correlation functions for the $(NH_3)_{16}$, $(NH_3)_{36}$ clusters and for the $(NH_3)_{54}$ cluster interior and surface states.

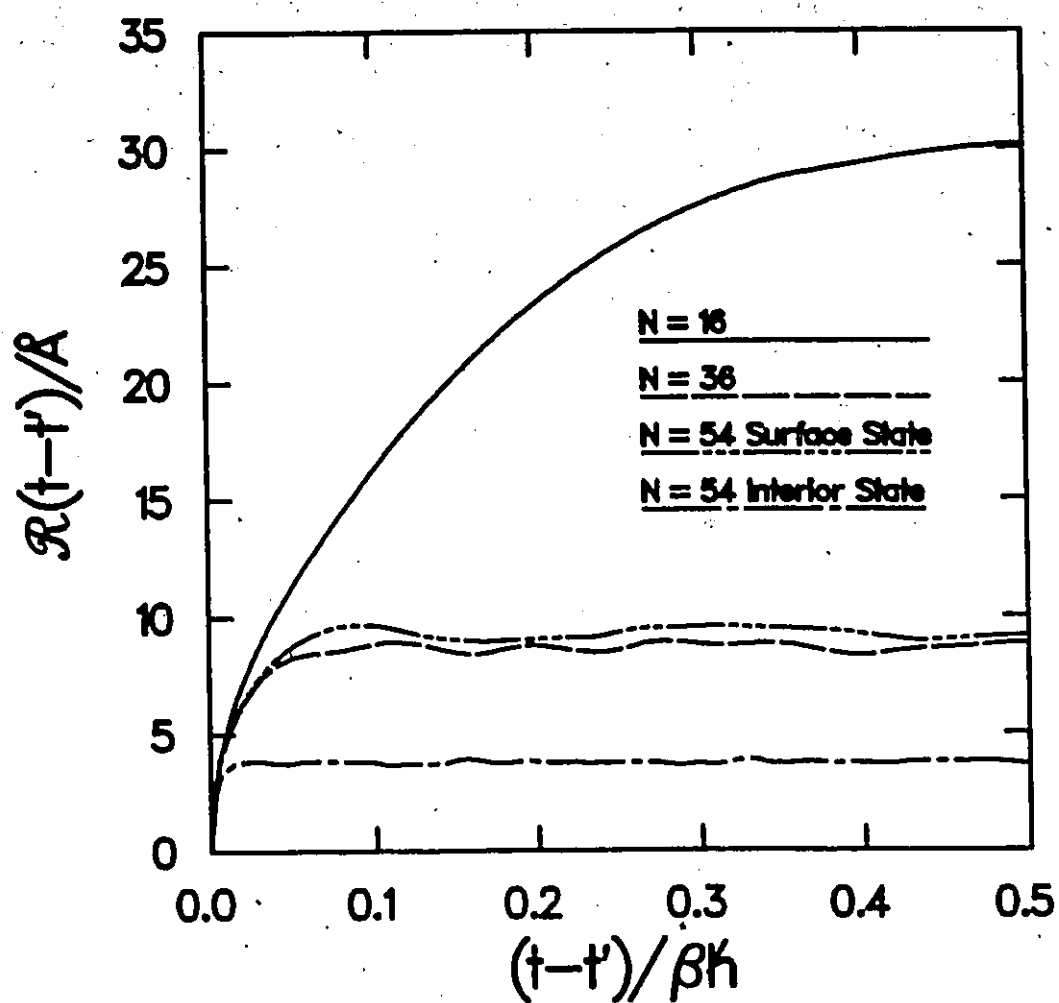


Figure 7.6:

Dipole correlation functions for the electron in liquid ammonia and for the electron in an interior and surface states bound to the $N = 54$ ammonia cluster. The correlation functions for the electron in bulk ammonia and the interior state include contribution from the first electron solvation sheath. About 10 neighbouring ammonia molecules are included in the calculation for the surface state.

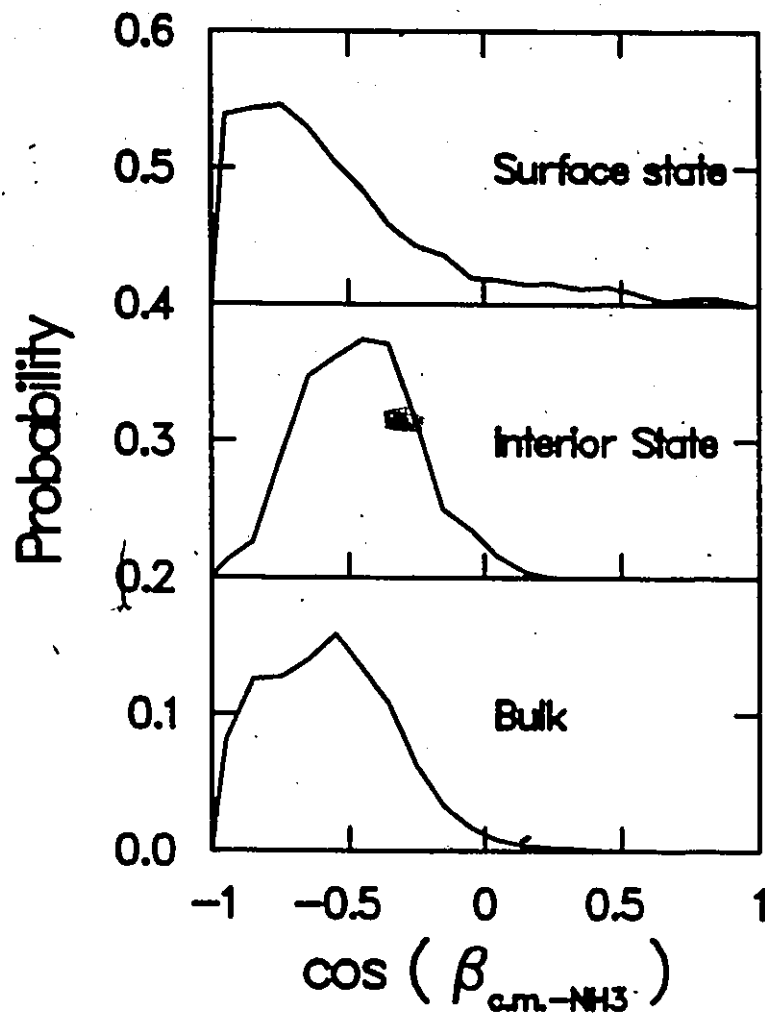
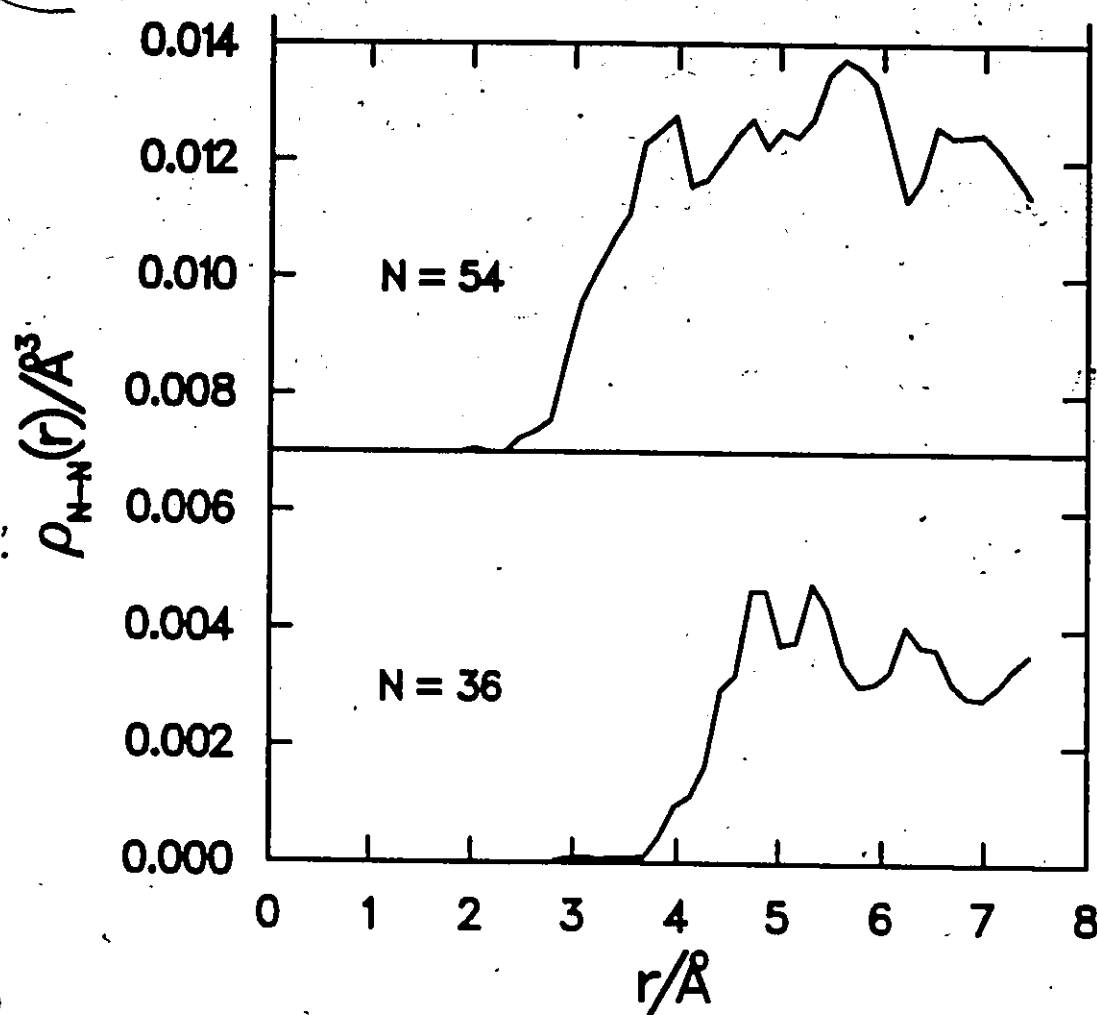


Figure 7.7:

Electron c.m.-nitrogen correlation functions for the surface states.



Chapter 8

Conclusions

In this thesis the path integral Monte Carlo method has been applied to some solvation problems involving quantum solutes. Thermodynamics quantities like partial molar volume and entropy change associated with the electron solvation process have been calculated. The ionization of alkali atoms in liquid ammonia and the electron attachment to ammonia clusters have been investigated.

Path integral MC simulations at constant pressure have lead to an expansion of the simulation box in satisfactorily agreement with the experimental molar volume. The simulations were carried out by regarding the polymer degrees of freedom as independent of the volume fluctuations. The structure of the solvated electron at constant pressure was found to be very similar to the one at constant volume. The electron wavefunction was only slightly expanded.

The Debye charging trick was used to calculate the free energy of the solvated electron at constant volume. The experimental solvation entropy at constant pressure was reproduced only when a correction due to the volume expansion was introduced. The contribution to the entropy due to the ordering of the ammonia molecules induced by the electron is negative. A major result is clear from this calculation : the expansion work, performed by the liquid when the electron is introduced, is responsible for the positive experimental entropy.

Two model pseudopotentials were used to study alkali atoms in ammonia. Spontaneous ionization was observed only for Na and Cs when the HC model was employed. The SC model leads to the formation of dipolar atoms when tested with Li and Cs. A dipolar Li atom was observed even for the HC model. The HC Li was much more polarized than the SC Li. These calculations predict that the minimum energy state for at least Na and Cs is indeed the separately solvated ions. This is agreement with the experimental evidence.

In the study on neutral and negatively charged ammonia clusters at $T = 200$ K the $N = 16, 36$ and 54 neutral-clusters of ammonia were found unstable. The introduction of an excess electron does not increase their stability and they spontaneously break apart. In contrast, at $T = 100$ K only the $n = 16$ cluster fails to bind the electron. For both the $N = 36$ and 54 a most stable surface state was found. The (meta)stable internal state for the $N = 54$ cluster was higher in energy than the surface one.

- These results are in agreement with Landman's work on water,[66,100] but disagree with the continuum theory.[103]

Despite the limitations of the method and interaction models adopted in this thesis, the results obtained are in satisfactory agreement with experiment. More importantly, the path integral Monte Carlo method is able to offer deep insights in the structural aspects of the systems examined and to make predictions on their minimum energy states.

Bibliography

- [1] M. L. Klein. *Ann. Rev. Phys. Chem.*, 36:525, 1985. and references therein.
- [2] J. P. Valleau, and S. G. Whittington. In B. J. Berne, editor, *Statistical Mechanics*, page 137, Plenum Press, New York, 1977. and references therein.
- [3] M. Parrinello, and A. Rahman. *J. Chem. Phys.*, 80:860, 1984.
- [4] B. DeRaedt, M. Sprik, and M. L. Klein. *J. Chem. Phys.*, 80:5719, 1984.
- [5] M. Sprik, R. W. Impey, and M. L. Klein. *J. Chem. Phys.*, 83:5802, 1985.
- [6] A. Wallqvist, D. Thirumalai; and B. J. Berne. *J. Chem. Phys.*, 86:6404, 1987.
- [7] R. Car, and M. Parrinello. *Phys. Rev. Lett.*, 55:2471, 1985.

- [8] A. Selloni, P. Carnevali, R. Car, and M. Parrinello. *Phys. Rev. Lett.*, 59:823, 1987.
- [9] R. P. Feynman, and A. R. Hibbs. *Quantum Mechanics and Path Integrals*. McGraw-Hill, New York, 1965.
- [10] R. P. Feynman. *Statistical Mechanics*. Benjamin, Reading, 1972.
- [11] D. Chandler, and P. G. Wolynes. *J. Chem. Phys.*, 74:4073, 1981.
- [12] D. M. Ceperley, and E. L. Pollock. *Phys. Rev.*, B30:2555, 1984.
- [13] J. Schnitker, and P. J. Rossky. *J. Chem. Phys.*, 86:3471, 1986.
- [14] D. M. Ceperley, and E. L. Pollock. *Phys. Rev. Lett.*, 56:351, 1986.
- [15] D. F. Coker, B. J. Berne, and D. Thirumalai. *J. Chem. Phys.*, 86:5689, 1987.
- [16] M. Sprik, R. W. Impey, and M. L. Klein. *Phys. Rev. Lett.*, 56:2326, 1986.
- [17] W. Weyl. *Ann. Phys.*, 197:601, 1863.
- [18] J. C. Thompson. *Electron in Liquid Ammonia*. Clarendon, Oxford, 1976.
- [19] F. Y. You, and G. R. Freeman. *J. Phys. Chem.*, 85:629, 1981.
- [20] P. Krebs. *Ber. Bunsenges, Phys. Chem.*, 88:275, 1984.

- [21] P. Krebs. *J. Phys. Chem.*, 88:3702, 1984.
- [22] U. Scindewolf. In J. V. Acrivos, N. F. Mott, and A. D. Joffe, editor, *Physics and Chemistry of Electrons and Ions in Condensed Matter*, Reidel, Dordrecht, 1984.
- [23] . In J. Jortner, and N. R. Kestner, editor, *Electrons in Fluids*, Springer-Verlag, Berlin, 1973.
- [24] H. Haberland, H. G. Schindler, and D. R. Worsnop. *Ber. Bunsenges, Phys. Chem.*, 88:270, 1984.
- [25] H. Haberland, C. Ludewigt, H. G. Schindler, and D. R. Worsnop. *Surf. Sci.*, 156:157, 1985.
- [26] J. O. Hirschfelder, C. F. Curtis, and R. B. Bird. *Molecular Theory of Gases and Liquids*. Wiley, New York, 1954.
- [27] D. M. Ceperley. In M. H. Kalos, editor, *Monte Carlo Methods in Quantum Problems*, page 47, D. Reidel, Dordrecht, 1984.
- [28] S. G. Anderson, and D. P. Santry. *J. Chem. Phys.*, 74:5780, 1981.
- [29] E. Clementi, and G. Corongiu. *Int. J. Quantum Chem.*, 10:31, 1983.
- [30] M. Wojcik, and E. Clementi. *J. Chem. Phys.*, 85:3544, 1986.
- [31] I. G. Kaplan, and O. B. Rodimova. *Usp. Fiz. Nauk*, 126:403, 1973.

- [32] A. J. Pertsin, and A. I. Kitaigorodsky. *The Atom-Atom Potential Method*. Springer-Verlach, Berlin , 1987.
- [33] O. Matsuoka, E. Clementi, and M. Yoshimine. *J. Chem. Phys.*, 64:1351, 1976.
- [34] H. J. Bohm, R. Alrichs, P. Scharf, and H. Schiffer. *J. Chem. Phys.*, 81:1389, 1984.
- [35] T. Aoyama, O. Matsuoka, M. Nakagawa. *Chem. Phys. Lett.*, 67:508, 1979.
- [36] F. Mulder, G. Van Dijk, and A. Van der Avoird. *Mol. Phys.*, 39:407, 1980.
- [37] . In O. Chalvet, R. Daudel, S. Diner, and J. P. Malrieu, editor, *Localization and Delocalization in Quantum Chemistry*, D. Reidel, Dordrecht, 1975.
- [38] R. F. W. Bader, and P. M. Beddall. *J. Chem. Phys.*, 56:3320, 1972.
- [39] R. F. W. Bader, P. M. Beddall, and J. Peslak, Jr. *J. Chem. Phys.*, 58:557, 1972.
- [40] R. F. W. Bader, S. G. Anderson, and A. J. Duke. *J. Am. Chem. Soc.*, 95:305, 1979.
- [41] R. F. W. Bader. *Accounts of Chemical Research*, 18:9, 1985.

- [42] K. B. Wiberg, R. F. W. Bader, and C. D. H. Lau. *J. Am. Chem. Soc.*, 109:1001, 1986.
- [43] Z. Gamba, and H. Bonadeo. *J. Chem. Phys.*, 76:6212, 1982.
- [44] M. Marchi, and R. Righini. *Chemical Physics*, 94:465, 1984.
- [45] D. E. Williams. *J. Chem. Phys.*, 45:3770, 1966.
- [46] D. E. Williams. *J. Chem. Phys.*, 47:4680, 1967.
- [47] J. C. Phillips, and L. Kleinman. *Phys. Rev.*, 116:287, 1959.
- [48] M. H. Cohen, and V. Heine. *Phys. Rev.*, 122:1821, 1961.
- [49] W. A. Harrison. *Pseudopotentials in the Theory of Metals*. W. A. Benjamin, New York, 1966.
- [50] M. A. Morrison, and L. A. Collins. *Phys. Rev.*, A 17:918, 1978.
- [51] J. Schnitker, and P. J. Rossky. *J. Chem. Phys.*, 86:3462, 1986.
- [52] A. Wallqvist, D. Thirumalai, and B. J. Berne. *J. Chem. Phys.*, 85:1583, 1986.
- [53] N. Metropolis, A. W. Rosenbluth, M. N. Rosenbluth, A. H. Teller, and E. Teller. *J. Chem. Phys.*, 21:1087, 1953.
- [54] J. P. Hansen, and I. R. McDonald. *Theory of Simple Liquids*. Academic Press, London, 1986.

- [55] W. Feller. *An Introduction to Probability Theory and its Applications*. Volume 1, John Wiley, New York, 1950.
- [56] D. J. Evans, and S. Murad. *Mol. Phys.*, 34:327, 1977.
- [57] M. P. Allen, and D. J. Tildesley. *Computer Simulation of Liquids*. Oxford University Press, Oxford, 1988.
- [58] M. F. Herman, E. J. Bruskin, and B. J. Berne. *J. Chem. Phys.*, 76:10, 1982.
- [59] M. Sprik, M. L. Klein, and D. Chandler. *Phys. Rev.*, B31:4234, 1985.
- [60] M. Sprik, M. L. Klein, and D. Chandler. *J. Chem. Phys.*, 83:3042, 1985.
- [61] L. D. Fosdick, and H. F. Jordan. *Phys. Rev.*, 143:143, 1966.
- [62] D. Chandler, Y. Singh, and D. M. Richardson. *J. Chem. Phys.*, 81:1975, 1984.
- [63] A. L. Nichols III, D. Chandler, V. Singh, and D. M. Richardson. *J. Chem. Phys.*, 81:5109, 1984.
- [64] A. L. Nichols III, and D. Chandler. *J. Chem. Phys.*, 84:398, 1986.
- [65] M. Sprik, and M. L. Klein. *Computer Physics Reports*, 7:147, 1988.
- [66] R. N. Barnett, U. Landman, C. L. Cleveland, and J. Jortner. *J. Chem. Phys.*, 88:4492, 1988.

- [67] C. Deutsch, and M. M. Gombert. *J. Math. Phys.*, 17:1077, 1976.
- [68] R. W. Shaw. *Phys. Rev.*, 174:769, 1968.
- [69] I. R. McDonald. *Mol. Phys.*, 23:41, 1972.
- [70] N. F. Mott. *Metal-Insulator Transitions*. Taylor and Francis, London, 1974.
- [71] Z. W. Salsburg, J. D. Jacobson, W. Fickett, and W. W. Wood. *J. Chem. Phys.*, 30:65, 1959.
- [72] J. P. Valleau, and G. M. Torrie. In B. J. Berne, editor, *Statistical Mechanics*, page 169, Plenum Press, New York, 1977. and references therein.
- [73] D. A. Chestnut. *J. Chem. Phys.*, 39:2081, 1963.
- [74] W. G. Hoover, and F. H. Ree. *J. Chem. Phys.*, 47:4873, 1967.
- [75] W. G. Hoover, and F. H. Ree. *J. Chem. Phys.*, 49:3609, 1968.
- [76] J. P. Valleau, and D. N. Card. *J. Chem. Phys.*, 57:5457, 1972.
- [77] G. M. Torrie, and J. P. Valleau. *J. Comput. Phys.*, 23:187, 1977.
- [78] M. C. Moody, J. R. Ray, and A. Rahman. *J. Chem. Phys.*, 84:1795, 1986.
- [79] C. H. Bennett. *J. Comp. Phys.*, 22:245, 1976.

- [80] A. Rahman, and G. Jacucci. *Il Nuovo Cimento*, D 4:341, 1984.
- [81] R. W. Impey, and M. L. Klein. *Chem. Phys. Lett.*, 104:579, 1984.
- [82] R. L. Mills, D. H. Liebenberg, and Ph. Pruzan. *J. Phys. Chem.*, 86:5219, 1982.
- [83] R. L. Mills, D. H. Liebenberg, R. LeSar, and Ph. Pruzan. *Mat. Res. Symp. Proc.*, 22:43, 1984.
- [84] J. C. Thompson. In J. Jortner, and N. R. Kestner, editor, *Electrons in Fluids*, Springer-Verlag, Berlin, 1973.
- [85] R. S. Allgaier. *Phys. Rev.*, 185:227, 1969.
- [86] R. L. Schroeder, J. C. Thompson, O. L. Oertel. *Phys. Rev.*, 178:298, 1969.
- [87] N. W. Hashcroft, and G. Russakoff. *Phys. Rev.*, A 1:39, 1970.
- [88] R. L. Schroeder, J. C. Thompson. *Bull. Am. Phys. Soc.*, 13:397, 1968.
- [89] R. W. Impey, M. Sprik, and M. L. Klein. *J. Am. Chem. Soc.*, 109:5900, 1987.
- [90] S. F. Smith, J. Chandrasekha, and W. L. Jorgensen. *J. Phys. Chem.*, 86:3308, 1982.
- [91] A. M. Stacy, and M. J. Sienko. *Inorg. Chem.*, 21:2294, 1982.

- [92] V. Heine, and I. V. Abarenkov. *Phil. Mag.*, 9:451, 1964.
- [93] W. Andreoni, A. Baldereschi, E. Biémont, and J. C. Phillips. *Phys. Rev.*, B20:4814, 1979.
- [94] D. E. Logan. *Phys. Rev. Lett.*, 57:782, 1986.
- [95] P. F. Meier, R. H. Hauge, and J. L. Margrave. *J. Am. Chem. Soc.*, 100:2108, 1978.
- [96] M. Armbruster, H. Haberland, and H. G. Schindler. *Phys. Rev. Lett.*, 47:323, 1981.
- [97] M. Knapp, O. Echt, D. Kreisle, and R. Recknagel. *J. Chem. Phys.*, 85:636, 1986.
- [98] M. Knapp, O. Echt, D. Kreisle, and R. Recknagel. *J. Chem. Phys.*, 91:2601, 1987.
- [99] R. N. Barnett, U. Landman, C. L. Cleveland, and J. Jortner. *Phys. Rev. Lett.*, 59:811, 1987.
- [100] R. N. Barnett, U. Landman, C. L. Cleveland, and J. Jortner. *J. Chem. Phys.*, 88:4421, 1988.
- [101] U. Landman, R. N. Barnett, C. L. Cleveland, J. Luo, D. Scharf, and J. Jortner. In D. A. Micha, editor, *The Few Body Problem and Multiple Particle Dynamics*, A.I.P. to be published.

- [102] R. N. Barnett, U. Landman, C. L. Cleveland, and J. Jortner. *Chem. Phys. Lett.*, 148:249, 1988.
- [103] P. Stampfli, and K. H. Benneman. *Phys. Rev. Lett.*, 58:3042, 1985.